University of Nottingham
UK | CHINA | MALAYSIA

PHD THESIS

Model Order Reduction for Electromagnetic Design in Power Electronics

XINNING GAO, MEng

Thesis submitted to the University of Nottingham for the degree of Doctor of Philosophy, Jan 2022

Abstract

With the development of Wide Band Gap (WBG) power devices and their application in power electronics system, the evaluation of the key component electromagnetic (EM) behaviour is becoming increasingly important due to the fast switching speed and resulting dV/dt and dI/dt. Issues with WBG (Wide Band Gap) devices application such as EMI (electromagnetic interference) therefore must be considered at the design stage. Predicting electromagnetic effects using simulation tools is difficult because 3D models of design geometry and accurate semiconductor switching models must be coupled. These simulations require large numbers of time-steps to be applied to large simulation models.

This thesis considers electromagnetic modelling in power electronics and potential methods for improvement for its simulation time. An electromagnetic simulation process using a numerical modelling method (Partial Element Equivalent Circuit (PEEC) method) is derived and evaluated in the thesis. The EM (Electromagnetic) modelling method is evaluated on impedance prediction and current density prediction.

Model Order Reduction (MOR) techniques are then proposed to accelerate the simulation. Firstly, Standard, single-point MOR (Model Order Reduction) techniques are applied and evaluated through simple examples. The analysis on simulation results and experimental results with conventional MOR method shows the limitation on 3D simulation.

A modified multi-point MOR technique is proposed in this thesis to enhance the accuracy with 3D simulation and compared with the conventional MOR method. An eigenvalue analysis method is derived and used to evaluate different MOR techniques explain the limitations of standard single-point MOR methods and the advantages of the multi-point approach. Further analysis on expansion point selection and its effect on simulation results are then given.

Acknowledgements

I would like to thank my supervisors Dr. Paul Evans, Prof. Mark Johnson, Dr. Ke Li for their guidance and advice throughout this study. Many thanks to my external assessor Prof. Christopher Bailey and my internal assessor Dr. Thomas Cox for their correction advice to my thesis.

Finally, I want to thank my husband Jiawei Zhang for his support and encouragement.

Table of Contents

List of Figures

List of Tables

List of Symbols

E - Electric field

H - Magnetic field

D - Electric flux density in Maxwell's equation

B - Magnetic flux density in Maxwell's equation

ρ_v - Volume charge density

J – Electric current density

Z – Impedance

A - Magnetic vector potential

ϕ – Electric scalar potential

σ – Conductivity

r – Observation point

μ – Permeability

ϵ - Permittivity

P – Potential coefficient

Q – Charge

I – Current

C_s - Short circuit capacitance matrix

R – Resistance

C – Capacitance

λ - Eigenvalue

$\alpha + \omega i$ - Complex eigenvalue

τ - Time constant

σ_r - Expansion point

Matrix symbol:

u – input vector

y – output vector

M, A, B, C: Original system matrix

O – output matrix

G, R – modified system matrix for control theory method

J, K – modified system matrix used in Arnoldi based method

$G(s)$ - transfer function

M_i - Moments

W_r, V_r – Transfer matrix generated from Lanczos algorithm

V_r - Transfer matrix generated in Arnoldi based method

Kr – Subspace

$H_r(s)$ - Reduced order system transfer function.

M_r, A_r, B_r, C_r- System matrix in reduced order model

A_s B_s – Modified system matrix used in eigenvalue analysis

$\boldsymbol{w}$, $\overline{\boldsymbol{w}}$ - conjugate pair of eigenvectors

X_p -Matrix represents steady state solution

D – contribution coefficient matrix

Chapter 1

1 Introduction and Background

1.1 Application of Wide Band Gap Devices for Power Electronics System

Modern power electronic systems operate with a trend of increasing semiconductor switching speeds, voltage, power and temperature. These characteristics mean that electromagnetic compatibility(EMC) or electromagnetic interference (EMI) of the systems can become a significant concern, due to high dV/dt and high dI/dt. Existing design tools cannot satisfy the demands associated with these increasing operating frequencies because they are usually designed for one domain or ignore the influence of high switching frequency[1]. One domain could be refer to circuit domain, physical domain, thermal domain, electromagnetic domain, or mechanical domain. Design tools that can couple accurate semiconductor models with efficient 3D electromagnetic models in time-domain simulation are required to enable a Virtual Prototyping design process. This is a timely problem due to the increasingly widespread application of extremely fast-switching wide-bandgap (WBG) devices in areas such as AC electric drives[2], hybrid /electric vehicles[3] and renewable energy systems[4].

Wide-bandgap devices can operate at high frequency, high voltage, and high temperature, which can offer significant benefits in power electronic application[5].

Operating frequency of WBG devices is higher than traditional silicon devices. Traditional silicon devices usually operate from a few hundred Hz to a few thousand Hz. Silicon carbide WBG devices can operate above 100kHz. GaN devices can achieve even higher operating frequency above 1 MHz. For example, higher switching frequencies can reduce the volume of the power system. WBG devices operating at higher voltage can reduce the amounts of devices being used, which will improve both power density and reliability. Higher operating temperature up to 400℃ make WBG devices more suitable for many industrial applications such as automotive and aerospace. Therefore, systems using WBG devices will be more compact and efficient.

However, fast voltage and current switching may cause the electromagnetic interference (EMI). The thermal management[6] is also very important for power electronics and can become a limiting factor in power dense power electronics enabled by wide bandgap semiconductors.

1.1.1 Advances in WBG Devices

A WBG semiconductor is one with large band gap energy, which means the energy difference between the top of the valence band and the bottom of the conduction band. In semiconductor physics, the energy band structure is shown in Figure 1.1:

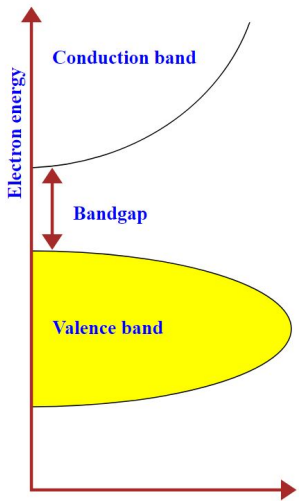

Figure 1.1 The Energy Band Structure[7]

The bandgap of WBG materials are higher than conventional materials of semiconductors such as silicon. This larger bandgap means that WBG devices can operate at higher voltages and/or frequencies, and temperatures. These characteristics make them an ideal solution for in high-performance, high-power power electronic applications. For example, Silicon Carbide (SiC) is anticipated to be widely used in future automotive traction invertors and aerospace power conversion[8] and Gallium Nitride (GaN) is seen as an ideal solution for automotive battery chargers[9, 10].

1.1.2 Challenges in WBG Devices and Their Applications

Higher operating frequencies of WBG devices allows the use of smaller and lighter passive filters components which usually make up a significant proportion of the overall system weight[11], and their higher allowable operating temperatures allow smaller thermal management systems.

With these advantages comes additional design challenges: electromagnetic interference (EMI) and compatibility (EMC) issues and power dense systems with increased semiconductor operating temperatures require careful thermal design to ensure reliable operation. With existing design techniques it is hard to predict how potential system designs will perform at the design stage[12].

1.1.3 The Importance of Electromagnetic Design in Power Electronics

The component choice, system geometry and construction techniques should be considered during the WBG system design. Effects such as electromagnetic interference and reliability are also notoriously difficult to predict[13] with extensive experience. Virtual Prototyping is the use of computer simulation tools to accurately predict how a design will perform, this reduces the need for physical prototype construction testing before production and therefore it will save money and time. It will enable faster design and allows engineers to develop high performance WBG systems more quickly.

EMI refers to the coupling between waveforms in a power electronic circuit and other, external circuits. This can be through conducted mechanisms (circuit physically connected to the system) or radiated mechanisms (coupling through electromagnetic fields created by the system). Both of these effects are design geometry dependent and should be predicted by virtual prototyping tools. The system's design can also influence its own performance and this effect is often explained through the concept of parasitic circuit elements. For example, the effects of parasitic elements can be seen from Figure 1.2 :

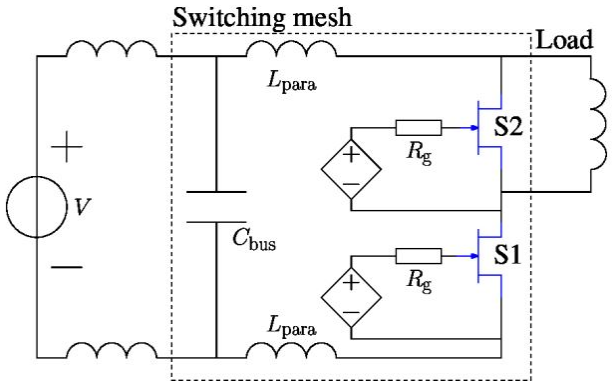

Figure 1.2 JEET Half Bridge Electrical Circuit[14]

The parasitic inductances can be found in the switching current loop. High switching frequency increases the interaction between devices and parasitic circuit. The source of the parasitic impedance depends on device packaging, circuit layout, such as PCB track of a half bridge circuit. Parasitic capacitance also contributes to power loss [15].

In addition, switching over-voltages are generated in the transistors and diodes due to high dI/dt in parasitic inductances. This increase turn off power dissipation and voltage stress in the power semiconductors. High-frequency oscillations in the range of some MHz may be generated in connection with parasitic impedance. It is important to develop 3D Virtual Prototyping tools (simulation software) that can predict how potential system designs will perform at the design stage.

1.2 Review of Commercial Simulation Tools

1.2.1 3D Electromagnetic Simulation

1.2.1.1 Ansys Maxwell

Some commercial software such as Ansys Electromagnetic Suite can provide EM simulation. Ansys Maxwell is used for low frequency EM field simulation, such as electric machines[16], actuators and other mechanical devices.

Ansys Maxwell is widely used by engineers at the stage of design and optimize a new product more efficient without buying costly physical prototype. It is based on the finite element analysis method, the meshing is optimized automatically based on the user's requirements. It is widely used in low frequency electromagnetic field simulation. The drawback of Ansys Maxwell is that the electric field and magnetic field cannot be coupled.

1.2.1.2 Ansys HFSS

Ansys HFSS is used for high frequency EM field simulation software, such as antennas, antenna arrays, RF or microwave components etc.[17] For example, a HFSS model of microstrip bend is shown in Figure 1.3:

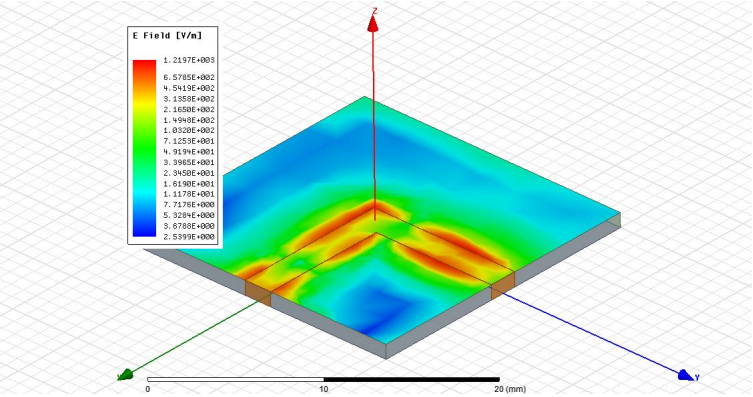

Figure 1.3 The electric field distribution in a microstrip bend

This model is a microstrip transmission line with 90 degree bend. Analysis is done at the frequency of 10GHz. HFSS is usually used for EM simulation at GHz.

HFSS is suitable for RF and high-speed design with a 3D full wave solver. HFSS breaks the cycle of repeated design iterations and length for physical prototyping[18]. Post process is needed for field, conducting current J, Near field E, H, and port power parameters etc. In HFSS, it is focus on the structure design of physical model. To set up a physical model, definition of boundary and excitation are needed. The boundary condition could be sources, surface approximations, and material properties etc. The excitations are defined to allow energy to flow into and out of a structure. The limitation is that Ansys HFSS is designed for high frequency EM simulation and cannot combine the power electronic circuits to the geometry model. The electrical characteristics of power electronics cannot be modelling directly in HFSS because the circuit elements application includes lumped circuit element or a block box representation in the HFSS solution.

In HFSS, the circuit components cannot connect directly to the HFSS model without model transformation, and geometry design cannot be modified in the circuit simulation software. There is no direct coupling of the circuit and HFSS model.

1.2.1.3 Ansys Q3D

Ansys Q3D is a simulation tool which can extracts and calculates the parasitic parameters, such as resistance, inductance, capacitance and conductance for electronic products.

Q3D extractor is widely used at the design stage for advanced high-speed electronic equipment. It is also used to extract parasitic parameters for power converter components used in electrical power distribution, power electronics and electric drive systems.

Ansys use MOR algorithms to accelerate the simulation speed for applications such as digital twin in aerospace industry.

1.2.2 Circuit Simulation

1.2.2.1 PLECS

PLECS is a software designed for power electronics and easy to use in system-level simulation, because ideal semiconductor switching model is implemented in PLECS. It typically consists of electrical power circuit[19], electrical load, digital controls and thermal networks. The advantage is that PLECS provides fast and efficient simulation with ideal switches for instantaneous switching.

PLECS is kind of circuit and system level modelling, but cannot provides 3D modelling. It will become difficult for designers if the layout of circuit board design is required to optimize based on the electromagnetic and thermal performance of the PCB board.

1.2.2.2 SPICE

SPICE[20] is a circuit simulator and can be used to predict the circuit behaviour. It includes many accurate semiconductor device models. In addition, it had many other elements, such as resistors, capacitors, inductors (including coupling), current and voltage sources. It allows the user to view the transient behaviour of current and voltage waveforms for the circuit simulation.

The SPICE software can be used for power electronics and electric power simulation, the disadvantage is that it cannot coupled with geometry model and cannot give a 3D view of the model.

1.2.3 Coupled System Simulation

The geometry model of HFSS can be exported as a black box and imported to a circuit simulator, but the structure inside is invisible. Only the behaviour seen from the port defined can be observed. It is difficult to coupling with accurate semiconductor models.

The combination of circuit model and HFSS model is shown in Figure 1.4:

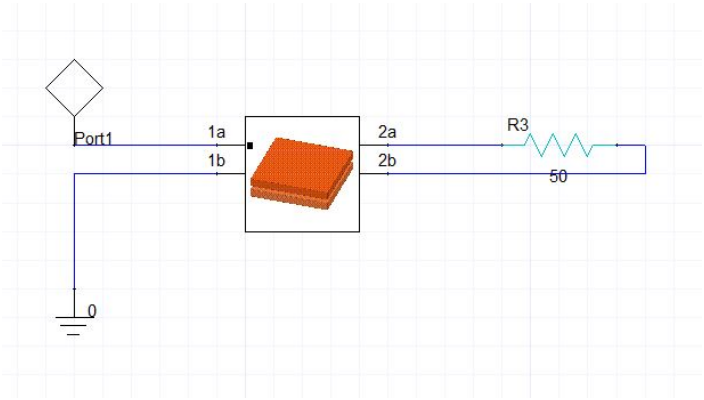

Figure 1.4 Combination Model with Circuit and HFSS

The HFSS model is a simple parallel capacitor, but the geometry cannot modified in the circuit simulator.

1.3 Motivation and Contribution

The electromagnetic modelling in power electronic is important, but existing simulation tool cannot meet the requirement in WBG devices application. In general, the motivation of this PhD is to find appropriate numerical methods which can be used for fast time-domain electromagnetic simulation of power electronics systems. The target is a method that can evaluate a coupled 3D physical model and wide-bandgap semiconductor models, and provide analysis of the electric field and magnetic field in a 3D view. A key technical objective is enhancing the simulation speed to allow a rapid, iterative virtual prototyping design process.

A design tool, developed at the University of Nottingham is proposed in [21], it enables virtual test to save cost and time[22], however, initial results from this design tool (prior to this PhD) show that it is unable to perform fast and accurate

electromagnetic modelling and suffers from poor performance at high frequencies. The tool uses a Model Order Reduction (MOR) algorithm to accelerate 3D electromagnetic models to provide analysis capabilities similar to finite element software such as Ansys, but with much faster simulation times and an ability to easily couple with semiconductor device models. The principle of MOR will be explained in chapter 3.

The main contribution of this PhD is the development of a new model-order reduction algorithm which provides this accelerated 3D electromagnetic simulation capability but is accurate over a much larger frequency range.

1.4 Thesis Outline

The thesis is structured as follows.

Chapter 2 introduces the basic concepts of electromagnetic modelling process. Several electromagnetic analyse methods are reviewed. The principles of an electromagnetic simulation technique, the Partial Element Equivalent Circuit (PEEC) method is introduced in detail as this forms the basis of the simulation techniques used in later chapter. Several examples are used to evaluate the PEEC method when applied to power electronic systems.

Chapter 3 introduces the standard MOR methods which have been used previously. Several MOR techniques are reviewed and then technical details of the PRIMA algorithm, designed specifically for PEEC type electromagnetic models, are described. An evaluation of the standard PRIMA MOR technique for impedance prediction, simulation speed, and current density prediction is then performed. The results from this work are used to illustrate the limitations of the standard PRIMA MOR method and justify the research undertaken by this PhD project.

Chapter 4 introduces an eigenvalue analysis method which is a secondary contribution of this PhD. The method is presented and the principles of dominant eigenvalue analysis are explained. Several examples are given to show how the

eigenvalue analysis method works. It is then used to illustrate why standard MOR techniques are not suitable for this application through analysis of the simulation results from chapter 3.

Chapter 5 introduces a multi-point MOR technique, the primary contribution of this PhD. First some background and a review of multi-point Krylov subspace method are described. A modified multi-point PRIMA algorithm is proposed and evaluation of this algorithm is given on terminal impedance and current density distribution. The eigenvalue analysis method is then applied to both conventional MOR algorithm and multi-point MOR algorithm to understand the advantages of the proposed method over the standard PRIMA algorithm.

Chapter 6 provides further analysis on the proposed multi-point MOR method. Optimal selection of expansion points is investigated and recommendations for use of the algorithm are given.

Chapter 7 concludes the thesis.

Chapter 2

2 The PEEC method and MOR

2.1 Introduction

As shown in the previous chapter, virtual prototyping tools able to evaluate electromagnetic performance in power electronics are becoming increasingly important due to the increasing use of WBG devices. The main reason why doing numerical simulation and modelling within the area of research and industries is to test the products before production. This will save money and time if the electromagnetic performance of a new product can be predicted using a 3D virtual prototyping design tool.

This chapter will review 3D Electromagnetic (EM) simulation techniques. A more in-depth review of the PEEC method is then given as it is chosen to be the electromagnetic modelling technique used in this work. The EM simulation process and the evaluation of PEEC method will be illustrated and the results of experimental tests will be given in this chapter.

2.2 Introduction on Numerical Methods

Methodologies for electromagnetic modelling are either based on differential or integral forms of Maxwell's equation. The electromagnetic behaviour of a system is evaluated by solving Maxwell's equations for a range of quantities including electric and magnetic fields, current density, voltage, and even equivalent impedances between points in the geometry depending on requirements. The integral form of Maxwell's equation is shown in Equation 2.1:

$$\begin{aligned} \oint_L \vec{H} \cdot d\vec{l} &= \int_S \left(\vec{J} + \frac{\partial \vec{D}}{\partial t} \right) \cdot d\vec{S} \\ \oint_L \vec{E} \cdot d\vec{l} &= -\int_S \frac{\partial \vec{B}}{\partial t} \cdot d\vec{S} \\ \oint_S \vec{D} \cdot d\vec{S} &= \int_v \rho_v \cdot d\vec{S} \\ \oint_S \vec{B} \cdot d\vec{S} &= 0 \end{aligned} \qquad (\mathbf{2}.1)$$

The differential form of Maxwell's equation is shown in Equation **2**.2:

$$\begin{aligned} \nabla \times \vec{H} &= \vec{J} + \frac{\partial \vec{D}}{\partial t} \\ \nabla \times \vec{E} &= -\frac{\partial \vec{B}}{\partial t} \\ \nabla \cdot \vec{D} &= \rho_v \\ \nabla \cdot \vec{B} &= 0 \end{aligned} \qquad (\mathbf{2}.2)$$

And:

$\vec{E}$ - Electric field

$\vec{H}$ - Magnetic field

$\vec{D}$ - Electric flux density

$\vec{B}$ - Magnetic flux density

ρ_v - Volume charge density

$\vec{J}$ - Electric current density

The relationship between displacement field D and the electric field E, as well as the relationship between the magnetizing field H and the magnetic field B is shown in Equation 2.3:

$$D = \varepsilon E, \quad H = \frac{1}{\mu} B \tag{2.3}$$

ε is permittivity and μ is permeability. The changing magnetic field produced an electric field, the changing electric field produces a magnetic field. The selection of integral or differential form of Maxwell's equations depends on the problem being solved and what kind of solution is needed, such as the solution domain and field variables. The differences between integral equation methods and the differential equation methods will explained in the next section.

A typical standard electromagnetic(EM)simulation process is shown in Figure 2.1:

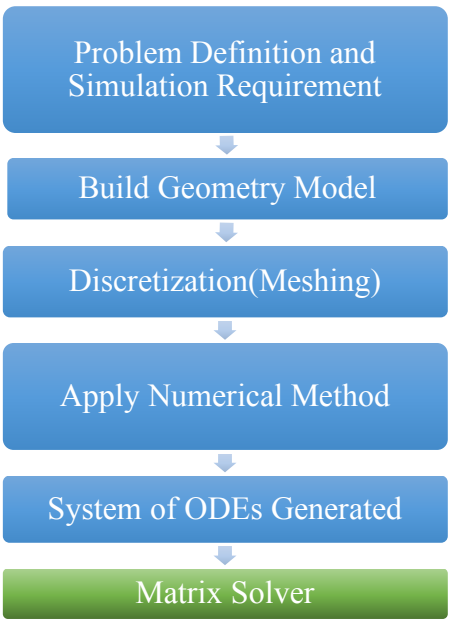

Figure 2.1 Basic EM Simulation Process

The general procedure for EM modelling is shown in the diagram. The first step is to define the EM problem, it is important because the choose of modelling

technique depends on the requirements of solution, such as output variables, simulation speed etc. The comparison of differential mesh and integral mesh is shown in Figure 2.2:

PEEC Model(Integral)	Ansys (Differential)
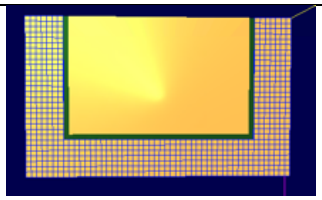	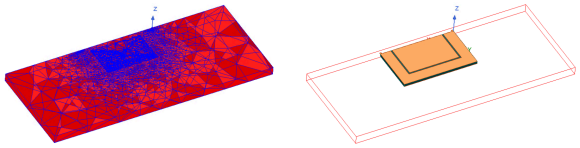

Figure 2.2 Comparison of Differential Mesh and Integral Mesh

A spatial discretization procedure is needed in EM simulation process, this involves dividing the solution domain into smaller regions and is used to allow Maxwell's partial differential equations (PDEs) to be converted into a large system of ordinary differential equations (ODEs). Different discretization methods are applied depending on which kind of EM solvers is chosen. For example, volume-cell discretization methods used in finite element method, "Yee's method" [23]used in FDTD method to discretize Maxwell's equations in space. More details about meshing process will be given later.

Refer to basic EM simulation process shown in Figure 2.1, the next step is to apply a numerical method after discretization which results in ODEs being generated in matrix form. PEEC method is one of the numerical methods which will be used in this thesis. The coefficients in the matrix can be determined by numerical methods, some numerical methods produce sparse matrices with lots of zero, some produce dense matrices with few zero. For example, FEM method described in section 2.3.1.2 produces sparse matrices because only non-zero entries at point i,j where i and j are nodes that both exist in the same mesh cell. Integral methods typically result in smaller matrices that very dense however it is much easier to solve the large, sparse matrices from differential methods efficiently.

The EM simulation can be done in time domain or frequency domain. The simulation speed is related to the mesh size and number of time steps or frequency

steps needed in simulation. MOR can be applied to increase the simulation speed which described in Chapter 3.

2.3 Introduction and Review of Numerical Methods for EM Simulation

2.3.1 The Differential Equation Methods

The differential form methods require the meshing of the entire domain in which the electromagnetic fields existed as they solve for the E and B fields directly. Everything including the surrounding air need to be meshed which means more equations and larger matrices will be generated. Differential methods are good but meshing can be very difficult, and coupling with circuits is slightly more difficult.

This kind of differential equation based methods are better when used in large system simulation because the versatility and sparsity of the observed system matrix. The common methods in the form are FDM and FEM methods.

2.3.1.1 FDM Method

Finite-difference time-domain method is a numerical analysis technique used for modelling electromagnetic problems. The differential form of Maxwell's equation is used in FDTD method. To derive the solution of field variables, the process of whole computational domain discretization is needed.

The discretization uses central-difference approximations to the whole space and time. The updated value of electric field derived from the solution of Maxwell's equation is related to the E-field stored and the H-field at the point in space. It is similar for the calculation of the components of H-fields[24].

The elements size after meshing is dependent on the frequency and model size, also need to consider the thinnest structure in the geometry model. The Yee's scheme[24] is used in FDTD method. The initial conditions, excitation and

boundary conditions of the model are needed to be identified. Selection of an appropriate time step is also important to avoid the EM wave propagation exceeding the speed of light in one time step. The meshing process with Yee's cell scheme requires the electric fields and magnetic fields are orthogonal, and will cause high storage requirement when used with complex geometries.

The Yee cell used for FDTD is shown in Figure 2.3:

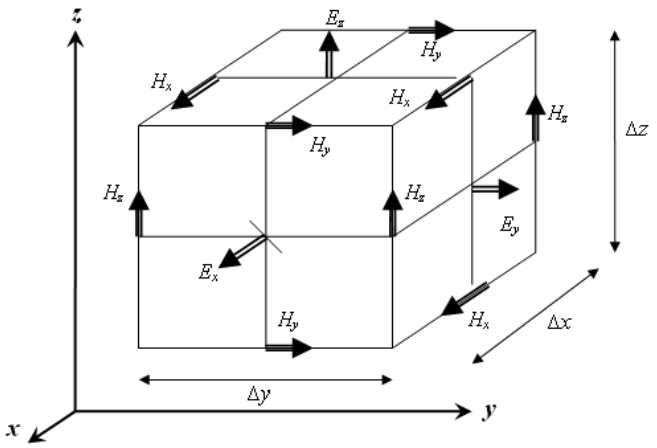

Figure 2.3 Yee cell used in FDTD technique[25]

The Yee algorithm is work as below [26]:

1. Discretize space and time to ensure E-fields and H-fields are staggered in both space and time.
2. Solve the differential equation to derive the 'update equation' which represents the future field components (unknown) related to past fields (known).
3. Evaluate the H-field one time-step into the future (now known and seen as past field).
4. Evaluate the E-field one time-step into the future (then become past field).
5. Repeat the previous two steps until obtain the whole fields.

In summary, the FDTD method can calculate the field variables, such as electric field and magnetic field.

2.3.1.2 FEM Method

FEM is another differential numerical method to solve EM field problems. FEM method can handle very complex geometry problems in a wide range of engineering area. The discretization requires discretization of the complete field space like the FDM. This method is used in both time domain and frequency domain.

FEM method discretizes a geometry structure into several elements and then connects these elements which are connected at their vertices by common nodes, or solution point. This process results in number of equations.

The procedure to obtain the results is by replacing an entire continues domain by number of sub-domains so that some unknown components can be replaced by interpolation functions with unknown coefficients. These sub-domains are the elements after discretization.

The most usual elements is shown in Figure 2.4:

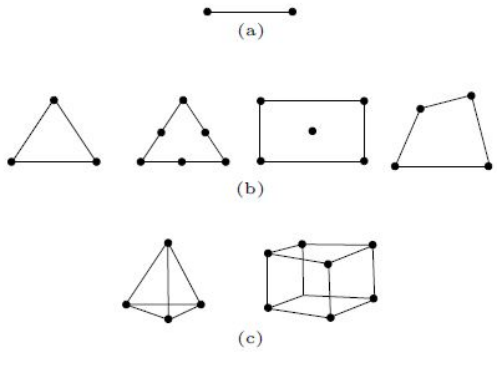

Figure 2.4 Different 1D, 2D and 3D elements[27]

The summary of process of the FEM method is:

1. Identify the analysis and element type (3D), material properties etc.
2. Discretization of geometry to obtain nodes and apply the boundary conditions.

3. Setup the equations of the system.
4. Solve the equations of the system.

The discretization of FEM method is important because it is related to the requirement of the storage, which is directly influence the computation time and the accuracy of the approximated results. The FEM is similar in characteristics to the FDM and isn't the subject of this PhD so won't be explained in detail.

2.3.2 The Integral Equation Methods

The integral equation methods only require a discretization of the source of the EM fields, that is the charge and current density. The size of the system using the integral method is smaller than using the differential form because it does not require a discretization of the surrounding environment. The main disadvantage of these methods is that they can required a lot of memory to store and to solve the resulting ODEs which results in high computational cost with the increasing problem size. PEEC method and MoM method are both common integral equation methods.

The integral equation methods are much easier to mesh because the surrounding air is not included in meshing process, and get fewer equations. The integral equation methods get coupling between almost all discrete elements, so the generated matrices are dense, which is the primary reason for increased memory requirements and computationally expensive solves.

2.3.2.1 MoM Method

The MoM method is predominantly used in frequency domain, but sometimes also used in time domain. The concept of MoM method is using a serious of known functions to represent the variables needed. The solution can be derived through a sum of basis functions, and the weighting coefficient to each basic function are made to best fit[27]. For example, to derive the wanted unknown surface current J,

it can be expanded into a series of known function, u_i ,with unknown weighting coefficient I_i. The relationship can be expressed as:

$$J = \sum_{i=1}^{n} I_i u_i \tag{2.4}$$

To derive the unknown coefficient, the problem can be transformed to linear equations in matrix form after discretization. This can be expressed as follows:

$$[Z][I] = [V] \tag{2.5}$$

Where the matrices *Z*, *I*, and *V* are the impedance ,current and voltage matrices. The unknown I_i can be derived by matrix inversion. In summary, the method is suitable for small size problem. If the system size is large, the estimated results may not accurate[28].

2.3.2.2 PEEC Method

The Partial Element Equivalent Circuit or PEEC method is commonly used for computational electromagnetics modelling in power electronic systems[29].

PEEC method is suitable for analysing the interaction and coupling of electromagnetic field but naturally describes the solution in terms of coupled circuit variables – current and voltage. This makes the method a common choice for application to the analysis of power devices in power electronics whereas many other electromagnetic solvers are used for evaluating the performance of antenna in high frequency but not often used in the area of power electronics.

PEEC is a method using integral equation form of Maxwell's equations. It is more convenient to use in a large and complex problems because the method doesn't need to model non-conducting sub-domains which simplifies meshing and reduced the size of the ODE matrices. The 3D electromagnetic model is expressed in the circuit domain as a network of partial circuit elements. Due to this circuit

formulation, other electrical components can easily be included, such as passive components, source etc.

For example, PEEC method can be applied on a PCB model, and the mesh is shown in Figure 2.5:

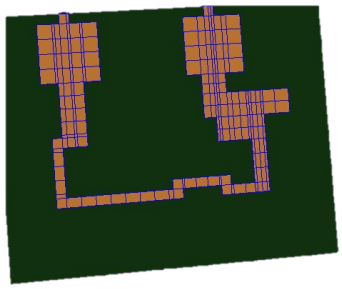

Figure 2.5 Mesh Structure

The top copper layer is meshed from the Figure 2.5, an voltage source can be added between the two ends of the copper track as a boundary condition. The blue lines show the mesh which forms a circuit of PEEC equivalent circuit components. For example, one type of the equivalent circuit model for a PEEC cell is shown in Figure 2.6:

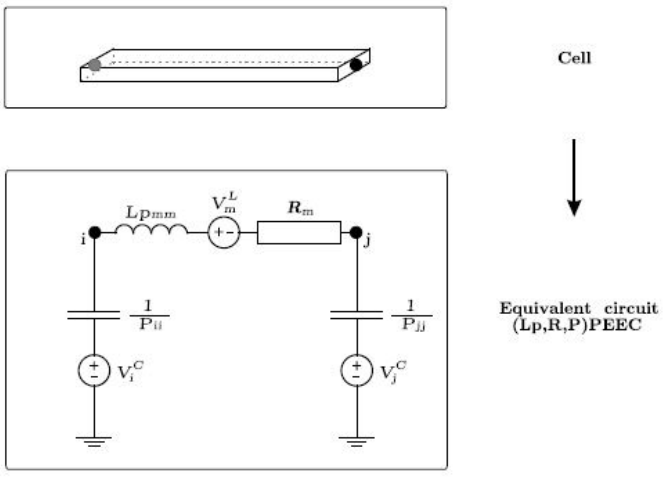

Figure 2.6 Equivalent Circuit Model for PEEC Method[27]

The equivalent circuit consist of partial inductance, partial capacitance and partial resistance. Sometimes capacitance coupling can be removed if it does not affect the accuracy, in power electronic systems capacitive effects typically become significant at high frequencies, and can be ignored at lower frequencies. For example, the parasitic capacitance will increase between two closely spaced windings or conductors at high frequencies which can affect the operation of the circuit. Removal of capacitive effects can reduce the problem size and complexity and therefore increase simulation speed.

The application areas of PEEC method include:

- Radiated electromagnetic field evaluation.
- Prediction of AC losses.
- Optimization of antenna array arrangements[30].
- Prediction of coupled noise in PCB circuit, including from radiated and conducted emissions.

Results from the PEEC method are circuit variables, post-processing is needed to obtain EM field components.

2.3.3 Comparison Between Different Methods

There are several differences of PEEC method and MoM method. Firstly, the definition of the structure used to solve is different. For differential form: The air around the geometry model needs to be discretized of cells, but for integral form: Only the materials, such as conductors, dielectric and magnetic materials need to be considered.

Secondly, the variables derived from the solutions are also different. For the differential form: The solution is predominantly the field variables, such as E or H. This kind of methods are suitable for antenna scattering, radiation and excited field structure problems[27]. Post processing is needed when the currents and voltages is required.

For the methods with integral forms, currents and voltages are directed from the solution. Post processing is usually needed when the EM fields variables are required.

Different numerical methods suitable for various application. For instance: PEEC can be used for the simulation for printed circuit board, electrical interconnect packaging, mixed circuit and EM problem. FEM method is good at the analysis for scattering problem. MoM method is good at Antenna design[31]. More details are concluded in the Table 2-1:

Table 2-1 Comparison of different EM simulation techniques[27]

Method	PEEC	MoM	FEM	FDM
Formulation	Integral	Integral	Differential	Differential
Solution Variables	Circuit	Circuit	Field	Field
Advantages	Circuit & EM Flexibility	Cell Flexibility	Cell Flexibility	Easy to Use Robust
Disadvantages	Heavy Computation	Heavy Computation	Solve Large Linear System	Large Storage Requirement

The table shows the solution variables, advantages and disadvantages of different methods. The solution variables could be either circuit variables (currents, voltages) or field variables (electric or magnetic fields). For the differential equation methods, the whole structure which including the air needs to be discretized. So differential equation methods require larger number of meshing cells. The PEEC method is suitable for EM modelling in power electronics because it naturally describes the solution in terms of coupled circuit variables.

2.4 Numerical Methods for Thermal models

The thermal management becomes important because the high operating frequency and high operating temperature in power electronics system etc. The heat equation is the basic theory to solve thermal problems.

Some methods for thermal modelling such as FEM and FDM can give the solution in time domain. These methods existed for thermal modelling can be found in [32]

The thermal modelling technique used in power electronics is proposed in [33] to generate compact thermal models. The thermal system can be represented in state space models. The thermal modelling technique has been applied on analysis of power modules in [34]. This section is for completeness but this isn't the subject of the PhD.

2.5 PEEC Methods for EM Simulation

PEEC method can obtain circuit variables directly. For example, PEEC method can be used in extraction of parasitic inductance in wiring pattern SiC half bridge module to minimize the EMI for SiC power module during the design process. The PEEC method can also be used to analyse the influence of radiation when changing geometry model[35].

However the PEEC method does have disadvantages when applied to a large and complex problem because it requires a large amount of memory to store the dense matrices and significant computational effort to solve them at each time or frequency step. For dense matrix, it will have N^2 entries, for sparse matrix it may have 7N entries. To reduce the limitation, an effective method is needed to make the simulation faster with larger problems. One method is model order reduction to reduce the simulation time. Model order reduction technique will be described in chapter 3.

PEEC method does not need air to be meshed as it implicitly accounts for the surrounding air by assuming homogenous material properties. This does however make it difficult for the PEEC method to be applied to a model including magnetic

materials. μPEEC method is proposed in [36], towards the simulation of a piece of iron and analysis the impact of eddy currents on busbar. The magnetic core can be taken into account with PEEC model for power electronics in the future. A review of EM simulation methods has been described in section 2.3, the PEEC method is suitable for power electronics application and more details of PEEC method will be illustrated in next section.

2.6 Meshing Process of PEEC Model Generation

The PEEC method is based on the integral equation form of Maxwell's equation. The first step of PEEC model generation is to generate a mesh structure to allow discretization of Maxwell's equations. The model matrix is then constructed by evaluating Maxwell's integral equations on this mesh. The last step is to get the matrix solution and post-processing maybe needed sometimes.

Meshing is a process for finite element analysis in simulation. The mesh influences the accuracy, overall efficiency and the speed in simulation. Meshing technology is an important factor in the finite element simulation software.

Geometry model will be discretized as volume cells after meshing process. For each volume cell: nodes, branch conductors and surface cells are defined based on the mesh structure.

The general process of discretization is: Meshing → Get the mesh structure → Number the nodes → Number the conductors → Number the surface panels → Number the boundaries.

2.6.1 The Placement of Nodes in 3D Geometry

The first step of PEEC modelling is to decide the node placement, one option is to set the nodes on the vertex of a volume cell after meshing and to obtain a node distribution. One example of node distribution is shown in Figure 2.7:

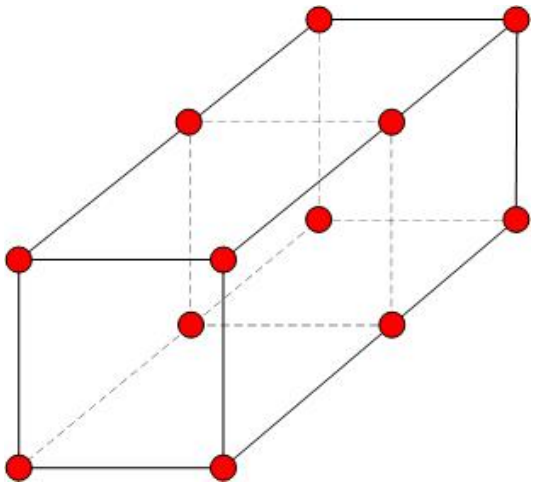

Figure 2.7 Node Distribution of a Cube

2.6.2 The Discretization Structure of Inductive Partitions

After numbering the nodes, the next step is conductor cell distribution. 3D geometry model can be discretized in 3 directions due to the currents can appear in all three directions. For example, conductor cells after discretized in z direction is shown in Figure 2.8:

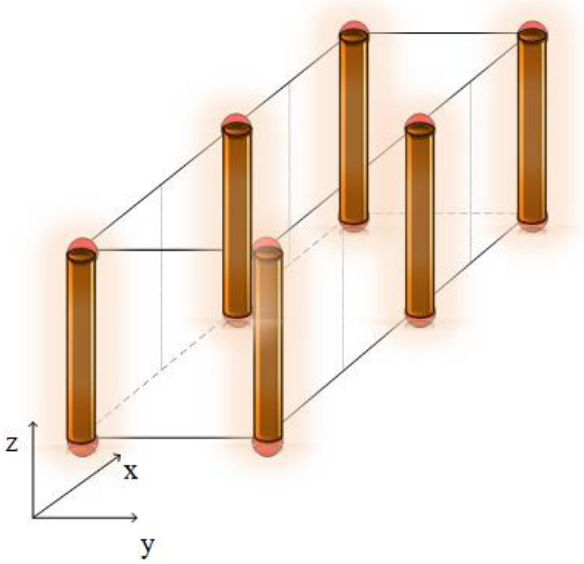

Figure 2.8 Conductor Cells in Z Direction

For inductive cell partition, a 3D geometry model needs to be divided into conductors in different directions. For each conductor cell, equivalent circuit need

to be defined. The 3D discretization of the geometry and the equivalent circuit is shown in Figure 2.9:

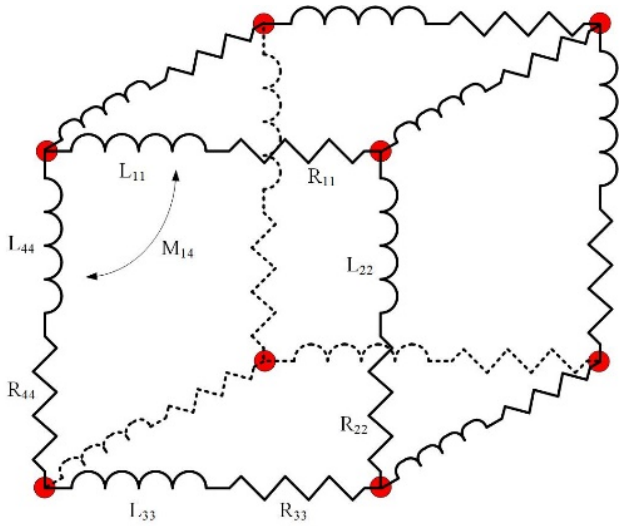

Figure 2.9 3D Discretization in the inductive Partition

Where L_{11} and R_{11} represents the self-inductance and self-resistance of conductor 1, M_{14} represents the mutual-inductance between conductor 1 and conductor 4.

2.6.3 The Discretization Structure of Capacitive Partitions

For capacitance modelling, surface cells need to be divided for partial coefficients of potential calculation. For example, discretization of surface cells is shown in Figure 2.10:

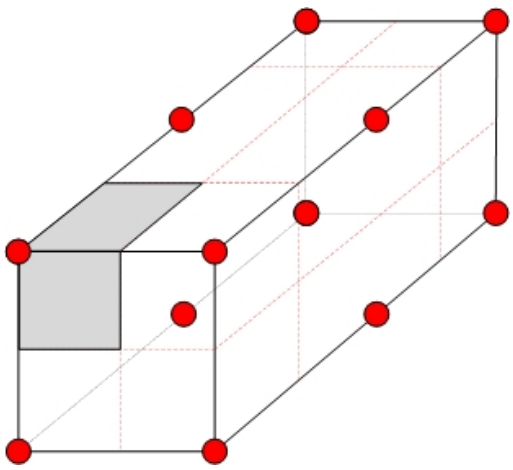

Figure 2.10 Surface Cell Discretization

For capacitive discretization, an example of 3 surface cells model and the corresponding equivalent circuit is shown in Figure 2.11:

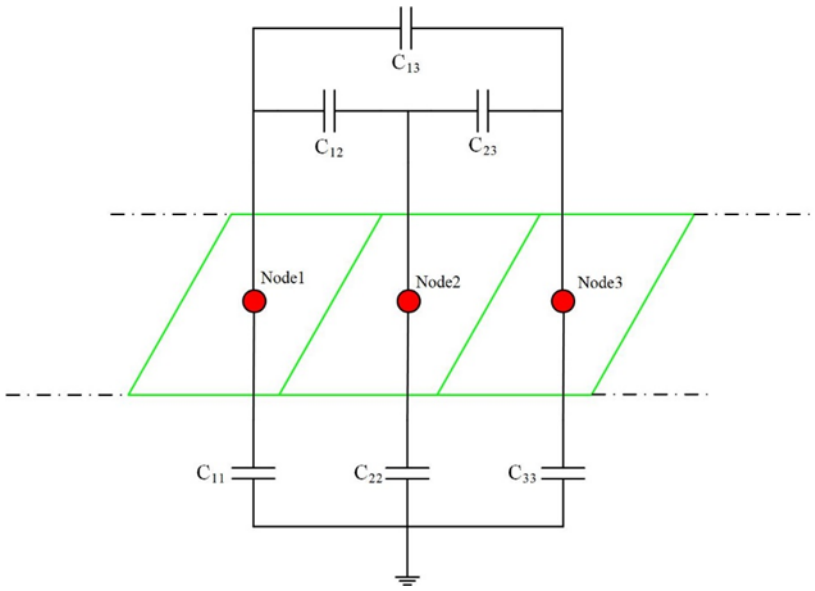

Figure 2.11 Equivalent Circuit of Capacitance PEEC Model

The geometry model is discretized and the surface panels are defined based on the meshed structure which is shown in Figure 2.10. The partial capacitance is defined between different surface cell. For each surface cell, it has self-capacitance to the ground and mutual-capacitance to another surface cell. The structure of PEEC model in matrix form has been described.

There are several issues towards meshing process. Firstly, how to decide the size of meshing cells need to be carefully considered based on the 3D geometry structure and the simulation frequency. Secondly, the meshing need to meet the requirement of accuracy, some effects such as skin-effect and dielectric loss need to be considered during meshing process.

In summary, the meshing size require even smaller cells compared to the wavelength. Non-uniform cell discretization maybe needed to reduce the number of cells and reduce the solver's simulation time. The values for each element in system matrix will be illustrated in next section.

2.7 PEEC Circuit Parameter Calculation

The previous section has shown how the PEEC method generate an equivalent circuit from the meshed geometry. The values for each *L, M, C, R* can be found by using an integral formulation of Maxwell's equation. The integral form of Maxwell's equation has shown in Equation **2**.1. Magnetic field *B* can be written as the curl of a vector field *A*, which is shown in Equation 2.6:

$$B = \nabla \times \mathrm{A} \tag{2.6}$$

This can substitute into Maxwell's Equation, and combines the electric field and the time derivative of the magnetic vector potential, then the electric scalar potential ϕ and the magnetic vector potential *A* can be defined in Equation 2.7:

$$\begin{gathered} E = -\frac{\partial A}{\partial t} - \nabla \phi \\ \mathrm{B} = \nabla \times \mathrm{A} \end{gathered} \tag{2.7}$$

The electric field *E* corresponding to the fields from all sources. The PEEC method is derived from the equation for the total electric field[27, 37]. From Ohm's law, the electric field is related to the current density. The total electric field from conducting current can be defined by Equation 2.8:

$$E = \frac{J}{\sigma} \tag{2.8}$$

The scattered field E can be rewritten after considering external incident field E^i and integrating Equation2.8, The equation of electric field becomes Equation 2.9:

$$E^i(r,t) = \frac{J(r,t)}{\sigma} - \frac{\partial A(r,t)}{\partial t} - \nabla \phi(\mathrm{r},\mathrm{t}) \tag{2.9}$$

Where *r* is the observation point, *A* is the magnetic vector and ϕ is the electric potential.

The solutions to scalar potential and vector potential is given by Equation 2.10:

$$A(r,t) = \frac{\mu}{4\pi}\int_{V'}\frac{J(r',t')}{|r-r'|}dV'$$
$$\phi(r,t) = \frac{1}{4\pi\epsilon}\int_{S'}\frac{q(r',t')}{|r-r'|}dS' \tag{2.10}$$

The free space Green function is used to calculate the electromagnetic potentials at the observation point *r*. The static Green's function in free-space is shown in Equation 2.11:

$$G(\boldsymbol{r},t) = \frac{1}{4\pi}\frac{1}{|\boldsymbol{r}-\boldsymbol{r}'|} \tag{2.11}$$

The EFIE (Electric Field Integral Equation) can be rewritten based on Equation 2.10 and Equation 2.11 into Equation 2.9. The electric field integral equation can be defined in Equation 2.12:

$$\begin{aligned} n\times E^i(r,t) = n\times&\left[\frac{J(r,t)}{\sigma}\right] \\ &+ n\times\left[\sum_{k=1}^{K}\mu\int_{vk}G(r,r')\frac{\partial J(r',t_d)}{\partial t}dv_k\right] \\ &+n\times[\sum_{k=1}^{K}\frac{\nabla}{\varepsilon_0}\int_{vk}G(r,r')q(r',t_d)\,dv_k] \end{aligned} \tag{2.12}$$

The EFIE describes the electric field contributions from all sources. The left hand side is the externally applied field. The first right hand side term corresponds to the components due to current flow through a local resistance, the second term corresponding to the component due to the rate of change of current density, and the third term corresponds to the component due to resistance, inductance and capacitance respectively. All these three terms are linked to the mesh structures. For example, the partial inductance is calculated on branch conductor cells from

mesh structure. The calculation of partial element is based on Equation 2.12, The details of each term in the equation are described in later sections.

2.7.1 Resistive Equivalent Circuits

The partial resistance is calculated use the Equation 2.13:

$$R = \frac{l}{a \cdot \sigma} \tag{2.13}$$

Where l is the length of the volume cell, a means the cross section of the volume cell. σ means the electrical conductivity. When add the resistance value to the matrix A, need to multiply by -1.

2.7.2 Inductive Equivalent Circuits

The calculation of partial inductance can be derived from the second term of Equation 2.12, the partial inductance is defined by Equation 2.14:

$$Lp_{\alpha\beta} = \frac{\mu}{4\pi}\frac{1}{a_\alpha a_\beta}\int_{v\alpha}\int_{v\beta}\frac{1}{|r_\alpha - r_\beta|}dv_\alpha dv_\beta \tag{2.14}$$

r_α, r_β are the positions in conductor cell α and β. The a_α, a_β are the cross-sectional areas of conductor cell α and β. The mesh structure of conductor cell definition is show in Figure 2.8, For inductance part, the inductance matrix is symmetrical, so only need to calculate the upper triangle element, because $L_{ij} = L_{ji}$.

2.7.3 Capacitive Equivalent Circuits

2.7.3.1 Calculation for Coefficient of Potential

If capacitive effects are of interest, the coefficients of potential P, need to be calculated to build the system matrix. The P coefficients relate charge on one

surface panel, to potential at a specific point in the model and can be thought of as the inverse of capacitance. The relationship between the charge and potential is shown in Equation 2.15:

$$\begin{aligned} C_s \cdot \Phi &= \mathrm{Q} \\ \mathrm{P} \cdot \mathrm{Q} &= \Phi \end{aligned} \tag{2.15}$$

The partial coefficient of potential can be derived based on the third term of Equation 2.12, the partial coefficient of potential between surface cell *i* and surface cell *j* can be calculated by Equation 2.16:

$$P_{ij} = \frac{1}{S_i S_j} \frac{1}{4\pi\varepsilon_0} \int_{S_i} \int_{S_j} \frac{1}{|r_i - r_j|} dS_j dS_i \tag{2.16}$$

The P coefficient is the inverse of capacitance. To obtain the nodal capacitances, additional calculations are needed.

2.7.3.2 P Matrix Generation

Voltage is always defined relative to a reference. Self-capacitance is connected to ground. The voltage on one conductor is in terms of the total change including the effect of self-coefficient and mutual-coefficient corresponding to the conductor. The relation between them is shown in Equation 2.17:

$$\begin{aligned} v_1 &= P_{11}q_1 + P_{12}q_2 + P_{13}q_3 + \cdots \\ v_2 &= P_{21}q_1 + P_{22}q_2 + P_{23}q_3 + \cdots \\ &\vdots \end{aligned} \tag{2.17}$$

The structure of matrix *P* is shown in Equation 2.18:

$$\begin{bmatrix} P_{11} & \cdots & P_{1n} \\ \vdots & \ddots & \vdots \\ P_{n1} & \cdots & P_{nn} \end{bmatrix} \tag{2.18}$$

Where the partial coefficient of potential P represents the self and mutual coefficient of potential. The P matrix can be calculated directly by evaluating individual coefficients using Equation 2.16. The P matrix relates voltage to charge, and the relationship is shown in Equation 2.19:

$$v = [P]q \qquad (2.19)$$
$$q = [P]^{-1}v$$

In the PEEC formulation, the partial coefficient of potential need to be transferred to equivalent capacitance in the circuit formulation, and the circuit equation can be expressed in Equation2.20:

$$I = [P]^{-1}\frac{dv}{dt} = [C]\frac{dv}{dt} \qquad (2.20)$$

In summary, the P matrix must be explicitly or implicitly inverted before it can be included in the PEEC model.

2.7.3.3 Short Circuit Capacitance Matrix Generation (Invert P)

In matrix form, the relationship between the voltage and coefficient P can be written as $v = Pq$. Short circuit matrix can be derived by invert the matrix P, the relationship between P matrix and short circuit capacitance matrix is shown in Equation 2.21:

$$C_s = P^{-1} \qquad (2.21)$$

Where ${P_{ij}}^{-1}$ is a capacitance, but the voltage used to calculate the potential coefficient is relative to a common reference, the capacitance derived is short circuit capacitance.

The short circuit capacitance matrix is shown in Equation 2.22:

$$C_s = \begin{bmatrix} Cs_{11} & \cdots & Cs_{1n} \\ \vdots & \ddots & \vdots \\ Cs_{n1} & \cdots & Cs_{nn} \end{bmatrix} \tag{2.22}$$

The C_s matrix is symmetrical. i.e $Cs_{ij} = Cs_{ji}$. The matrix C_s corresponding to the submatrix C in the system matrix M of PEEC model. The drawbacks of this approach are that the P matrix need to be explicitly inverted which is slow.

2.7.3.4 Capacitance Matrix Transformation

The potential used to calculate the short circuit capacitances is defined to connect to a common node representing infinity, but the issue is that capacitances connected between two surface panels is given by Equation 2.23:

$$C_{ij} = \frac{Q_{ij}}{(\phi_i - \phi_j)}, i \neq j \tag{2.23}$$

Because the voltage across the mutual capacitor is $V = \phi_i - \phi_j$, for example: in a two surfaces panel model, the total charge on the surface panel 1 is given by Equation 2.24:

$$Q_1 = Q_{11} + Q_{12} = (Cs_{11} + Cs_{12})\phi_1 - Cs_{12}\phi_2 \tag{2.24}$$

So the circuit capacitance matrix are derived using short circuit matrix but need some modifications shown below:

- The diagonal element is obtained by the sum of each row element in the short circuit matrix.
- The off diagonal element need to multiply by minus 1.

In summary, the relationship between short circuit capacitance matrix and circuit capacitance matrix is shown in Equation 2.25:

$$C_{ii} = Cs_{i1} + Cs_{i2} + Cs_{i3} + \cdots \tag{2.25}$$

$$C_{ij} = -Cs_{ij}$$

The capacitance matrix is shown in Equation 2.26:

$$C=\begin{bmatrix} Cs_{11}+\cdots+Cs_{1n} & -Cs_{12} & \cdots & -Cs_{1n} \\ -Cs_{21} & Cs_{21}+\cdots+Cs_{2n} & \cdots & -Cs_{2n} \\ \vdots & \vdots & \ddots & \vdots \\ -Cs_{n1} & -Cs_{n2} & \cdots & Cs_{n1}+\cdots+Cs_{nn} \end{bmatrix} \quad (2.26)$$

2.8 MNA Analysis

The equivalent circuit system equations are illustrated through the Kirchoff's current law and Kirchoff's voltage law. More specifically, MNA[38, 39] analysis can generate three parts of circuit equations: KCL node equation; KVL branch equation; Boundary equation.

2.8.1 Node Equation Generation

The relationship of currents flow into and out of a node can be represented in Equation 2.27:

$$\sum_{j=1}^{n} I_j = 0 \quad (2.27)$$

The basic idea is to find the branch currents flowing into or away from each node. The branch currents flowing into a node must sum to zero. The KCL equation can be written for each node.

The definition of the current direction is that the current flows from the positive node to the negative node. If the node connected to the positive end of the conductor, the sign of current is -1; If the node connected to the negative end of the conductor, the sign of current is +1. In summary, the branch currents are written as a function of node voltages.

More specifically, a diagram of the current flow through a node can be shown in Figure 2.12:

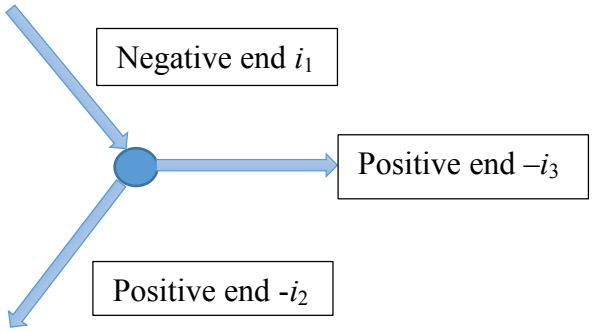

Figure 2.12 KCL Node Equation diagram

From the diagram, it can be shown the KCL equation of the node is shown below:

$$i_1 - i_2 - i_3 = 0 \tag{2.28}$$

If the capacitive effect is enabled, the current through the capacitance will be added, so capacitance terms need to be added into the node equation. Populating the C sub matrix derived in section 2.7.3.4 to the system matrix *M*, because it is part of the *M* matrix.

2.8.2 Branch Equation Generation

The branch equation is based on Kirchhoff's voltage law. For each branch in meshing structure, the potential differences between the positive node and negative node in the branch can be represented by the voltage drop through partial resistance and partial inductance.

The corresponding circuit of a branch equivalent circuit is shown in Figure 2.13:

Figure 2.13 Branch Equivalent Circuit

The corresponding KVL equation of the branch with one partial resistor and one partial inductor is shown in Equation 2.29:

$$L_b \frac{dI_b}{dt} = -RI_b + (V_p - V_n) \tag{2.29}$$

For the sign of the KVL equation, it is 1 for positive node and -1 for negative node.

2.8.3 Boundary Contributions

Electric boundary terms also contribute to the equation. Excitation will be added to the model as boundary condition. The PEEC model of the geometry must be coupled at certain terminals with other circuit components. For example, a voltage source can be added between two defined terminals of the geometry model as an excitation.

At each terminal, there will be two coupled variables: voltage and current. The voltage and current will cross the defined boundary and enter the PEEC model. Both the voltage and current should be consistent and shared between the PEEC model and coupled circuits.

Either voltage or current will be defined as an input of the PEEC model linked via the input. the other variable will be defined as an output. The matrix structure will be illustrated in next section.

Both voltage and current can be defined as boundary condition, but voltage input source has advantages because the model is guaranteed to have a standalone steady-state solution. However, there is no absolute potential reference with current input

source until the PEEC model is coupled with other equations that provide this reference, this is an important consideration for MOR methods where the equations are solved before coupling.

One thing need to be note is that boundary is connected to an area of the geometry model, boundary current is shared with node area, so need to calculate the index of the proportion of boundary current that overlaps node.

2.9 Matrix Structure of the PEEC model

After the capacitive and inductive discretization, the partial elements values including partial capacitance, partial inductance and partial resistance are calculated to build a PEEC model based on the modified nodal analysis (MNA) formulation of the equivalent circuit model. The matrix structure of the PEEC model of a 3D geometry model is given by Equation **2**.30:

$$\begin{aligned} M\dot{x} &= Ax + Bu \\ y &= Cx \end{aligned} \tag{2.30}$$

Where the state vector x represents the unknown node voltages and inductive branch currents; u and y are the input voltage source and output currents respectively, and:

$$\begin{aligned} M &= \begin{bmatrix} C & 0 \\ 0 & L \end{bmatrix} \\ A &= \begin{bmatrix} 0 & D \\ -D^T & -R \end{bmatrix} \end{aligned} \tag{2.31}$$

The dimensions of A and M are n×n, where n is the total number of unknowns (number of branch currents + number of node voltages). Within the A matrix, the D submatrix describes the interconnectivity of the circuit nodes and branches and the R submatrix is a diagonal matrix of conductor resistances, A is therefore a sparse matrix. For the inductance part of system matrix, only need to calculate the upper triangle element because the inductance matrix is symmetrical. The L and C

submatrices contain inductive and capacitive coupling coefficients and are extremely dense.

2.9.1 Output Matrix Generation

In order to plot current density, matrix *O* needs to be defined to represent the relationship between current density distribution at each mesh node in x, y, z direction and branch current of corresponding connected conductors to this node.

The structure of the O matrix is shown in Equation 2.32:

$$\begin{bmatrix} V_1 \\ \vdots \\ V_n \\ J_{1x} \\ J_{1y} \\ J_{1z} \\ \vdots \\ J_{nx} \\ J_{ny} \\ J_{nz} \end{bmatrix} = \begin{bmatrix} 1 & \cdots & 0 & 0 & \cdots & 0 \\ \vdots & \ddots & \vdots & \vdots & \ddots & \vdots \\ 0 & \cdots & 1 & 0 & \cdots & 0 \\ 0 & \cdots & 0 & \frac{W_{1x}}{Csa_x} & \cdots & \cdots \\ \vdots & \vdots & \vdots & \frac{W_{1y}}{Csa_y} & \ddots & \vdots \\ \vdots & \vdots & \vdots & \frac{W_{1z}}{Csa_z} & \cdots & \cdots \\ \vdots & \vdots & \vdots & \vdots & \cdots & \vdots \\ \vdots & \vdots & \vdots & \cdots & \cdots & \cdots \\ \vdots & \vdots & \vdots & \vdots & \ddots & \vdots \\ 0 & \cdots & 0 & \cdots & \cdots & \cdots \end{bmatrix} \begin{bmatrix} V_1 \\ \vdots \\ V_n \\ I_1 \\ \vdots \\ I_m \end{bmatrix} \tag{2.32}$$

Where the element in *O* matrix is determined in terms of how many conductor cells are connected to each node. W_{1x} means the x components of the conductor 1 which is connected to the node 1. The Csa_x means total current carrying area in *x* direction.

In summary, the number of state vector = the number of nodes + the number of conductor + the number of boundary.

2.10 Evaluation of PEEC Method on Example

The PEEC model generation has been described in previous section, two examples will now be used to validate the accuracy of partial element calculation. There are

three parts of the evaluation, they are partial inductance calculation, partial capacitance calculation and current density distribution.

2.10.1 Evaluation of Partial Inductance Calculation

2.10.1.1 Test case model for partial inductance calculation

An experimental test PCB board is selected to validate the partial inductance extraction using PEEC method. The PEEC code is on the development which is implemented in custom design tool software, VPPE. The PCB board is shown in Figure 2.14:

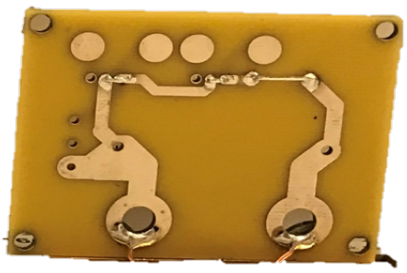

Figure 2.14 Test Case Model of Partial Inductance

The test case is a piece of PCB board, the dimension of this PCB board is 67mm× 53mm. the thickness of the copper track is 0.07mm. the dielectric material is FR4 and the thickness is 1.8mm. The material of ground plane is copper and the thickness is 0.1mm.

2.10.1.2 Simulation Results in VPPE

The PCB board model built in VPPE is shown in Figure 2.15:

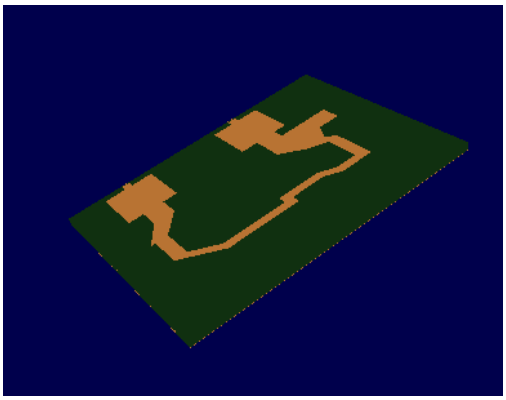

Figure 2.15 PCB Model in VPPE

The model is excited by coupled additional circuit components to the PEEC model, if an ideal current source is added between two terminals of the PEEC model then the resulting voltage across this source represents the terminal impedance. The meshing process generates 1050 capacitive nodes, and 2751 current carrying conductors, which results in 3804 equivalent circuit equations for the system. In this case, the inductance dominates the PCB track impedance. Experimental tests of the PCB board using ENA Analyzer and Impedance Analyzer are given as reference. The comparison of the terminal impedance between experimental result and simulation result is shown in Figure 2.16:

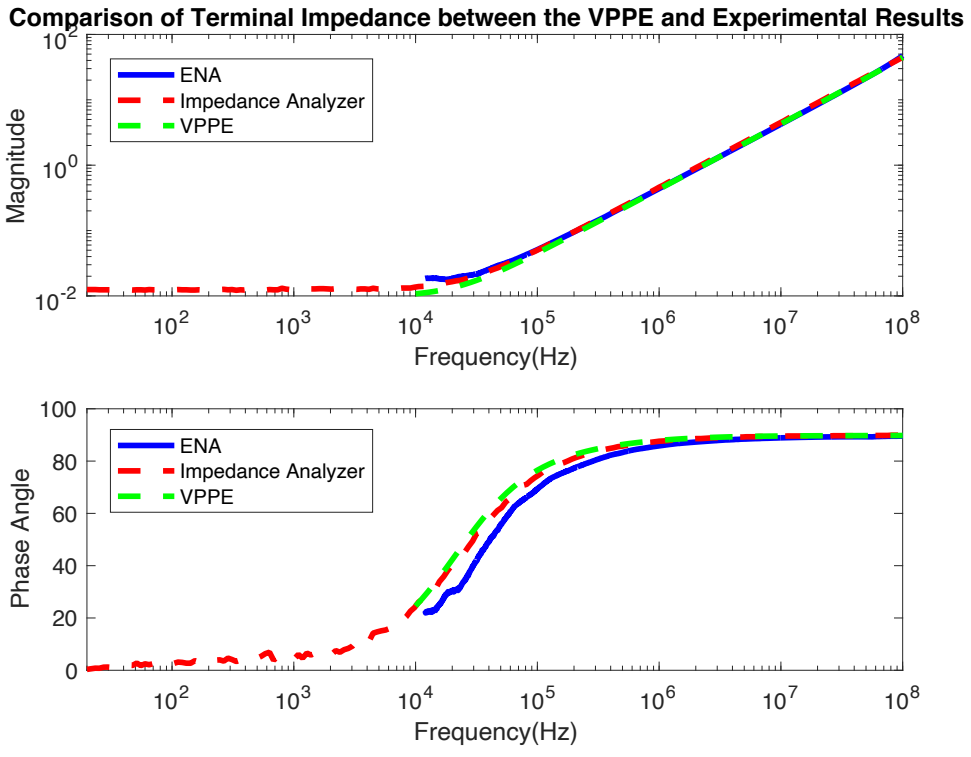

Figure 2.16 Comparison of Terminal Impedance between the VPPE and Experimental Results

The parasitic inductance can be extracted from the terminal impedance through post processing. A comparison of the inductance value between simulation and experimental results is shown in Figure 2.17:

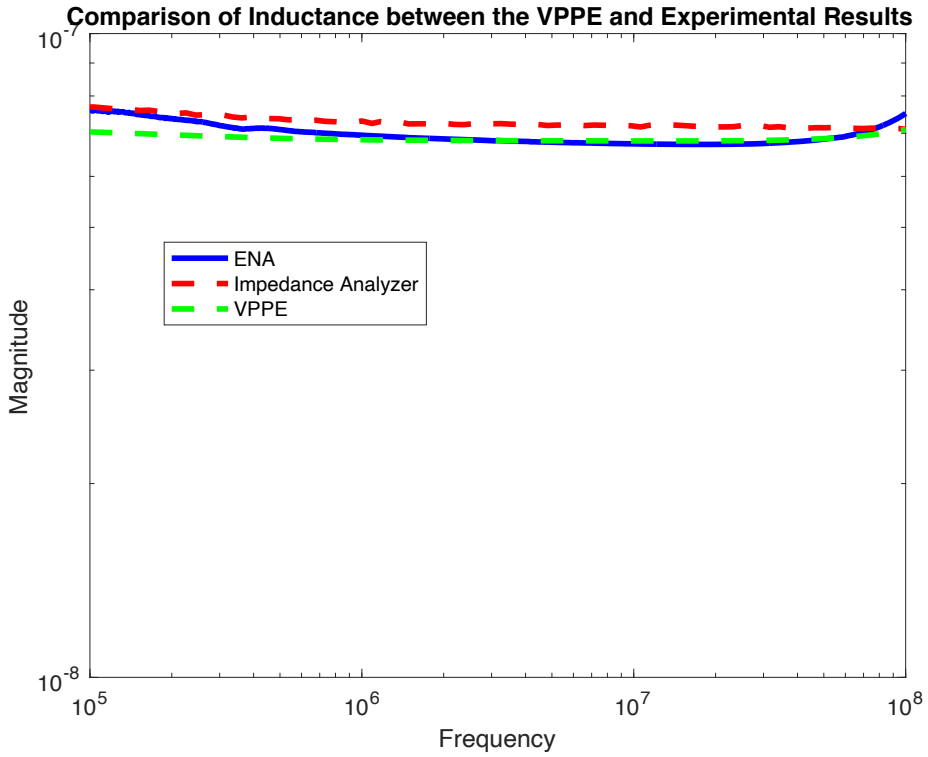

Figure 2.17 Comparison of Inductance between the VPPE and Experimental Results

The parasitic inductance of the copper track in the PCB is around 682 μH. It is clear that the PEEC simulation results accurately match measurements made using both a low frequency impedance analyser and high frequency network analyser.

The error between the simulation results and experimental results are shown in Figure 2.18:

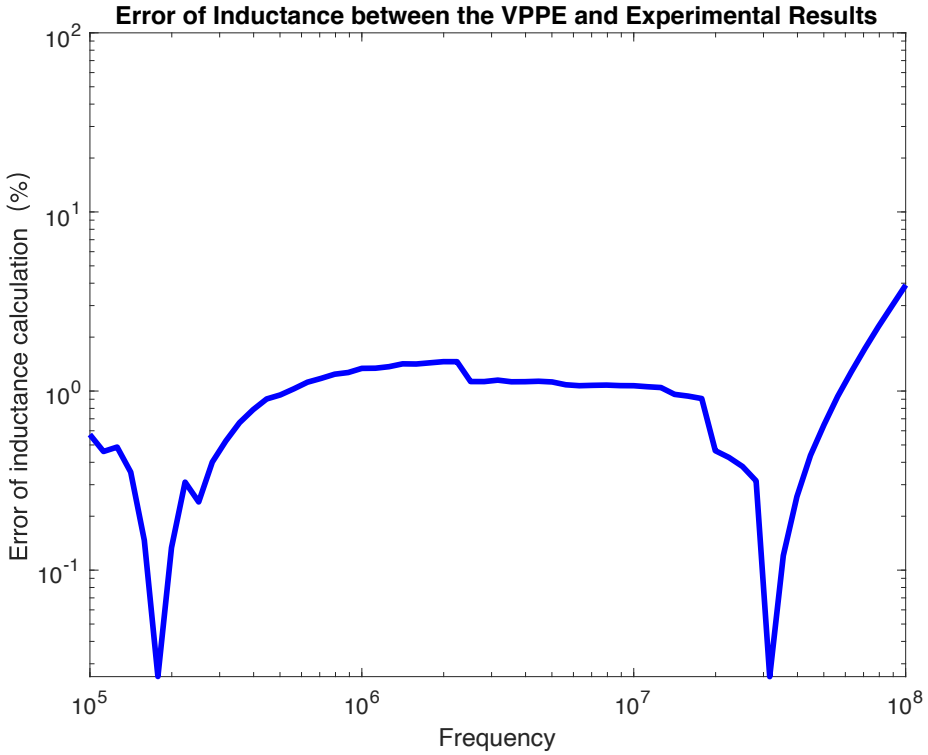

Figure 2.18 Error of Inductance between the VPPE and Experimental Results

The same model is also simulated in Ansys HFSS. The model built in HFSS is shown in Figure 2.19:

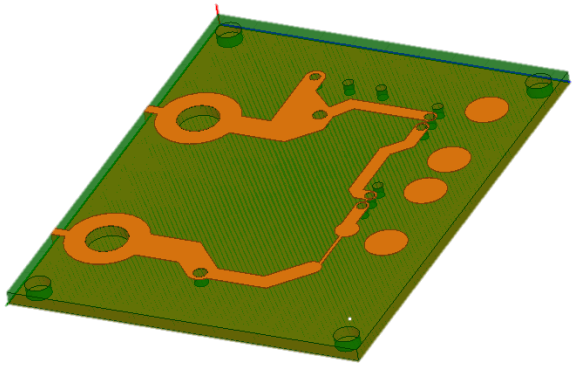

Figure 2.19 Test Case Model in HFSS

The shape of the model in HFSS model is a bit different from the VPPE model. This is because circles cannot be drawn in VPPE. The circles are approximated by rectangles.

The comparison of simulation results in HFSS and Experimental results is shown in Figure 2.20:

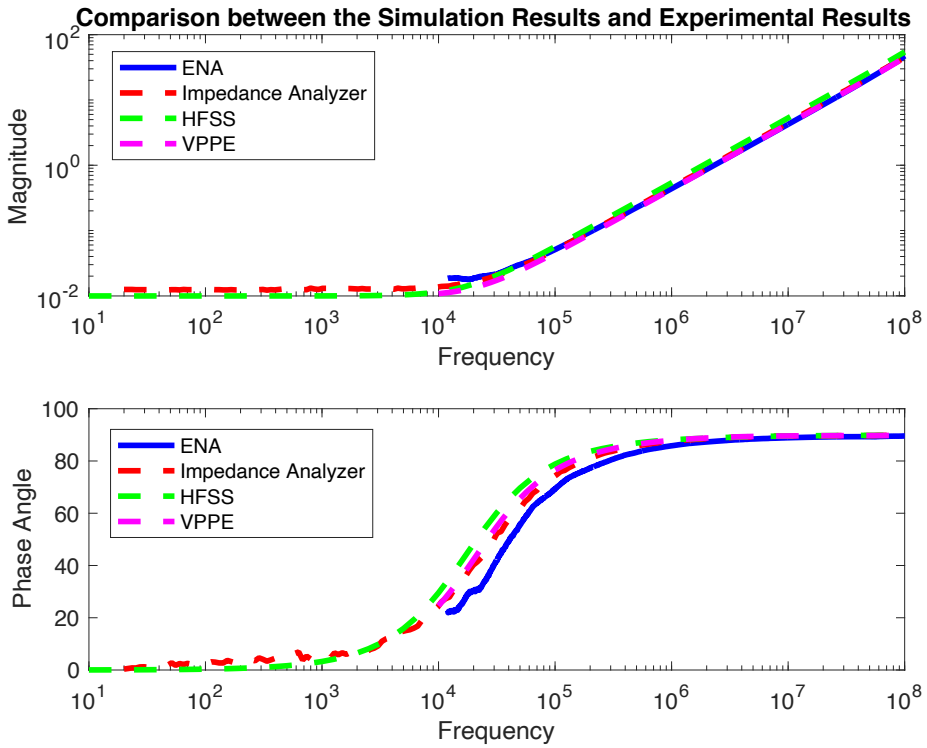

Figure 2.20 Comparison between experimental results and HFSS results

And the simulation time of HFSS is 255s and the simulation time of VPPE is 137s. The Z parameter extracted from HFSS matched the experimental results. In other words, it means the PEEC method can extracted the parasitic inductance accurately.

2.10.2 Evaluation of Partial Capacitance Calculation

2.10.2.1 Test Case Model for Partial Capacitance Calculation

In this section, an example will be given to evaluate the capacitance calculation using PEEC method. An example of a PCB board from another project is given in Figure 2.21:

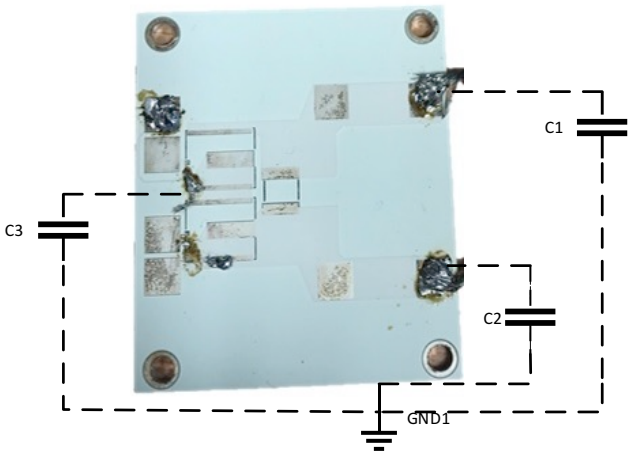

Figure 2.21 Test Case Model for Capacitance Calculation Evaluation

The equivalent circuit of the model is shown in Figure 2.22:

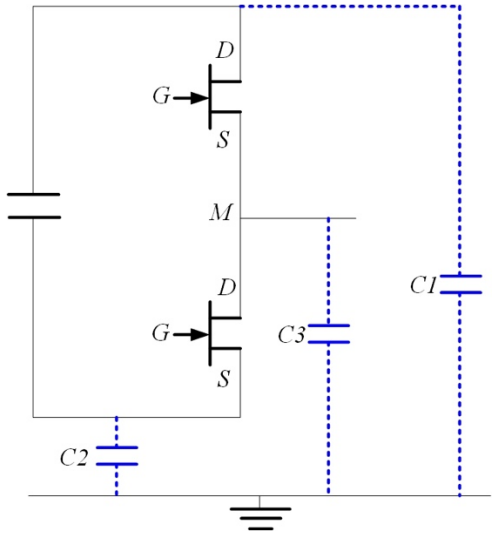

Figure 2.22 Equivalent Circuit of the Substrate Model

This is a GaN half bridge circuit in IMS substrate. There are three main parasitic capacitances in the circuit due to the capacitive coupling as shown in Figure 2.22. The same model is built in VPPE which is shown in Figure 2.23:

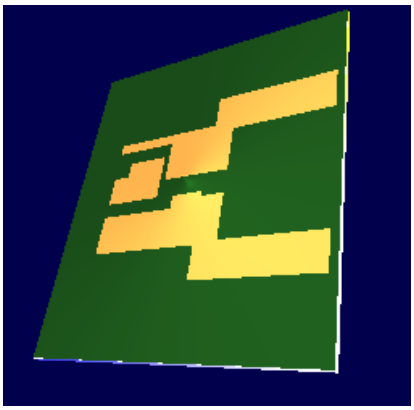

Figure 2.23 Test Case Model in VPPE for Capacitance Calculation Evaluation

An excitation can be added between the copper track and ground plane as electrical boundary condition. For example, the impedance curve of one of the terminal from PEEC model is shown in Figure 2.24:

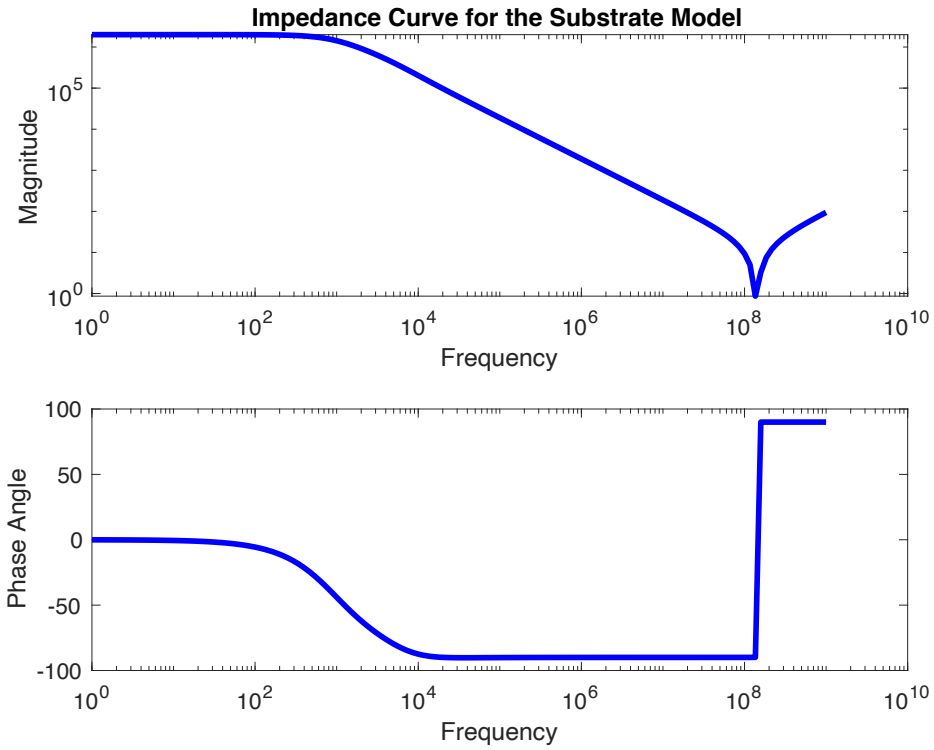

Figure 2.24 Impedance Curve of the Substrate PEEC Model

The parasitic capacitance *C1* can be extracted through the impedance curve in Figure 2.24. *C2* and *C3* can be extracted using the same method. So the parasitic

capacitance can be extracted by Z parameter obtained from VPPE. The theoretical value of each parasitic capacitance can be estimated through Equation 2.33:

$$C = \frac{\varepsilon A}{d} \tag{2.33}$$

Where ε is the permittivity of the dielectric, A is the area of plate overlap and d is the distance between the plates. The comparison of capacitance value between simulation results and theoretical value is shown in Table 2-2:

Table 2-2 Evaluation of Capacitance Calculation in VPPE

	C1(pF)	C2(pF)	C3(pF)
Theoretical Value	92.9	118	35.8
Simulation Value(PEEC)	84	112	34
Ansys Value	87	113	35
Accuracy of PEEC (%)	9.6%	5%	5%
Accuracy of Ansys (%)	6.4%	4.2%	2,2%

The simulation results shown the accuracy of parasitic capacitance calculation of PEEC method. The accuracy of PEEC method are 9.6%, 5%, and 5% for C1, C2, and C3 respectively.

2.10.3 Evaluation on Current Density Distribution

There are some concerns about high current density operation, because it may cause in higher temperature due to increased heat generation. So the current density distribution is important for thermal management. PEEC method can be used to predict current density and the details has been described in section 2.9.1, The same example used for capacitance calculation evaluation will be used to evaluate

current density as well. The comparison of the simulation results in VPPE and Ansys HFSS is shown in Figure 2.25:

Frequency	VPPE	HFSS
1KHz	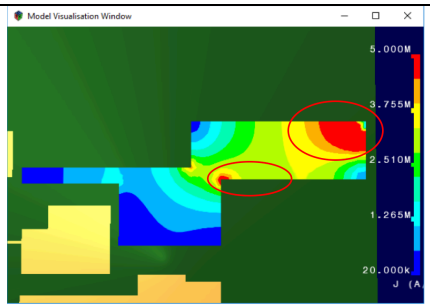	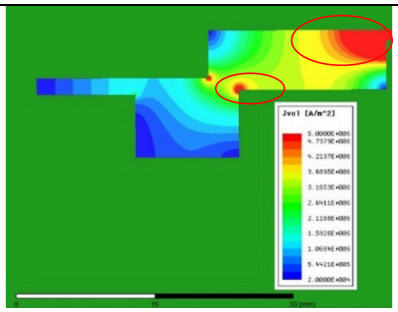
1MHz	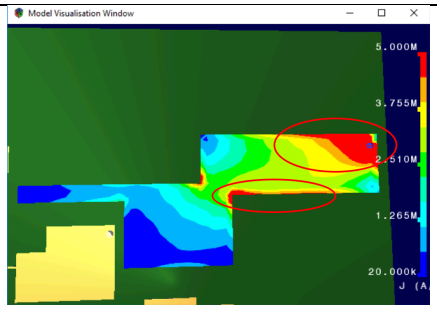	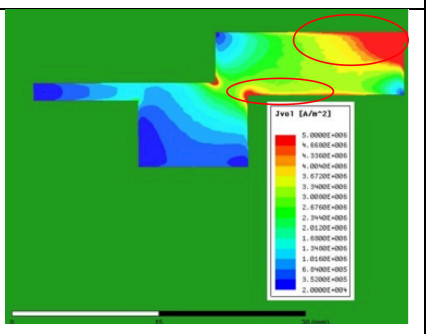

Figure 2.25 Simulation Results of Current Density in VPPE and HFSS

The current density is plot at 1KHz and 1MHz. The first column is the results from PEEC method and the second column is the results from Ansys software. The current density is higher around the top right of this copper track, which is shown in red colour. When the frequency increases to 1MHz, the current density distribution in the top right area starts to change and towards the edge of the copper track. It is clear that the PEEC simulation results accurately match the HFSS results on current density prediction.

2.11 PEEC Method for Magnetic Material

Magnetic components are included in some power electronic applications. Such as the core materials of the converter circuit, the new ferrite materials operating at megahertz frequencies etc. [40] Skin effects and core losses in magnetic components becomes an issue at high frequencies [41], The PEEC models can

include magnetic materials for problem solving with magnetic components for power electronics.

2.11.1 PEEC Model with Magnetic Materials

Magnetic materials problems are applied in power electronics, transformers or motors[42, 43], so it is important to enable the magnetic materials modeling at the design stage of power electronics system. The PEEC method is based on the expression of electric field integral equation (EFIE) in free space.

The usual integral equation used in quasi-static PEEC model is shown in Equation 2.34:

$$\boldsymbol{E}^i(\boldsymbol{r}, s) = \boldsymbol{E}^T(\boldsymbol{r}, s) + s\boldsymbol{A}(\boldsymbol{r}, s) + \nabla\emptyset(\boldsymbol{r}, \mathrm{s}) \tag{2.34}$$

Where: $\boldsymbol{E}^T(\boldsymbol{r}, s) = \frac{\boldsymbol{J}(\boldsymbol{r},s)}{\sigma}$

The s is the Laplace variable. The PEEC method is start with expression of electric field. $\boldsymbol{E}^i(\boldsymbol{r}, s)$ represents the external electric field corresponding to the external sources. $\boldsymbol{E}^T(\boldsymbol{r}, s)$ can be expressed by the current density in a conductor. The first term is corresponding to the partial resistance in conductors.

The second term of Equation 2.34 corresponding to the inductance part, which represents the magnetic coupling between conductors in air. If no magnetic materials medium is considered, the partial inductance can be derived.

The third term of Equation 2.34 corresponding to the capacitance part and can be represents by the gradient of potential $\emptyset$. The potential is related to charges and turn into capacitive elements in PEEC model.

When the effect of magnetic materials are considered, an additional term will need to be added to the EFIE equation. So the equation is shown in 2.35:

$$\boldsymbol{E}^i(\boldsymbol{r},s) = \boldsymbol{E}^T(\boldsymbol{r},s) + s\boldsymbol{A}(\boldsymbol{r},s) + s\boldsymbol{A}_m(\boldsymbol{r},s) + \nabla\emptyset(\boldsymbol{r},\mathrm{s}) \tag{2.35}$$

In the Equation 2.35, the added term $\boldsymbol{A}_m(\boldsymbol{r},s)$ corresponding to the partial inductance on magnetic conductor. The magnetic inductance is the additional term which is needed to be included in the MNA formulation process. After including inductive magnetic coupling, the system matrix will be changed to a new structure. For example, the normal system matrix of PEEC model is shown in Equation 2.36:

$$\begin{aligned} M &= \begin{bmatrix} C & 0 \\ 0 & L \end{bmatrix} \\ A &= \begin{bmatrix} 0 & D \\ -D^T & -R \end{bmatrix} \end{aligned} \tag{2.36}$$

The system matrix of PEEC model with magnetic materials can be shown in Equation 2.37:

$$\begin{aligned} M_M &= \begin{bmatrix} C & & \\ & L & L_M \\ & & \end{bmatrix} \\ A_M &= \begin{bmatrix} & D & \\ -D^T & -R & \\ & -\beta_c & \alpha - \beta_m \end{bmatrix} \end{aligned} \tag{2.37}$$

There are new parameters in the matrix. The discretization of magnetic material will generate volume cells. The magnetic inductance is related to magnetization cells, the submatrix L_M represents the magnetic inductance. The method to calculate these new parameters are proposed in [37].

The PEEC model for magnetic materials is useful when components with magnetic materials are needed. It could be developed in the design tool and used for power electronics design in the future.

The PEEC modelling for magnetic materials is another research direction and not related to this PhD's work, so it will not be discussed in this thesis.

2.12 Summary

Introduction of EM modelling process and different numerical methods are illustrated in this chapter. PEEC method is applied when doing electromagnetic modelling. The process to generate PEEC model is described step by step, including meshing process and circuit parameter calculation and matrix model generation.

The evaluation of the PEEC method is done with some example case. It can be seen from the simulation results and analysis on capacitance calculation, inductance calculation and current density plot that the PEEC method works for EM modelling.

Chapter 3

3 Reduced Order Modelling Techniques

3.1 Introduction

It has been shown that the PEEC method is suitable for electromagnetic modelling of power electronic systems but the challenge is to improve speed when PEEC method is used to solve a large size problem. Simulation time is specifically a problem for time-domain simulation with many time steps such as found in power electronics. One of the advantages of MOR is the simulation speed because it does not need to perform this large system solve at each step, another advantage is the storage, because it does not need to store a large solution at each step. Model Order Reduction (MOR) has been developed in the simulation of large scale models in mathematical and engineering area.

The matrix model can be generated through PEEC method. Modified Nodal Analysis (MNA) can be used to generate circuit equations. The process of MNA analysis has been described in chapter 2. The matrix equation from PEEC model is shown in Equation 3.1:

$$M\dot{x} = Ax + Bu \tag{3.1}$$

$$y = Cx$$

Where *M* matrix represents the contributions of the partial capacitance and partial inductance. The matrix *A* represents the resistances.

In general, a large system of ordinary differential equations will be generated by the PEEC method, and it needs a long computation time to solve. The system matrix *M*, *A*, *B*, *C* generated from PEEC model can be replaced by surrogate matrices which will significantly reduce the matrix dimension. MOR technique is used to reduce the dimension of the system matrix which makes the equations easier to solve. The input signal ***u*** and output signal ***y*** are unaffected, so the result is the same when applying MOR technique.

With development of the MOR technique, the MOR can also be used for optimization in the electromagnetic design for power electronics. MOR can highly reduce the simulation time with reasonable error.

The models for power electronics systems become larger and more complicated when physical structures are getting more complicated. There is demand for more details and accuracy at the design stage. It is very important to reduce the simulation time, so MOR technique can be used to reduce the size of the original model and approximate the behaviour of the original model properly and preserve the important information and characteristics. The aim of MOR is to get the accurate solution of the system with minimum error compared with original model.

The EM simulation process applying MOR is shown in Figure 3.1:

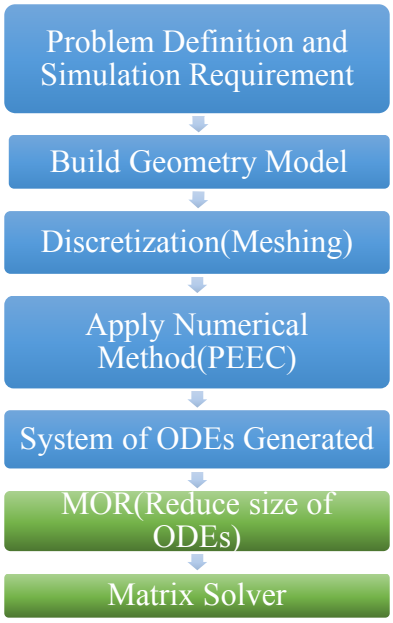

Figure 3.1 Basic EM simulation process with MOR

The diagram shows the basic process applying MOR. In conclusion, The MOR methods are based on the transformation of a high-dimension system of ODEs to a low-dimension one that give approximately the same results.

3.2 Standard MOR Technique

3.2.1 Introduction

The modelling of the 3D power electronic systems requires the solution of ordinary differential equations(ODEs) of very large systems. Model Order Reduction can reduce the size of the original system matrix, the reduced system can be solved faster and give a reasonable accurate result.

MOR technique is used to make a projection of a large-scale system to a low dimensional subspace. For example, some 3D objects can be represented by a single 2D picture. A 3D object exists in a 3D space, but a 2D representation (i.e. a picture) can be created on a 2D subspace (i.e. the camera angle) which captures the important features of a 3D object.

The principle of MOR technique is that it can take a low dimensional projection of a high dimensional model. This process is often termed "moment matching". Moments usually corresponding to the eigenvalues of the system. For example, in Krylov methods, the coefficients of the Taylor series expansion of the transfer function at expansion point are called moments. MOR approaches are based on moment matching around the expansion point, and sometimes multiple expansion points are needed to improve the accuracy which will be discussed in Chapter 5.

The MOR approach needs to accurately approximate the transfer function and effectively match the dominant eigenvalues of the high dimension model.

A projection based MOR technique [44] is used to define the subspace. The process to generate a reduced model is shown in Figure 3.2:

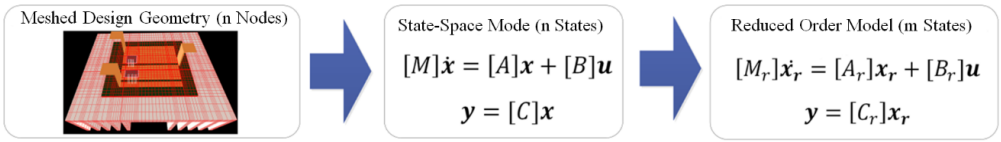

Figure 3.2 Reduced Model Generation Process[21]

$\boldsymbol{u}$ and $\boldsymbol{y}$ are input and output vectors of the system, and these two vectors are remain the same after MOR process. The relationship between the state vectors of the original and reduced model is shown in Equation 3.2:

$$\begin{aligned} \boldsymbol{x_r} &= [H]\boldsymbol{x} \\ \boldsymbol{x} &= [H]^T\boldsymbol{x_r} \end{aligned} \tag{3.2}$$

Where $H(m \times n)$ is the transfer matrix generated by projection process. This method allows to translate the original system into a reduced system. H matrix is usually orthogonal in most cases, so the original solution of the system can be recovered from the reduced order solution.

In conclusion, The MOR methods are based on the transformation of a high-dimension system of ODEs to a low-dimension one that give approximately the

same results. Two linear model order reduction methods are discussed later. They are Control Theory methods and Krylov Subspace methods[45].

3.2.2 Control Theory Method

This category of method is proposed in [45], The stable dynamic state space system is shown in Equation 3.3:

$$\begin{aligned} \dot{\boldsymbol{x}} &= G\boldsymbol{x} + R\boldsymbol{u} \\ \boldsymbol{y} &= C\boldsymbol{x} \end{aligned} \tag{3.3}$$

Where $\boldsymbol{x}$ is the state vector, $\boldsymbol{u}$ is the input vector, and $\boldsymbol{y}$ is the output. There are slight changes in the system matrix form compared with Equation 3.1, where:

$$\begin{aligned} G &= M^{-1}A \\ R &= M^{-1}B \end{aligned} \tag{3.4}$$

The control theory method is based the control theory concepts of controllability and observability.

A state is one of the variables that are used to describe a dynamical system. A state is controllable if any state is reachable in a finite time, and a system is controllable if all states are controllable. A system state at some given timestamp is observable if the knowledge of the input and output over a finite time segment allows the determination of the state at the timestamp. If all states of the system are observable, the system is said to be observable[46].

Controllability and observability can be represented by the means of the Gramians. The controllability Gramian P and the observability Gramian Q can be computed through Lyapunov equations. The method to solve Lyapunov equations can be found in [47]

The Gramians of controllability and observability are described in Equation 3.5 [48]:

$$P = \int_0^\infty e^{Gt} R R^T e^{G^T t} dt$$
$$Q = \int_0^\infty e^{Gt} R^T R e^{G^T t} dt \tag{3.5}$$

The P and Q matrices are solutions of Lyapunov equations related to Equation 3.3. The reduced model will be generated by restricting the system matrix to the dominant eigenvalues. The Gramians need to be solved and factorization in descending order to calculate Hankel singular values, which is used to form the projection matrices. In summary, the idea of control theory is to truncate the system matrix corresponding to the eigenvalues with lowest contribution.

3.2.2.1 Balanced Truncation Method

Balanced truncation method is an example related to control theory methods. The balanced truncation method is to obtain a reduced order model by transforming the system to a balanced representation. There are some algorithms mentioned in [49] to achieve the goal of balanced truncation, such as square root algorithm, balancing-free square root algorithm etc.

The Gramians of controllability and observability are important in the order reduction process. For example, there is a method suggested in [50] to balance the system, which obtains Hankel singular values(HSV) by setting both Gramians equal and diagonal. The Hankel singular values are the positive square roots of the eigenvalues of the product of the Gramians PQ, a diagonal matrix with the HSV values on its diagonal will be generated to build the projection matrices. The reduced model can be transformed through the projection.

In conclusion, the advantage of control theory method is that it has a global error estimate and also the control theory method is more suitable for small systems because it's computational complexity is greater than Krylov subspace method. It's difficulties arise for large systems because it involves eigenvalue computation of the product of Gramians, which increase the amount of computation.

3.2.3 Krylov Subspace Method

Krylov subspace techniques are an alternative MOR methods that require a matrix representation of a system. For a single input single output system, a left-hand side representation of the form[45] is shown in Equation 3.6:

$$\begin{aligned} J\dot{\boldsymbol{x}} &= \boldsymbol{x} + b\boldsymbol{u} \\ \boldsymbol{y} &= e^T \cdot \boldsymbol{x} \end{aligned} \tag{3.6}$$

Where:

$$J = A^{-1}M$$
$$b = A^{-1}B$$

The $\boldsymbol{u}$ and $\boldsymbol{y}$ are input and output vectors. The transfer function of the system can be obtained from Equation 3.6 and shown in Equation 3.7:

$$G(s) = e^T(I - sJ)^{-1}b \tag{3.7}$$

T is an operator which means the transpose of a matrix. Krylov method is to use low dimensional model to approximate the system transfer function. Taylor series expansion about expansion point s_0 is applied to $G(s)$ for Pade approximation[51]. The transfer function can be rewritten as Equation 3.8:

$$G(s) = \sum_{i=0}^{\infty} \frac{G^{(i)}(s_0)}{i!}(s - s_0)^i \tag{3.8}$$

$$= \sum_{i=0}^{\infty} \frac{-i!\, e^T J^i (I - s_0 J)^{-(i+1)} b}{i!} (s - s_0)^i$$

$$= \sum_{i=0}^{\infty} M_i \, (s - s_0)^i$$

Where $M_i = -e^T J^i (I - s_0 J)^{-(i+1)} b$, are called moments about expansion point s_0. The principle of Krylov method is to generate a series of basis vectors, which is called Krylov subspace. Each basis vector of the subspace corresponds to one moment defined in Equation 3.8.

The standard MOR method usually make the series expansion at one point $s_0=0$. The right Krylov subspace can be defined as equation 3.9:

$$K_r^R\{J, b\} = span\{b, Jb, \dots, J^{r-1} b\} \tag{3.9}$$

And the left Krylov subspace can be defined as equation 3.10:

$$K_r^L\{J^T, e\} = span\{e, J^T e, \dots, (J^T)^{r-1} e\} \tag{3.10}$$

The moments obtained in the reduced order mode contain information about the dominant eigenvalues. The basis vectors are effectively the eigenvectors corresponding to dominant eigenvalues of system.

In summary, the Krylov method is used to reduce the size of the original model, the process is to generate a subspace and make a projection of the original model onto the subspace. In other words, the methods generate a subspace to match the dominant eigenvalues of the original system with the eigenvalues of the reduced model, which is often termed “moment matching”

There are several methods frequently used in Model Order Reduction. For example, Lanczos method, Arnoldi method and its extended methods such as block Arnoldi algorithm and PRIMA algorithm. The details of these methods will be illustrated in later sections.

3.2.3.1 Lanczos Algorithm

The Lanczos method [45]can generate both left subspace basis and right subspace basis including *2m* basis vectors. They are a pair of biorthogonal basis, $W_r, V_r \in R^{n\times m}$. The relationship between the original system matrix and the reduced system matrix is shown in equation 3.11:

$$W_r^T J V_r = T_r \tag{3.11}$$

Where J is the original system matrix and T_r is the reduced system matrix after MOR process. The Lanczos algorithm is shown below:

Input: Matrix *J*, Right and left starting vectors $\boldsymbol{b}$ and $\boldsymbol{e}$.
Output: The orthonormal matrix V_r, W_r.

1. Set $\hat{v}_1 = b.\ \hat{w}_1 = e$, and $v_0 = w_0 = 0$, set $\delta_0 = 1$.

For *i=1,...,m* do (Build basis vector v_i, w_i)

2. Compute $h_{i,i-1} = \|\hat{v}_i\|$, and $h_{i,i-1}{}' = \|\hat{w}_i\|$
   If $h_{i,i-1} = 0$, or $h_{i,i-1}{}' = 0$ then stop.
3. Set $v_i = \hat{v}_i / h_{i,i-1}$, $w_i = \hat{w}_i / h_{i,i-1}{}'$.
4. Compute $\delta_i = w_i{}^T v_i$, if $\delta_i = 0$, then stop.
5. Set $h_{i-1,i} = h_{i,i-1}{}' \frac{\delta_i}{\delta_{i-1}}$, $\hat{v}_{i+1} = J v_i - v_{i-1} h_{i-1,i}$,
   Compute $h_{i,i} = \frac{w_i{}^T \hat{v}_{i+1}}{\delta_i}$, $h_{i,i}{}' = h_{i,i}$, $h_{i-1,i}{}' = h_{i,i-1} \frac{\delta_i}{\delta_{i-1}}$,
6. Set $\hat{v}_{i+1} = \hat{v}_{i+1} - v_i h_{i,i}$,
   $\hat{w}_{i+1} = J^T w_i - w_i h_{i,i}{}' - w_{i-1} h_{i-1,i}{}'$,

End_For
Set $V_r = [v_1\ v_2\ \cdots v_m]$, $W_r = [w_1\ w_2\ \cdots w_m]$.

The number of moments matched in Lanczos method is *2m*, where *m* represents the dimension of the reduced model. The advantage of this method is that the

reduced model can match 2m moments, however, the reduced model may not be stable sometimes.

3.2.3.2 Arnoldi Algorithm

Arnoldi process[45] is another iterative method, which use Gram-Schmidt process to set up a sequence of orthonormal vectors, which called Arnoldi vectors. The vectors from the right Krylov subspace. The matrix V_r is the transfer matrix, which can be considered as a projection of system matrix J onto the Krylov Subspace, and the order of reduced system is m. The standard Arnoldi process for SISO (Single Input Single Output system) is shown below :

Arnoldi Process

7. Set $\hat{v}_1 = b$.

For $i=1,\ldots,m$ do (Build Arnoldi vector v_j)

8. Compute $h_{i,i-1} = \|\hat{v}_i\|$.
   If $h_{i,i-1} = 0$, then stop.
9. Set $v_i = \hat{v}_i / h_{i,i-1}$.
10. Set $v_{i+1} = A_k v_i$.
11. For $j=1,\ldots,i$ do:
    Set $h_{j,i} = v_j{}^T \hat{v}_{i+1}$;
    $\hat{v}_{i+1} = \hat{v}_{i+1} - v_j \cdot h_{j,i}$
    End_For

End_For

The projection matrix V_r can be generated after the Arnoldi process, which $V_r = [v_1 \cdots v_m]$. The original system matrix J, b, can be transferred to the reduced system matrix J_r, b_r .The relationship between them is shown in equation 3.12:

$$\begin{aligned} J_r &= V_r{}^T J V_r \\ b_r &= V_r{}^T b \end{aligned} \tag{3.12}$$

$$C_r = CV_r$$

From the relationship between reduced system matrix and original system matrix, it is clear that the dimension of input and output vectors are remain the same after transformation. And the relationship between the transfer matrix V_r in standard Arnoldi process and the transfer matrix H in Equation 3.2 is $V_r = H^T$.

In summary, the Arnoldi method generates the right Krylov Subspace, described by a set of orthogonal basis vectors, and projects the original system to this subspace. The projection process is defined by the V_r matrix which is an output of the algorithm.

3.2.3.3 Block Arnoldi Algorithm

The standard Arnoldi method is suitable for SISO(single input single output) systems, that have only one column in the input matrix. For multi-inputs systems, it may not take account complete inputs however so called "block" variations of the Arnoldi algorithms are available for multi-input, multi-output systems. A new method based on Arnoldi method is proposed in[52] which is Block Arnoldi method. Block Arnoldi method is suitable for multi-input systems. In a single input single output system, the incidence matrix b is a vector. But in multi-input system with inputs described by a matrix B, with N columns where N is the number of inputs. The Block Arnoldi method is almost the same as the SISO method except that either matrix-vector products become matrix-matrix products or that an extra inner loop is added to deal with each column of the input matrix in turn.

In large scale dynamic systems, the systems can be represented in different matrix form. Block Arnoldi method is needed when the input number is more than one. For example, Block Krylov subspace methods can be used for solving large Sylvester equations[53]. Block SAPOR [54](block second-order Arnoldi method for passive order reduction) also applied to MIMO for solving RCL interconnect circuits.

In Block Arnoldi algorithm, The system matrix is represented in the form as Equation 3.13:

$$\begin{aligned} J\dot{\boldsymbol{x}} &= \boldsymbol{x} + K\boldsymbol{u} \\ \boldsymbol{y} &= C \cdot \boldsymbol{x} \end{aligned} \tag{3.13}$$

Where:

$$J = A^{-1}M$$
$$K = A^{-1}B$$

The transfer equation can be rewritten as Equation 3.14 in terms of s:

$$\begin{aligned} (sJ - 1)x(s) &= Ku(s) \\ y(s) &= C \cdot x(s) \end{aligned} \tag{3.14}$$

In frequency domain, then take Laplace transformation of the system equation and obtain the system transfer function matrix in Equation 3.15 :

$$H(s) = C(sJ - I_n)^{-1}K \tag{3.15}$$

The matrix $I_n \in R^{n\times n}$ is the identity matrix, Apply Taylor expansion to *H(s)* around *s=0*, we have:

$$H(s) = M_0 + M_1 s + M_2 s^2 + \cdots \tag{3.16}$$

Where M_0, M_1, M_2, …are the block moments of *H(s)*, where $M_i \in R^{N\times N}$. *N* is the number of inputs. the moments can be calculated as Equation 3.17:

$$M_i = -CJ^i K \tag{3.17}$$

The block Krylov subspace can be generated through matrices $J \in R^{n\times n}$ and $K \in R^{n\times N}$, the definition of the Krylov subspace is shown in Equation 3.18:

$$\begin{aligned} Kr(J,K,m) = colsp[K, JK, J^2K, \cdots, J^{d-1}K, \\ J^d k_1, J^d k_2, \cdots, J^d k_l] \\ where, d = \left[\frac{m}{N}\right], l = m - dN \end{aligned} \tag{3.18}$$

Block Arnoldi procedure can generate an orthogonal basis V_r spanning the subspace, then the original system can be projected on the subspace. The order of the original system can be reduced from *n* to *m*. The transformation between the reduced order model and original model is shown in Equation 3.19:

$$\begin{aligned} J_r &= V_r{}^T J V_r \\ K_r &= V_r{}^T K V_r \\ C_r &= C V_r \end{aligned} \tag{3.19}$$

The moments can be calculated from Equation 3.18. In Arnoldi based methods, there are *m* moments are matched. Two sided Arnoldi process is proposed to increase the number of matched moments[55], but it will increase the complexity of the algorithm.

3.2.3.4 PRIMA Algorithm

PRIMA method is based on Arnoldi method and can obtain passivity of RLC circuits. The original system can be stable and the original model has properties such as stability and passivity. The passive model means that the components in the model will only consume, but do not produce, energy. It is needed to guarantee the overall circuit stability. It is important to ensure that the reduced model has the same properties as the original model. But the basic Arnoldi method cannot guarantee the passivity of the reduced model. So the improved Arnoldi method is proposed in [44] which is PRIMA(Passive Reduced-Order Interconnect Macromodeling Algorithm) method.

The Block Arnoldi method doesn't work for MNA because it uses left-hand side matrix form to represent a first order ODE system but RCL interconnect models are inherently second order systems that can be represented as coupled first order

ODEs. The PRIMA algorithm overcomes this limitation as it is modified to suit the matrix type that results from a set of second order differential equations presents as a two coupled first order sets. The differential equations are obtained through MNA analysis (Modified nodal analysis). The details of MNA analysis and system matrix generation has been described in chapter 2.

Arnoldi method is used for first order type of problems, such as thermal conduction modelled with FDM or FEM method. RLC circuit model is fundamentally second order systems, but can be assembled as first order ODEs using MNA analysis. The system matrix obtained by MNA analysis including a partitioned structure: inductance part and coupled capacitance part.

PRIMA algorithm guarantees passivity of the original system. In PRIMA, extended block Arnoldi algorithm is applied to the original system matrix and then the circuit matrices are again projected onto the subspace spanned by the Arnoldi vectors.

The basis vectors of the Krylov subspace can be generated through Block Arnoldi algorithm. The algorithm will do [*m/N*]+1 iterations to obtain the transfer Matrix $V_r \in R^{n\times m}$. In summary,

$$\begin{aligned} colsp(V_r) &= Kr(J, K, m) \\ V_r{}^T V_r &= I_m \end{aligned} \tag{3.20}$$

The reduced order system transfer function is given in Equation 3.21:

$$H_r(s) = C_r(sM_r - A_r)^{-1}B_r\boldsymbol{u} \tag{3.21}$$

The PRIMA algorithm is shown below:

PRIMA Process:

Input: Matrix *A, B* and integer orders *m, N*.
Output: The orthonormal matrix V_r .

1. Solve $AK=B$. for Matrix K.
   qr factorization of K to obtain V_0
2. If $\frac{m}{N}$ is not an integer, set $n = \left[\frac{m}{N}\right] + 1$, else set $n = \frac{m}{N}$.
3. For $k=1,2,\ldots,n$
   Solve $AV_k^{(0)} = MV_{k-1}$ for $V_k^{(0)}$.
4. For $j=1,\ldots,k$
   Compute $H = V_{k-j}^T V_k^{(0)}$.
   $V_k^{(j)} = V_k^{(j-1)} - V_{k-j}H$.
   qr factorization of $V_k^{(k)}$ for V_k.
   End_For
   End_For

Set $V_r = [V_0\ V_1\ \cdots V_{k-1}]$ and truncate matrix V_r to make sure it has m columns only.
Compute $M_r = V_r{}^T M V_r, A_r = V_r{}^T A V_r$

The PRIMA algorithm will generate the transfer matrix V_r, the reduced system matrix can be calculated in Equation 3.22:

$$\begin{aligned} M_r &= V_r^T M V_r \\ A_r &= V_r^T A V_r \\ B_r &= V_r^T B \\ C_r &= C V_r \end{aligned} \tag{3.22}$$

The reduced system can be represented in Equation 3.23:

$$\begin{aligned} V_r^T M V_r \dot{\boldsymbol{x}}_{\boldsymbol{r}} &= V_r^T A V_r \boldsymbol{x}_{\boldsymbol{r}} + V_r^T B \boldsymbol{u} \\ \boldsymbol{y} &= C V_r \boldsymbol{x}_{\boldsymbol{r}} \end{aligned} \tag{3.23}$$

The size of the system matrices is very small after model order reduction process, typically about 10 to 30 equations. The maximum size of original model is around 7000-10000equations. The “outputs” of the system are arbitrary. The output can be terminal currents or voltage, and also can be interpolated values.

The PRIMA algorithm has advantages for large scale coupled RLC circuit compared with Block Arnoldi method as presented in [44]. PRIMA algorithm is able to capture the system response for a wider frequency range than block Arnoldi method. The PRIMA algorithm is based on Arnoldi method, but with guaranteed passivity and is able to produce passive reduced order model for RLC circuit network. Therefore, PRIMA is chosen as the MOR technique used in EM modelling.

3.3 Evaluation of Standard MOR Technique

In this section, the PRIMA is applied to a PEEC model in an electromagnetic domain simulation. The standard MOR method usually has one expansion point, effectively starting to match eigenvalues at a particular frequency which is usually 0Hz or DC. The accuracy of the reduced order model is therefore highest near the expansion point and reduces at frequencies further away. Some test cases will be chosen to validate the accuracy of the standard MOR method and the relationship between the accuracy and expansion point.

This section will evaluate the MOR method from three aspects: Terminal impedance, simulation speed and current density. The limitation of the standard MOR method will be illustrated in the end of this section.

3.3.1 Evaluation of MOR Based on Impedance Prediction

The first example is an experimental test PCB board which is selected to validate the MOR method. The PCB board is shown in Figure 3.3:

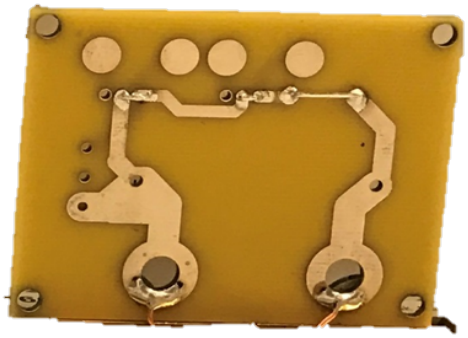

Figure 3.3 Test Case Model

The PEEC code development and optimization that described in Chapter 2 was implemented in the software called VPPE. The VPPE simulation tool can do simulation in frequency domain or time domain. The PCB board is simulated both in the commercial software (Ansys) and VPPE. The PCB board was available from another project.

This example will be used to validate the accuracy on Z parameter extraction and current density plot. The PCB board model built in VPPE is shown in Figure 3.4:

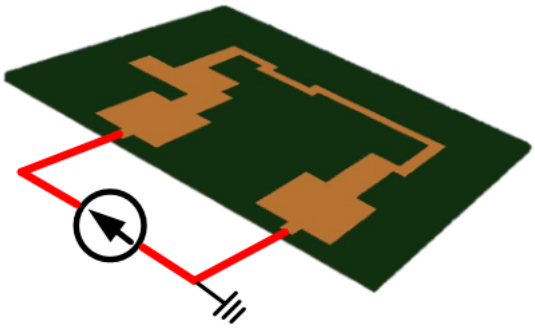

Figure 3.4 PCB Board Model in VPPE

Two nodes are defined at the terminal. Current source is connected between the nodes as an excitation. The meshing process generates 1948 capacitive nodes, and 4646 current carrying conductors, which results in 6597 equivalent circuit equations for the system. The terminal impedance will be used to evaluate model accuracy. Although the PEEC method computes terminal voltage and current, the software can easily be configured to give impedance curves by selecting a

frequency domain simulation and attaching a 1A current source between the terminals. A plot of inner-terminal voltage then represents the terminal impedance.

The terminal voltage magnitude and phase angle in VPPE are shown in Figure 3.5:

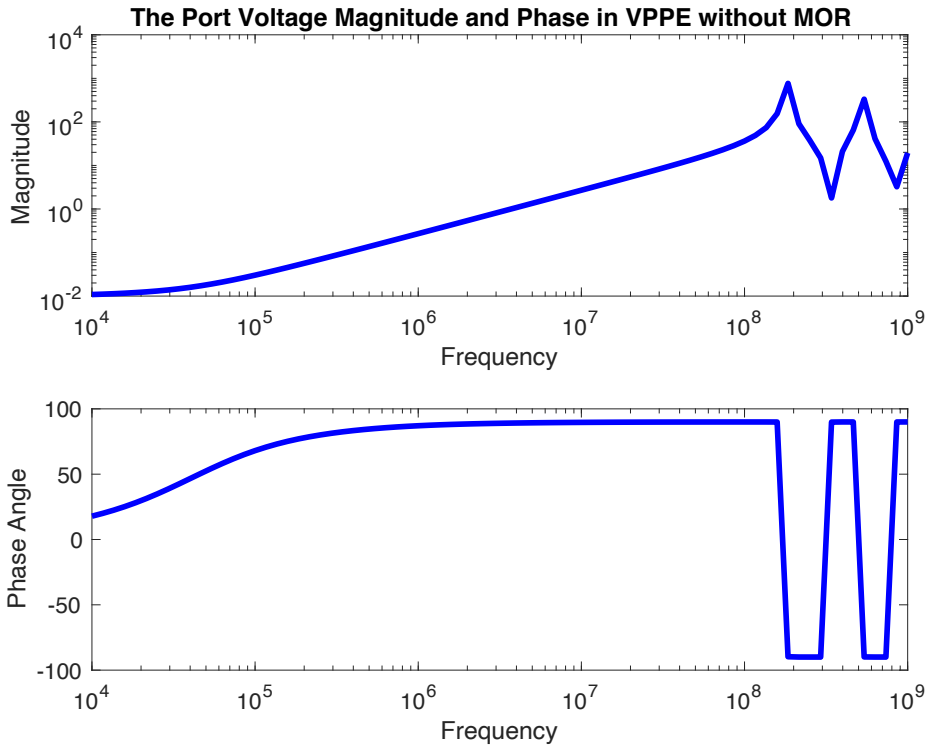

Figure 3.5 The Port Voltage Magnitude and Phase in VPPE

The port impedance can be easily derived from the port current because the current value is constant. The MOR can be applied to accelerate the simulation. The comparison of the impedance curve prediction in VPPE with and without MOR is shown in Figure 3.6:

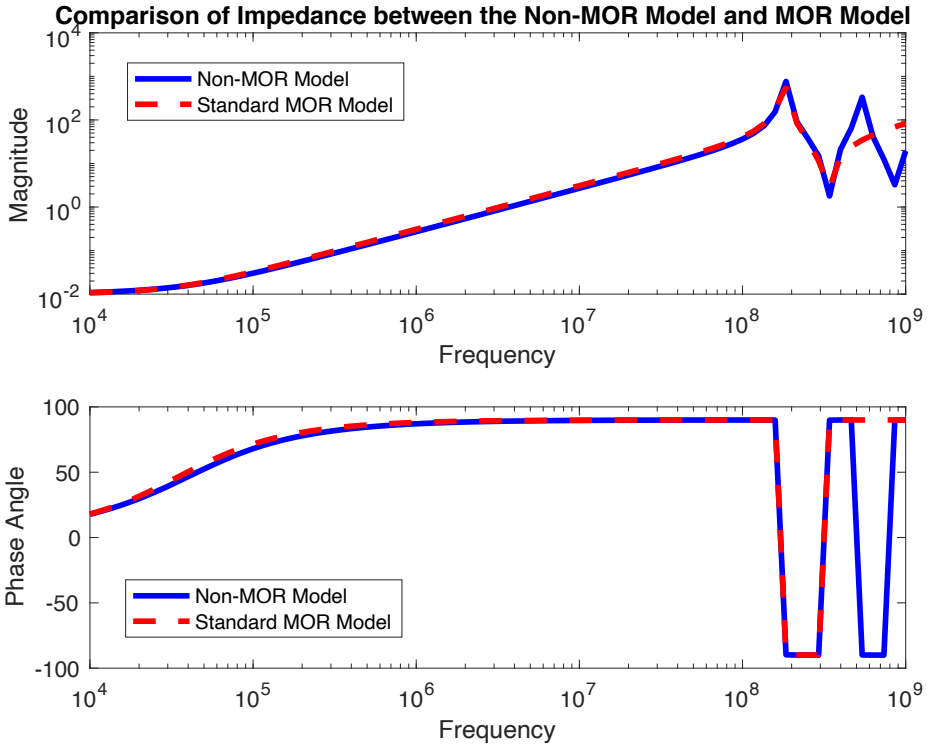

Figure 3.6 Comparison of Impedance between the Non-MOR Model and MOR Model

The error between the non-MOR model and MOR model is shown in Figure 3.7:

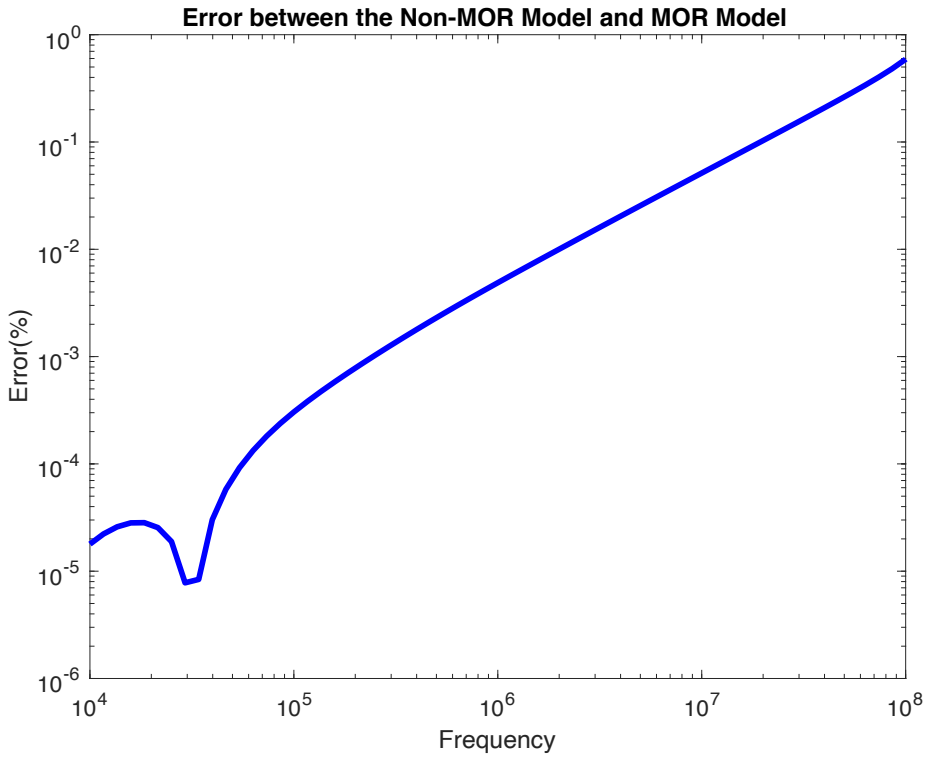

Figure 3.7 Error Between the non-MOR model and MOR model

The non-MOR model and MOR model are simulated using the same meshing and frequency stepping settings. From Figure 3.6, It is clear that the result with MOR is almost matching the non MOR model until 300MHz where the results begin to differ. Based on the expansion point theory described in section 3.2.3, the accuracy is higher when towards expansion point. And in this case the expansion point is at DC which is far away from high frequencies.

The simulation time for MOR model is 81s, but the simulation time for non MOR model is 7205s. The evaluation of the simulation speed of MOR will be illustrated in next section.

3.3.2 Evaluation of MOR based on Simulation Speed

The accuracy of simulation results depends on many factors. The non-MOR simulation requires meshing, matrix coefficient calculation through evaluation of the PEEC integrals, and frequency stepping. Meshing and matrix generation times are a function of the number of conductors and nodes in the mesh, frequency stepping is a function of the number of conductors and nodes in the mesh and the number of frequency steps.

An MOR enabled simulation requires meshing, matrix coefficient calculation through evaluation of the PEEC integrals, reduced order model generation, and frequency stepping. Meshing and matrix generation times are a function of the number of conductors and nodes in the mesh, reduced order model generation is a function of the number of conductors and nodes in the mesh and the chosen reduced order model size, frequency stepping is a function of the reduced order model size and the number of frequency steps.

The MOR approach involves an additional pre–processing step for reduced order model generation, but the frequency stepping procedure requires solution of the reduced order model rather than the original, much larger model.

Two main factor will be illustrated in this section. They are the number of equations (determined by the number of conductors and nodes in the mesh) and the number of frequency steps. The reduced order model size is usually required to be in the range 20-100 but variations within this range have little effect on the overall simulation time.

3.3.2.1 Relationship Between Total Simulation Time and Mesh Size

The relationship between the simulation time and the meshing in VPPE will be illustrated. The test case model is a PCB board as example 1. In low frequencies, only small number of conductors and nodes in mesh structure are needed to get accurate results, but in high frequencies large number of conductors and nodes in mesh structure are necessary. The number of equations depend on the number of conductors and nodes, also the frequency of interest. The number of equations also determines the size of the system matrix.

The relationship between the total simulation time and number of equations without MOR is shown in Figure 3.8:

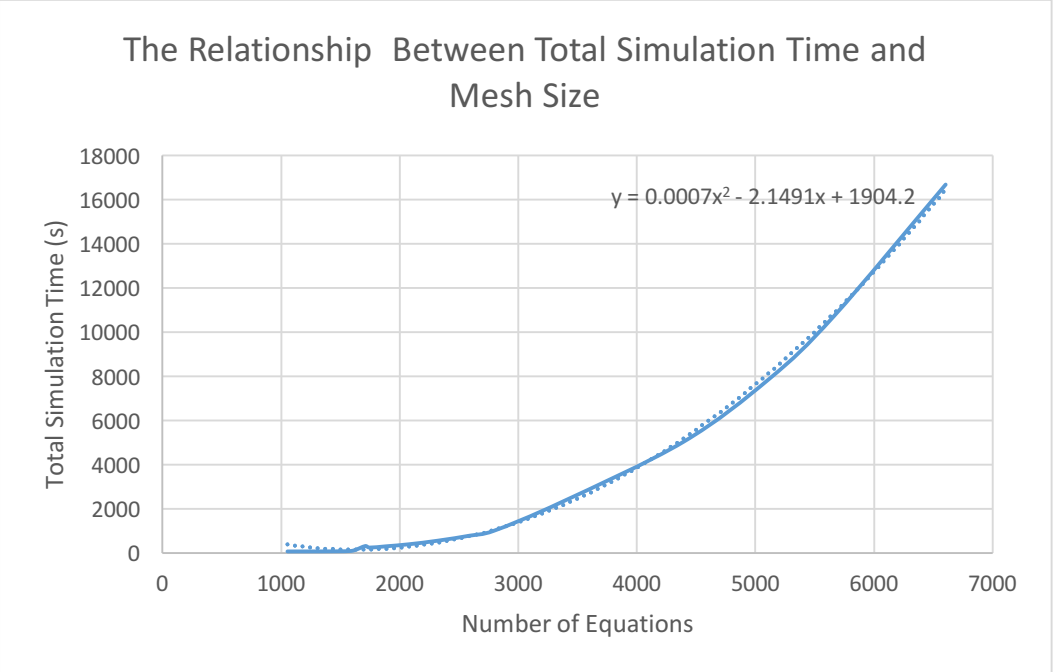

Figure 3.8 The Relationship Between simulation Time and Mesh Size

The model is simulated in VPPE, the *X* axis represents the number of equations and the *Y* axis represents the total simulation time. All the simulation settings are the same except for the mesh setting. The simulation is made in frequency domain in the range from 10Hz to 100MHz with 71 frequency steps. The relationship between the simulation time and number of equations can be given as a quadratic polynomial through the results, which is shown in the figure. It is clear that with the number of equations increasing, the simulation time with non-MOR model increased significantly. The disadvantage of the original PEEC model is that increasing the size of model will cause much longer simulation time.

When MOR is applied in the simulation, the simulation becomes faster than Non-MOR simulation in same condition.

The comparison of total simulation time between MOR and Non-MOR model in different mesh setting is shown in Figure 3.9:

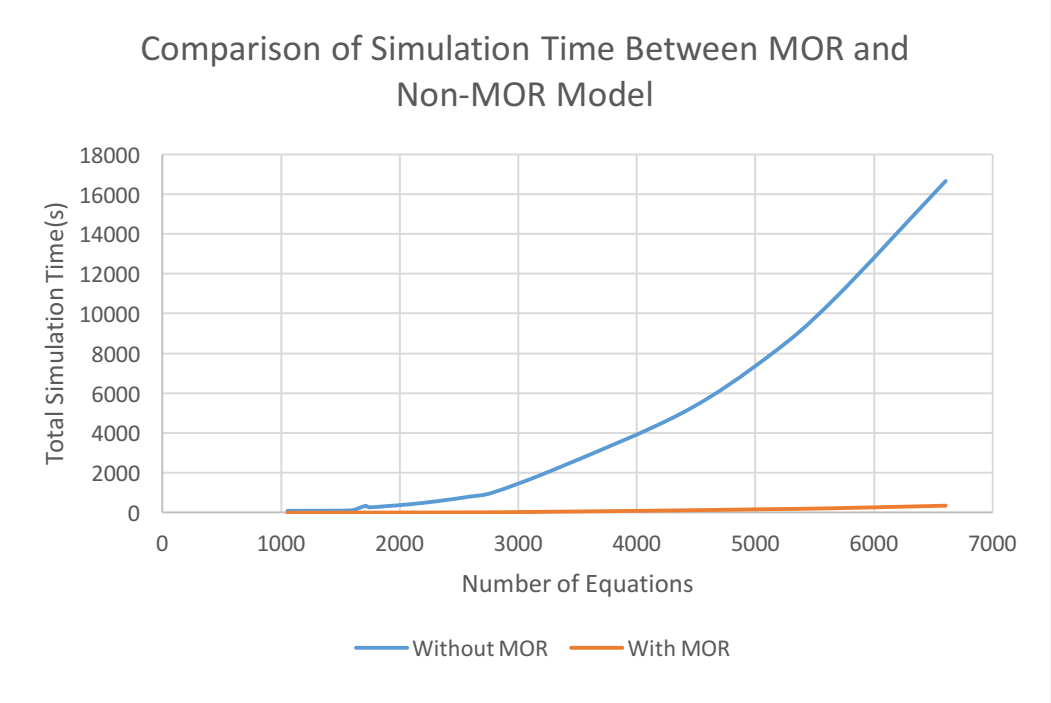

Figure 3.9 Comparison of Simulation Time Between MOR and Non-MOR Model

The numbers in *X* axis means the number of equations or dimensions of the model matrices. It can be seen from Figure 3.9 that the simulation time without MOR is

much longer comparing with the simulation time with MOR when the number of equations increases. For example, the simulation time with MOR is 13 times faster when the number of equations is 1500, and 48 times faster when the number of equations is 6600 compared with the simulation time without MOR. The MOR method has obvious advantages in high dimensional model.

In summary, the simulation with MOR is faster than the simulation without order reduction. That is because the dimension of the system matrix is reduced after MOR.

3.3.2.2 Relationship Between Total Simulation Time and Number of Steps

The simulation time and accuracy also depends on initial set up and how many time or frequency steps are configured. Although results are presented here for frequency-domain simulation, the simulation process is almost identical for time-domain simulation where, for example, large number of time-steps are needed to represent pulsed waveforms in power electronic simulation. Some simulations can easily require 100,000 time steps, so the dependency of simulation time on the time-stepping process becomes dominant. The same principle applies with frequency domain simulation: more frequency steps are needed if need to capture more details in a wide range of frequencies. If the time required to evaluate results at each step can be reduced, simulation speed will improve.

The same example will be used to evaluate the relationship between the total simulation time and the number of frequency steps. The simulation settings are all the same except for the number of frequency steps. The number of equations is 3773 equations. The frequency range of the simulation is from 10Hz to 100MHz. The relationship between simulation time and frequency steps without MOR is shown in Figure 3.10 :

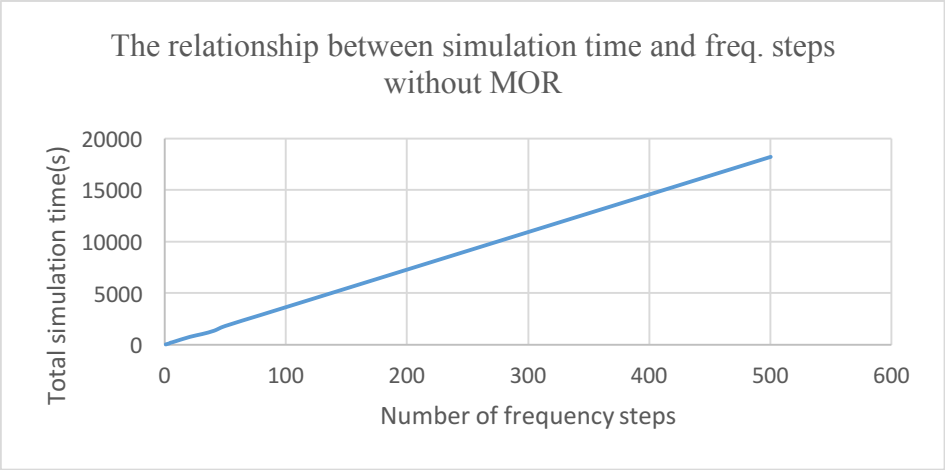

Figure 3.10 Simulation Time vs Frequency Steps

The simulation time for each frequency step is almost the same without MOR because the number of equations need to solve is the same at each stepping. From Figure 3.10, it can be found that the simulation time increases linearly with the frequency steps because it is one solve per step. The relationship between the simulation time and number of steps for this specific model is shown below:

$$t(s) \approx 30 + 36.45n \tag{3.24}$$

The average set up time for PEEC model generation is about 30s, and average simulation time per step is about 36.45s, and n means the number of steps. The relationship between simulation time and frequency steps with MOR is shown in Figure 3.11:

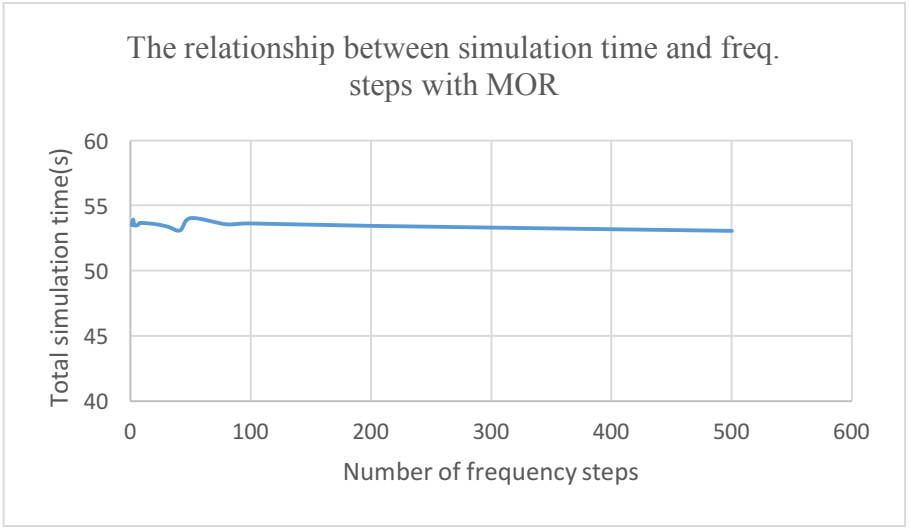

Figure 3.11 Simulation Time vs Frequency Steps with MOR

The simulation time does not change much regarding to the frequency steps when applying MOR. This is because the dimension of the system matrix after order reduction is very small. The initial 53.5s offset is the time for reduced model generation. The simulation speed for one frequency step is fast. The number of equations for the reduced model is less than the original model. Sometimes the total simulation time has a slight decrease when increase frequency steps, it is because frequency stepping takes a small proportion of the time.

The comparison of total simulation time between MOR and Non-MOR model with different number of frequency steps is shown in Figure 3.12:

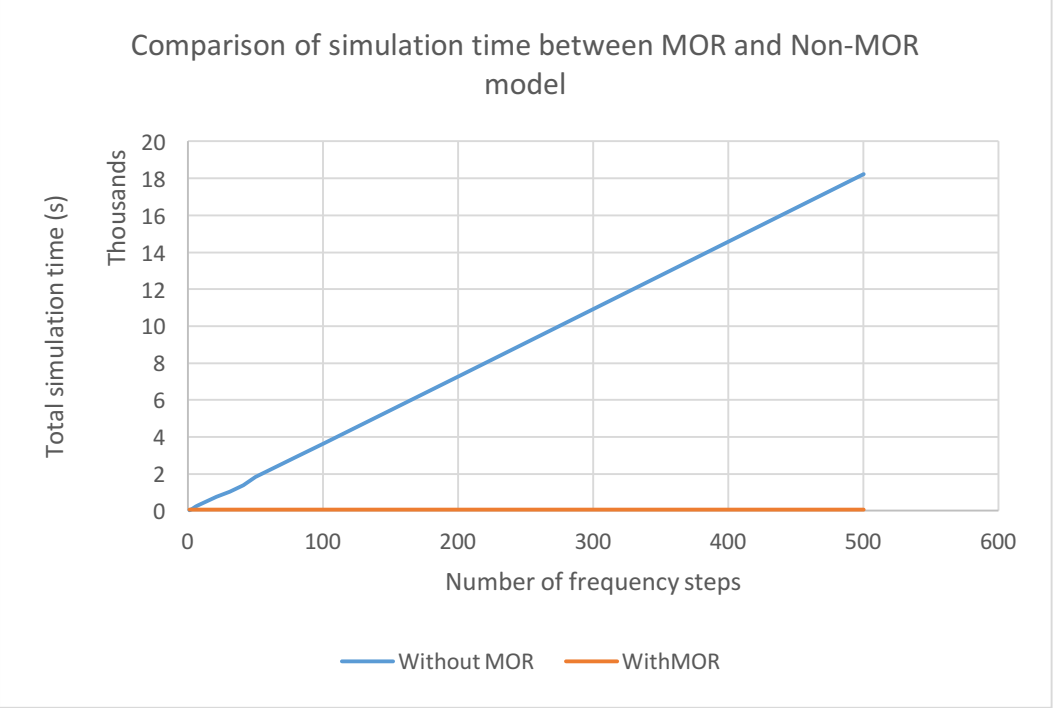

Figure 3.12 Comparison of Simulation Time Between MOR and Non-MOR Model with different number of frequency steps

It can be seen from Figure 3.12 that the simulation time without MOR increase linearly when the number of frequency steps increase. The simulation time with MOR doesn't change much when increasing the number of frequency steps. The simulation with MOR is about 54s. This comparison shows that simulation time can be reduced significantly with MOR.

3.3.3 Evaluation of MOR based on Current Density Prediction

In previous section, the terminal impedance has been evaluated. The benefit of MOR is that it is not only suitable for impedance prediction, it can also be used to extract internal distribution. The current density distribution is very important at high frequencies as it is not easy to predict and can affect losses in materials or circuit components.

3.3.3.1 Simulation results in VPPE without MOR

Firstly, the current density is simulated in VPPE without MOR, the example is the same as section 3.3.1, and the simulation results of the original model at 100Hz in VPPE with different mesh size is shown in Figure 3.13:

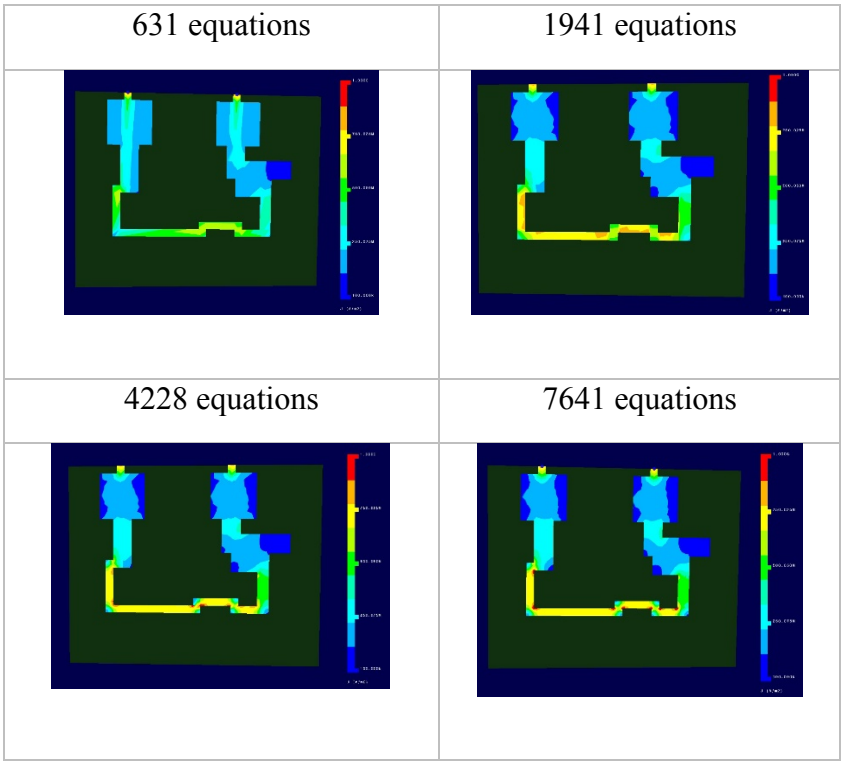

Figure 3.13 Current Density in VPPE at 100Hz

From Figure 3.13 , It's obviously that the simulation can capture more details when the number of equations increase. The number of equations means how many equations we got after discretization process. It can be seen that the accuracy of the

simulation result is related to the mesh size. The PEEC code is able to give accurate results when increasing the mesh size. From the simulation result (7641equations) in Figure 3.13, The current density is high at the corner of the thin copper track.

3.3.3.2 Simulation Results in Commercial Software

The same example will be simulated in Ansys HFSS as a reference. The model simulated in ANSYS HFSS is shown in Figure 3.14:

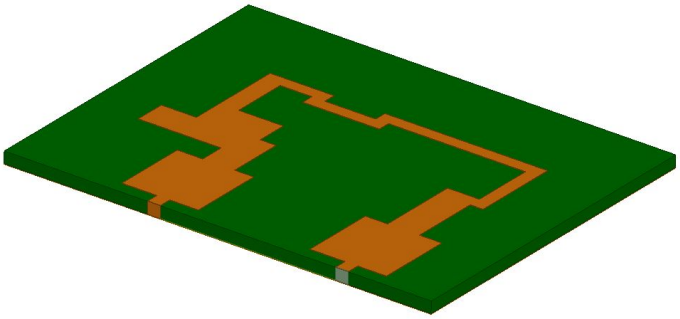

Figure 3.14 PCB Model in HFSS

In Ansys HFSS, the model dimension and excitation source are all the same as VPPE. The simulation results about current density will be shown in this section. The simulation result in HFSS at 100Hz is shown in Figure 3.15:

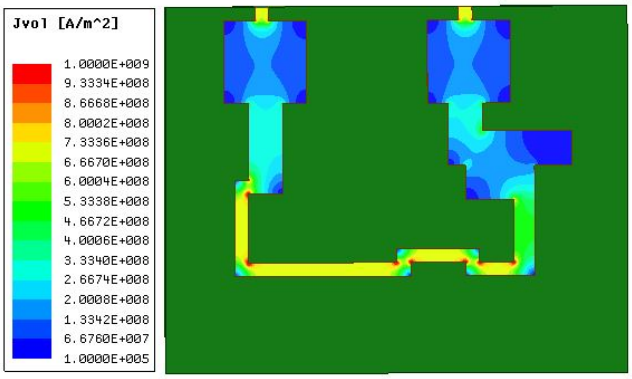

Figure 3.15 Current Density in HFSS at 100Hz

This model will be used for evaluate the accuracy of MOR enabled PEEC and also compared with the commercial software ANSYS. From the current density plot in Ansys HFSS, the VPPE can accurately predict the current density at 100Hz for this example without MOR. The evaluation of MOR will be illustrated in next section.

3.3.3.3 Evaluate the Simulation Results with MOR

The appropriate mesh size needs to be determined to get accurate simulation results. The section 3.3.3.1 has shown the simulation results in different mesh setting. In this section, the simulation results of the current density in VPPE with and without MOR will be illustrated. The accuracy of the simulation results is also very important.

MOR is applied in different settings trying to find out the effect of MOR with the accuracy. The MOR models can be used for both time- and frequency-domain simulations. The reason why we need to apply MOR is because the available technology nowadays is too slow in realistic system. The standard MOR technique uses a single point expansion point, which is usually chosen to be 0Hz or DC. In this test, three different MOR setting at different expansion points are evaluated to understand the effect of expansion point on model accuracy. The choice of expansion point was found to have a more pronounced effect of current density predictions than for terminal impedance. Apart from DC expansion point, another two expansion points at 100KHz and 10MHz is chosen based on the frequency of interest, because the WBG devices usually work at KHz to MHz. The simulation results in HFSS and VPPE with different MOR expansion points at 100Hz are shown in Figure 3.16:

Frequency	Current density at 100Hz excitation
HFSS	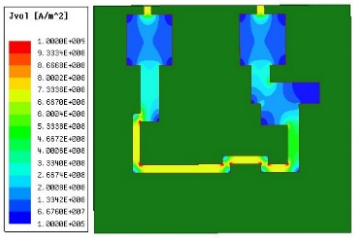
VPPE (without MOR)	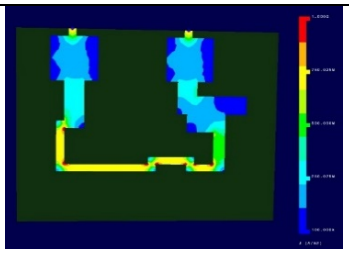
DC Expansion Point	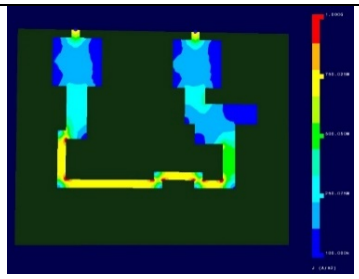
10KHz Expansion Point	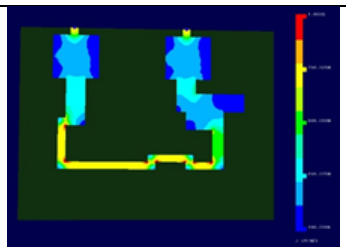
100MHz Expansion Point	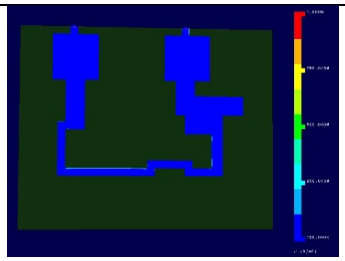

Figure 3.16 Simulation Result at 100Hz with Standard MOR at Different Setting

All the simulation results are for the frequency of 100Hz. From the simulation results, it is clear that the standard MOR method can only give accurate results around the frequency which is near the single expansion point. For example, the simulation results when choosing the expansion point at DC and 10000 are the same as the simulation result without MOR.

The simulation result is clearly incorrect when setting the MOR expansion point to 10^8, because the expansion point is far from 100Hz. Another example will be given to focus on analysing the limitation of standard MOR method.

3.4 Limitation of Standard MOR

3.4.1 Simple Model to show the Limitation of the Standard MOR Approach

A simple designed substrate model is used to further demonstrate the limitation of standard MOR method. The substrate model in VPPE is shown in Figure 3.17:

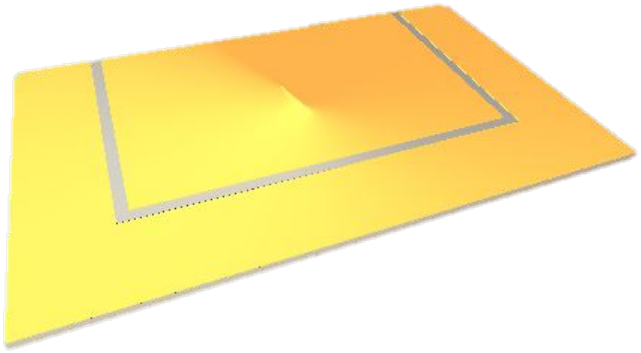

Figure 3.17 Substrate Model in VPPE

Current density can be plot in developed design tool VPPE. A simple substrate tile is used as an example to show the limitation of standard MOR method. The simulation results are shown in Table 3-1:

Table 3-1 Comparison between Non-MOR and Standard MOR

	Non-MOR	Single Expansion Point (DC)	Single Expansion Point (100MHz)
100Hz			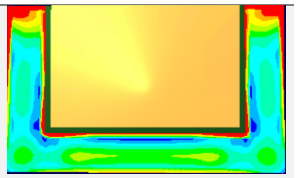
100 KHz	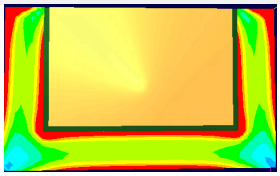	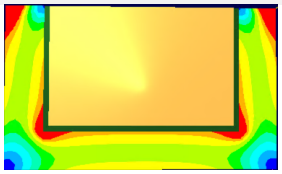	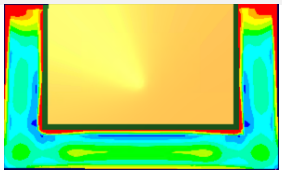
100MHz	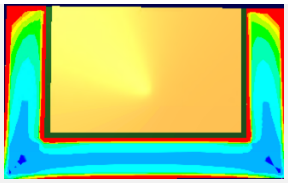	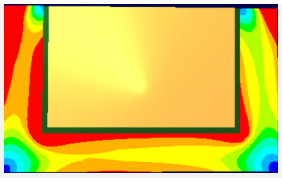	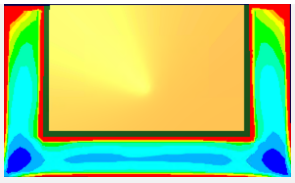
	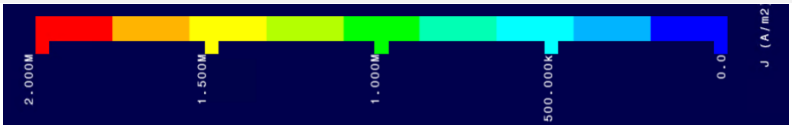		

From Table 3-1, the simulation result using low frequency expansion point only shows the low frequency behaviour, and the simulation result using high frequency expansion point only shows the high frequency behaviour. More specifically, current density plot is only accurate on 100Hz when using DC expansion point, and current density plot is only accurate at 100MHz when using 100MHz expansion point. All the simulation results are obtained with same mesh settings and the scale is from 0 (A/m^2) to $2e^6$ (A/m^2).

Compared with the simulation result without applying MOR, the standard MOR method cannot show accurate results over a wide range of frequencies, this effect is seen in both the terminal impedance curves and current distribution but is more pronounced in the current distribution predictions. Many applications of MOR concentrate on MOR as an equivalent impedance model generation tool and so overlook this effect, whereas for Virtual Prototyping of Power Electronics both

effects are of interest. The following chapters will present work that aims to overcome this limitation by modifying the standard PRIMA algorithm to generate reduced order models based on multiple expansion points.

3.5 Summary

Introduction of MOR technique and how it works are illustrated in this chapter. Krylov subspace method is applied to PEEC model when doing electromagnetic modelling. The MOR technique is very useful when the size of the system is large. There will be huge number of system equations need to be solved when the model becomes complicated. The complexity of geometry is related to the number of conductors and nodes in the mesh.

The evaluation of the standard MOR is done with some example case. The evaluation of the impedance and current density prediction in standard MOR technique are discussed in this chapter. It can be seen from the simulation results and analysis in section 3.4.1 that the standard MOR works for some examples, but it is unable to capture effects across all frequencies of interest.

Chapter 4

4 Eigenvalue Analysis Method

4.1 Introduction to eigenvalue analysis

From last chapter, the simulation results show the disadvantages of standard single point MOR method on current density prediction. Compared with a non-MOR Model, the single point MOR method only shows the low frequency behaviour if the expansion point is in low frequency range, or shows high frequency behaviour if the expansion point is in high frequency range. In conclusion, it is difficult to get the same simulation results as the original model in all frequencies. Single point MOR method has poor accuracy when the model is needed to simulate in a wide frequency range.

An Eigenvalue analysis method is now proposed to analyse why the reduced model cannot give accurate results at all frequencies. This chapter will illustrate the theory and process of the eigenvalue analysis.

In this chapter, section 4.2 shows the general structure of a dynamic system's solution, section 4.3 and 4.4 shows the process of dominant eigenvalue analysis of a dynamic system. section 4.5 shows how to extract dominant eigenvalues from a simple PEEC circuit, and how these eigenvalues influence the response of the

circuit, and evaluate the accuracy of the reduced model generated manually by dominant eigenvalues. Finally, in section 4.6, eigenvalue analysis is used to find out the reason why PRIMA algorithm cannot given the accurate response over wide frequency range.

4.2 The general system solution

4.2.1 Structure of the General solution

The electromagnetic system can be represented in state space formulation. The system is composed of ODEs. Both the MOR and Non-MOR models can be expressed in the matrix format, which is shown in equation 4.1

$$\begin{aligned} M\dot{\boldsymbol{x}} &= A\boldsymbol{x} + B\boldsymbol{u} \\ \boldsymbol{y} &= C\boldsymbol{x} \end{aligned} \tag{4.1}$$

For Non-MOR models, the matrix *M, A, B, C* can be generated through application of the PEEC method. For MOR models, they are generated by the MOR process. Where *u* and *y* are the input source and output signal, respectively, and the structure of the system matrix is shown in equation 4.2.

$$M = \begin{bmatrix} C & 0 \\ 0 & L \end{bmatrix} \quad A = \begin{bmatrix} 0 & D \\ -D^T & -R \end{bmatrix} \tag{4.2}$$

The matrix generation is based on the modified nodal analysis, so KCL and KVL equations are written and system matrix is then generated. Matrix *M* includes the parasitic capacitance and parasitic inductance. The Matrix *A* can be represented by the submatrix *R* and submatrix *D*, where *R* is the resistance submatrix and *D* is the incidence matrix of the branches.

The system matrix can be written in standard state-space form as shown in Equation 4.3:

$$\dot{\boldsymbol{x}} = A_s \boldsymbol{x} + B_s \boldsymbol{u} \tag{4.3}$$

Where :

$$\begin{aligned} A_s &= M^{-1} A \\ B_s &= M^{-1} B \end{aligned} \tag{4.4}$$

The general solutions of a system representing by differential equations can be presented as the form of eigenvalues[56]. The form of the general dynamic solution to differential equation system with real poles is shown in equation 4.5

$$\boldsymbol{x}(t) = c_1 e^{\lambda_1 t} \boldsymbol{v}^{(1)} + c_2 e^{\lambda_2 t} \boldsymbol{v}^{(2)} + \cdots + c_l e^{\lambda_l t} \boldsymbol{v}^{(l)} \tag{4.5}$$

Where λ is the eigenvalue of the system matrix and $\boldsymbol{v}$ is the corresponding eigenvector, and c_n is the constants for each one of the eigenvalues. The dynamic solution of the system is the linear combination of each independent fundamental set of solutions. The complete general solution is the combination of dynamic solution and steady state solution. There are two types of eigenvalues, which are real eigenvalues and complex eigenvalues. Usually the eigenvalues from original system matrix will have both the two types of eigenvalues.

The system matrix is real matrix. If there are complex eigenvalues, the eigenvalues must be in conjugate pairs, and the corresponding eigenvectors are also in conjugate pairs. The eigenvalues and eigenvectors can generate the complex solution, the form of the complex solution for one of complex eigenvalues is shown in Equation 4.6:

$$\boldsymbol{x} = e^{(\alpha + \omega i)t} \boldsymbol{v} \tag{4.6}$$

Where the vector $\boldsymbol{v}$ is the corresponding eigenvector of the eigenvalue. Naturally, for the PEEC model, the solution of the system will be purely real because the input is real however in the general case the solution is complex. The real part and imaginary part of the complex solution are also solutions to the system, so the

complex eigenvector can be separated into real part and imaginary part and build the new eigenvectors.

For example, with a real system matrix A, suppose that there has l real eigenvalues and k pairs of complex eigenvalues. Let $\boldsymbol{v}$ be real eigenvectors corresponding to the real eigenvalues, and $\boldsymbol{w}$, $\overline{\boldsymbol{w}}$ be the conjugate pair of eigenvectors to complex eigenvalues. The complex eigenvectors can be represented in the form as: $\boldsymbol{w}_j = \boldsymbol{a}_j + i\boldsymbol{b}_j$, $\overline{\boldsymbol{w}_j} = \boldsymbol{a}_j - i\boldsymbol{b}_j$, the new form of the matrix after separate the real part and imaginary part of original complex eigenvectors is shown in Equation 4.7:

$$V = [\boldsymbol{v}_1 \quad \boldsymbol{v}_2 \quad \cdots \quad \boldsymbol{v}_l \quad \boldsymbol{a}_1 \quad \boldsymbol{b}_1 \quad \cdots \quad \boldsymbol{a}_k \quad \boldsymbol{b}_k\,] \tag{4.7}$$

And from matrix V, the relation between system matrix A and V is shown in Equation 4.8:

$$AV = VD \tag{4.8}$$

Where D represents the eigenvalues of the system, the structure of matrix D is shown in Equation 4.9:

$$D = \begin{bmatrix} \lambda_1 & & & & & & & \\ & \ddots & & & & & & \\ & & \lambda_l & & & & & \\ & & & \alpha_1 & \omega_1 & & & \\ & & & -\omega_1 & \alpha_1 & & & \\ & & & & & \ddots & & \\ & & & & & & \alpha_k & \omega_k \\ & & & & & & -\omega_k & \alpha_k \end{bmatrix} \tag{4.9}$$

So the general real valued solution of the system is shown in Equation 4.10:

$$\begin{gathered} \boldsymbol{x}(t) = p_1 e^{\lambda_1 t}\boldsymbol{v}_1 + \cdots + p_l e^{\lambda_l t}\boldsymbol{v}_l + \\ e^{\alpha_1 t} Re\{q_1 e^{i\omega_1 t}\boldsymbol{w}_1\} + \cdots + e^{\alpha_k t} Re\{q_k e^{i\omega_k t}\boldsymbol{w}_k\} \end{gathered} \tag{4.10}$$

Where the first row means the dynamic solution for real eigenvalues, and the second row of the equation means the dynamic solution of the complex eigenvalues. The coefficients p and q can be derived from the initial condition of the system and represent the contribution each eigenvalue makes to the solution.

4.3 The Dominant Eigenvalue Analysis

4.3.1 Introduction to Dominant Eigenvalue Analysis

The size of the reduced model should be much smaller than the original model. The reduced order model has fewer eigenvalues compared with original model. The fewer eigenvalues need to accurately approximate the behavior of non-reduced model. The eigenvalue analysis method is developed to analysis how many eigenvalues in original system have a significant contribution to the solution.

Through the eigenvalue analysis, the dominant eigenvalue can be found. The number of the dominant eigenvalue depends on the specific model characteristics. If only a small number of the original eigenvalues make a significant contribution to the system, it means only these dominant eigenvalues need to be approximated by the reduced model.

For thermal domain simulation, it has been validated that the dominant eigenvalue can be extracted through MOR method and accurately give the same results of the original model[57]. The work presented in this chapter extends the eigenvalue analysis to the electromagnetic case to understand the frequency range limitation of electromagnetic reduced order models.

The dominant eigenvalues can be used to validate the accuracy of the reduced model. The contribution coefficient of each eigenvalue from the original model can be used as an indicator to identify the significance of the eigenvalue. The matrix D can be generated to represent the contribution coefficients for each eigenvalue in the original system. Comparison between the dominant eigenvalues of the original

system and the eigenvalues of the reduced model is a good way to check whether the reduced model can extract the important information accurately.

In this chapter, the eigenvalue analysis process will be illustrated and show how the eigenvalue solution can be computed. Firstly, a simple PEEC circuit will be analysed as an example test, then a more complicated substrate model will be analysed as a validation case. The simulation results of the substrate model are shown in Chapter 3.

4.3.2 Process of Dominant Eigenvalue Generation

The process to extract the contribution coefficient is shown as follow:

i. Calculate the eigenvalue and corresponding eigenvectors of the system matrix

The eigenvalues are:

$$\lambda_1, \lambda_2, \lambda_3, \dots\dots, \lambda_l, \alpha_1 + i\omega_1, \overline{\alpha_1 + \imath\omega_1}, \alpha_2 + i\omega_2, \overline{\alpha_2 + \imath\omega_2} \dots\dots \alpha_k + i\omega_k, \overline{\alpha_k + \imath\omega_k}$$

And the corresponding eigenvectors are in the form as:

$$\boldsymbol{v}_1, \boldsymbol{v}_2, \boldsymbol{v}_3 \dots\dots, \boldsymbol{v}_l, \boldsymbol{a}_1, \boldsymbol{b}_1, \boldsymbol{a}_2, \boldsymbol{b}_2, \dots\dots \boldsymbol{a}_k, \boldsymbol{b}_k$$

where $\boldsymbol{v}^i$ are the real eigenvectors and $\boldsymbol{a}_i$ and $\boldsymbol{b}_i$ are the real and imaginary part of the original conjugate pair of complex eigenvectors. The revised matrix of eigenvectors are all real vectors.

ii. Calculate the steady state solutions of the system

The steady state solution can be calculated when the derivative for state variables remains to be zero. The steady state solution can be calculated as shown in equation 4.11:

$$X_p = -A^{-1}B\boldsymbol{u} \tag{4.11}$$

iii. Calculate the constants of the system of differential equations by applying the initial conditions

The scaling constants, or constants of integration, of the system can be found by the equation below:

$$[\boldsymbol{v}_1, \boldsymbol{v}_2, \boldsymbol{v}_3 \dots\dots, \boldsymbol{v}_l, \boldsymbol{a}_1, \boldsymbol{b}_1, \boldsymbol{a}_2, \boldsymbol{b}_2, \dots\dots \boldsymbol{a}_k, \boldsymbol{b}_k]\boldsymbol{c} = \boldsymbol{X}_0 - \boldsymbol{X}_p \tag{4.12}$$

Where $\boldsymbol{X}_0$ is the initial condition of the system, and $\boldsymbol{X}_p$ is the steady state of the system.

iv. Calculate the contribution coefficient matrix

The contribution coefficient means how much contribution the corresponding eigenvalue contributes to the system solution. The calculation for contribution coefficients including two parts. The first part is to calculate contribution coefficients for real eigenvalues and the second part is for complex eigenvalues.

The contribution coefficients for real eigenvalues can be calculated as:

$$D_{ij} = v_{ji}c_j \tag{4.13}$$

The contribution coefficient for the *j*th pair of complex eigenvalues are shown as below:

$$\begin{aligned} D_{ij} &= c_j a_{ji} + c_{j+1} b_{ji} \\ D_{i(j+1)} &= c_{j+1} a_{ji} - c_j b_{ji} \end{aligned} \tag{4.14}$$

Where a_{ji} and b_{ji} means the *i*th real and imaginary part for each pair of conjugate eigenvector $\boldsymbol{a_j}$ and $\boldsymbol{b_j}$.

The contribution coefficient matrix D is calculated based on the process before. In conclusion, the coefficient calculation method is selected based on the type of eigenvalues.

4.4 The Dynamic Solution of the system

The dynamic solution of each state variable of the system is calculated as the sum of each eigen-functions and the steady state solution, so the dynamic solution can be calculated into two parts for each state variable. With *n* state variables, it means there are *n* solutions to the system. The general solution with real eigenvalues of the system can be calculated as follows:

$$\boldsymbol{x}_r = \begin{bmatrix} \sum_{j=1}^{l} \left(D_{1j} e^{\lambda_j t}\right) \\ \sum_{j=1}^{l} \left(D_{2j} e^{\lambda_j t}\right) \\ \cdots \\ \sum_{j=1}^{l} \left(D_{nj} e^{\lambda_j t}\right) \end{bmatrix} \tag{4.15}$$

The general solution with complex eigenvalue of the system can be calculated as:

$$\boldsymbol{x}_c = \begin{bmatrix} \sum_{j=1}^{k} \left(D_{1(l+2j-1)} e^{\alpha_j t} \cos\left(\omega_j t\right) + D_{1(l+2j)} e^{\alpha_j t} \sin\left(\omega_j t\right)\right) \\ \sum_{j=1}^{k} \left(D_{2(l+2j-1)} e^{\alpha_j t} \cos\left(\omega_j t\right) + D_{2(l+2j)} e^{\alpha_j t} \sin\left(\omega_j t\right)\right) \\ \cdots \\ \sum_{j=1}^{k} \left(D_{n(l+2j-1)} e^{\alpha_j t} \cos\left(\omega_j t\right) + D_{n(l+2j)} e^{\alpha_j t} \sin\left(\omega_j t\right)\right) \end{bmatrix} \tag{4.16}$$

The response to the system model is composed of steady-state, real eigenvalues and complex eigenvalues. The solution of the system model can be calculated in Equation 4.17:

$$\begin{bmatrix} x_1 \\ x_2 \\ \cdots \\ x_n \end{bmatrix} = \boldsymbol{x}_r + \boldsymbol{x}_c + \begin{bmatrix} x_{p1} \\ x_{p2} \\ \cdots \\ x_{pn} \end{bmatrix} \tag{4.17}$$

4.5 Eigenvalue Analysis on Simple PEEC Circuit Model

4.5.1 The PEEC Circuit Model Generation

The validation of the eigenvalue analysis will be illustrated on a PEEC circuit model. The model including 2 cells of PEEC circuit. The partial mutual inductance and partial mutual capacitance are assumed to be zero in this example. The circuit of the model is shown in Figure 4.1:

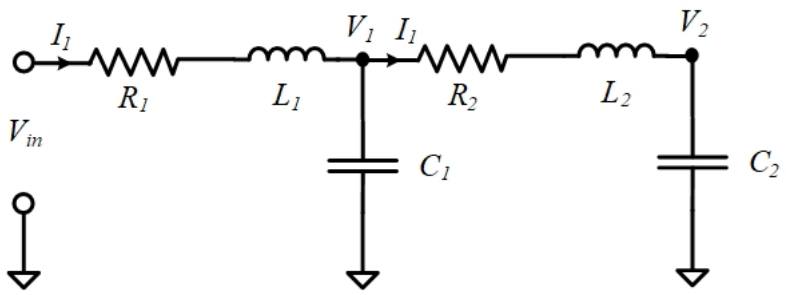

Figure 4.1 PEEC circuit with 2 cell

The system matrix of the PEEC circuit model can be generated based on KCL equations for nodes and KVL equations for branches. The system matrix can be generated as follows:

$$\begin{bmatrix} C_1 & & & \\ & C_2 & & \\ & & L_1 & \\ & & & L_2 \end{bmatrix} \begin{bmatrix} \dot{V}_1 \\ \dot{V}_2 \\ \dot{I}_1 \\ \dot{I}_2 \end{bmatrix} = \begin{bmatrix} 0 & 0 & 1 & -1 \\ 0 & 0 & 0 & 1 \\ -1 & 0 & -R_1 & 0 \\ 1 & -1 & 0 & -R_2 \end{bmatrix} \begin{bmatrix} V_1 \\ V_2 \\ I_1 \\ I_2 \end{bmatrix} + \begin{bmatrix} 0 \\ 0 \\ 1 \\ 0 \end{bmatrix} V_{in} \tag{4.18}$$

In the specific PEEC circuit model, after adding the elements values, the system matrices are:

$$M = \begin{bmatrix} 0.01 & & & \\ & 0.625 & & \\ & & 0.1 & \\ & & & 0.001 \end{bmatrix}$$
$$A = \begin{bmatrix} 0 & 0 & 1 & -1 \\ 0 & 0 & 0 & 1 \\ -1 & 0 & -2 & 0 \\ 1 & -1 & 0 & -10 \end{bmatrix} \quad (4.19)$$

The solution of this circuit is related to the system eigenvalue. The solution in time domain can be calculated using the process described in section 4.3.2, and the solution can be validated by circuit simulation software, such as Simulink.

4.5.2 Validation of Eigenvalue Analysis Method

4.5.2.1 Simulation Results of Original PEEC Circuit Model

Firstly, the PEEC circuit model is simulated in Simulink. A Simulink RLC circuit model is shown in Figure 4.2:

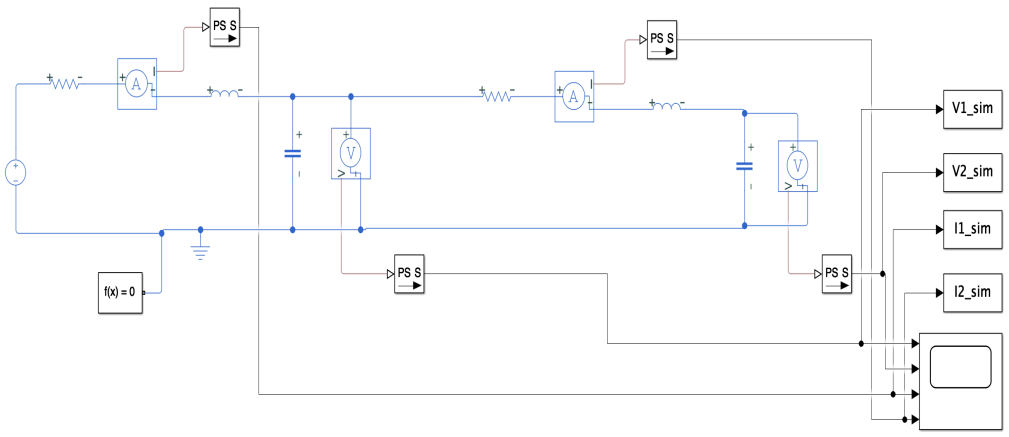

Figure 4.2 PEEC circuit model in Simulink

The time domain solution for each node voltage and branch current can be calculated by eigenvalue analysis method. The comparison between the calculated solution and simulation results is shown in Figure 4.3:

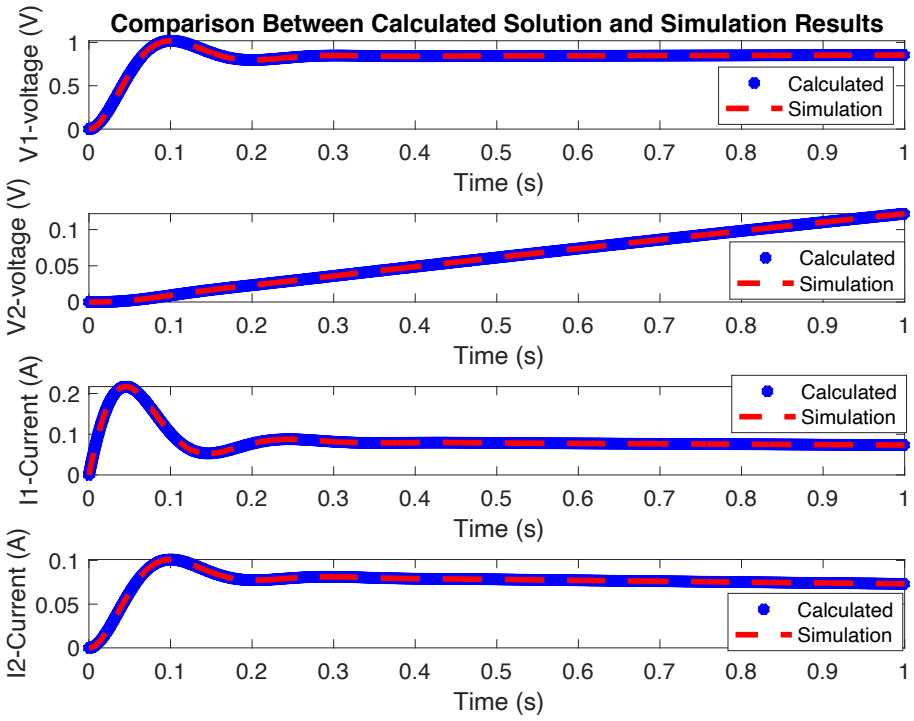

Figure 4.3 Comparison between the calculated solution and simulation results

The figure shows that the results for this simple circuit model matched each other very well. The calculated results are generated from the PEEC model and the simulation results are generated from the Simulink model. The calculated solution by eigenvalue analysis method can give the accurate results compared with Simulink. The error of the calculated solution can be used to show the accuracy of eigenvalue analysis method.

There is no significant error between calculated results and simulation results, so it means the eigenvalue analysis is correct. The error is calculated by the difference between the measured value and simulation results. The measured value for each state variable is calculated using the eigenvalues and eigenvectors of the system matrix.

4.5.2.2 Evaluation of Dominant Eigenvalue Analysis on Simple PEEC Circuit

The eigenvalue analysis methods will now be used to evaluate how a reduced model can be formed from the dominant eigenvalues of the original model. The eigenvalues of the original system, used to produce the results presented above, will be used to generate a reduced order model. The first step is to extract the dominant eigenvalue of the system using the process in section 4.3.2. The reduced model can be derived by building a transfer matrix based on the dominant eigenvectors, so the solution of the reduced model and the solution of the original model can be compared to validate whether the reduced model can give the accurate answer to the system.

Firstly, the eigenvalue of the original system matrix should be calculated. The dominant eigenvalue can be found by considering the contribution coefficient. Then the reduced model can be generated by transforming to the subspace. The transfer matrix between the original model and reduced model can be expressed as a set of "dominant" eigenvectors. There are three dominant eigenvalues found by contribution coefficient calculation, which is shown in table Table 4-1, so three eigenvectors are selected. The transfer matrix is related to the dominant eigenvectors of the original system. The matrix form of the reduced system is shown in Equation 4.20:

$$M_r \dot{x} = A_r x + B_r u \tag{4.20}$$

Where:

$$M_r = HMH^T = \begin{bmatrix} 0.601 & -7.5941e^{-4} & 0.0049 \\ -7.5941e^{-4} & 0.0092 & -0.0014 \\ 0.0049 & -0.0014 & 0.0088 \end{bmatrix}$$

$$A_r = HAH^T = \begin{bmatrix} -0.0802 & -0.1403 & -0.0967 \\ 1.0132e^{-4} & -0.0952 & 0.3096 \\ -6.4808e^{-4} & -0.2537 & -0.1757 \end{bmatrix}$$

$$B = HB = \begin{bmatrix} 0.0819 \\ -0.0473 \\ 0.2964 \end{bmatrix}$$

The matrix *H* is the transfer matrix and is calculated by extracting the eigenvector of the corresponding dominant eigenvalue. The eigenvalue and corresponding contribution coefficients and the eigenvalue of the reduced model are shown in Table 4-1:

Table 4-1 Eigenvalues of original model and reduced model

Original Eigenvalue ($\lambda, \alpha \pm \omega$)	**Contribution Coefficient (D)**	**Dominant?**	**Eigenvalue of MOR Model ($\lambda, \alpha \pm \omega$)**
-9.9898e+03	-1.007e-08	No	
-15.0184 + 31.22i	-0.166	Yes	-15.0184+31.22i
-15.0184 - 31.22i	-0.83	Yes	-15.0184-31.22i
-0.1334	-0.40	Yes	-0.1334

The contribution coefficient for the first eigenvalue of the original system is very small, So the other 3 eigenvalues are dominant eigenvalue. And the eigenvalue of the reduced model is almost the same with the dominant eigenvalue of the original model.

The comparison of the time domain solution between the original model and reduced model is shown in Figure 4.4:

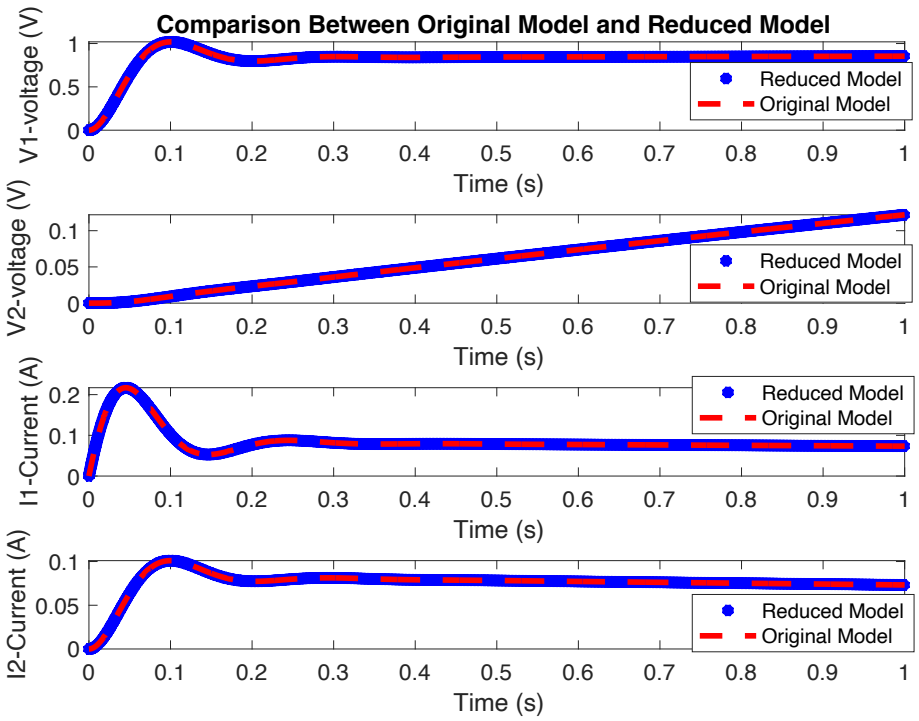

Figure 4.4 Comparison Between Original Model and Reduced Model

It's clear that the solution of the system matrix and the solution of the reduced model matches each other. In another word, it means that the reduced model can give the accurate solution if the dominant eigenvalue can be extracted. In the previous example, the reduced model is generated manually by selecting the dominant eigenvalues as an "ideal case" which is possible for simple circuits. Evaluation of MOR algorithms such as Arnoldi based algorithms will be illustrated later.

4.5.2.3 Evaluation of Terminal Impedance in Frequency Domain

In the meantime, the PEEC circuit is simulated in the VPPE design tool. PEEC circuit is shown in Figure 4.1. The impedance curve of the simple PEEC circuit is shown in Figure 4.5:

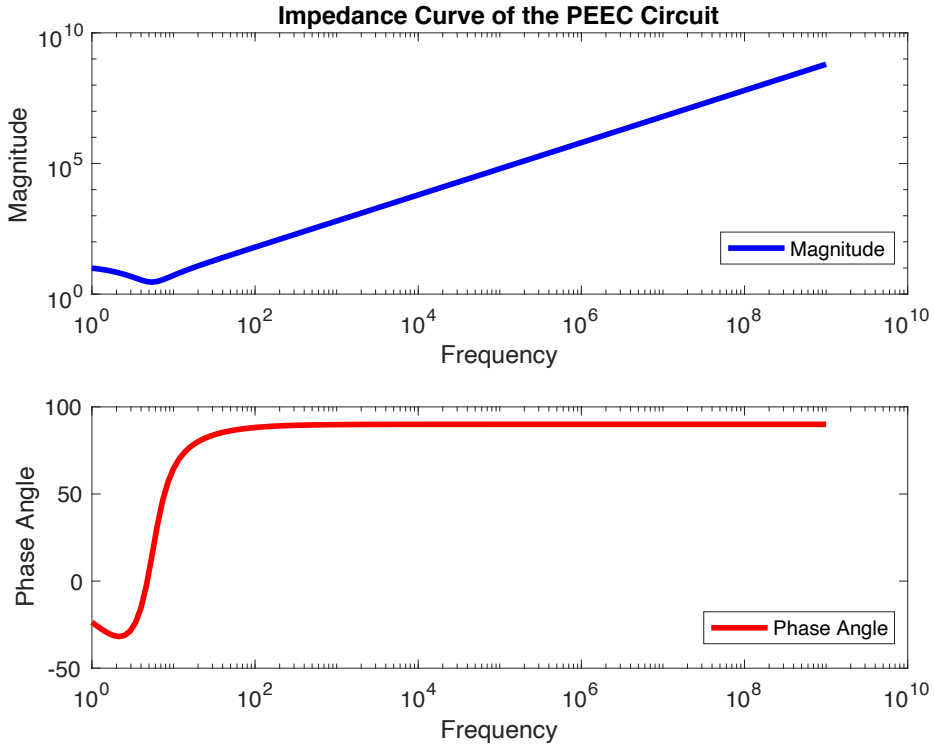

Figure 4.5 Impedance Curve of the PEEC Circuit

It is clearly shown from the impedance curve Figure 4.5, that the turning point happened at low frequency around 10*Hz*. The port impedance fluctuates at low frequencies, then the parasitic inductance play the dominant part in the frequency range from 100Hz to 1GHz.

The dominant frequency range is between 0 and 100Hz. So compared with Table 4-1, the dominant eigenvalue is located within the low frequency range, and the eigenvalue -9.9898e+03 is located at the much higher frequency, which is far from the low frequency range which includes important information.

The terminal impedance can be analysed by eigenvalue analysis as well, and all eigenvalues are used to predict the terminal impedance. The comparison of impedance curve between the simulation results in VPPE design tool and eigenvalue analysis method is shown in Figure 4.6:

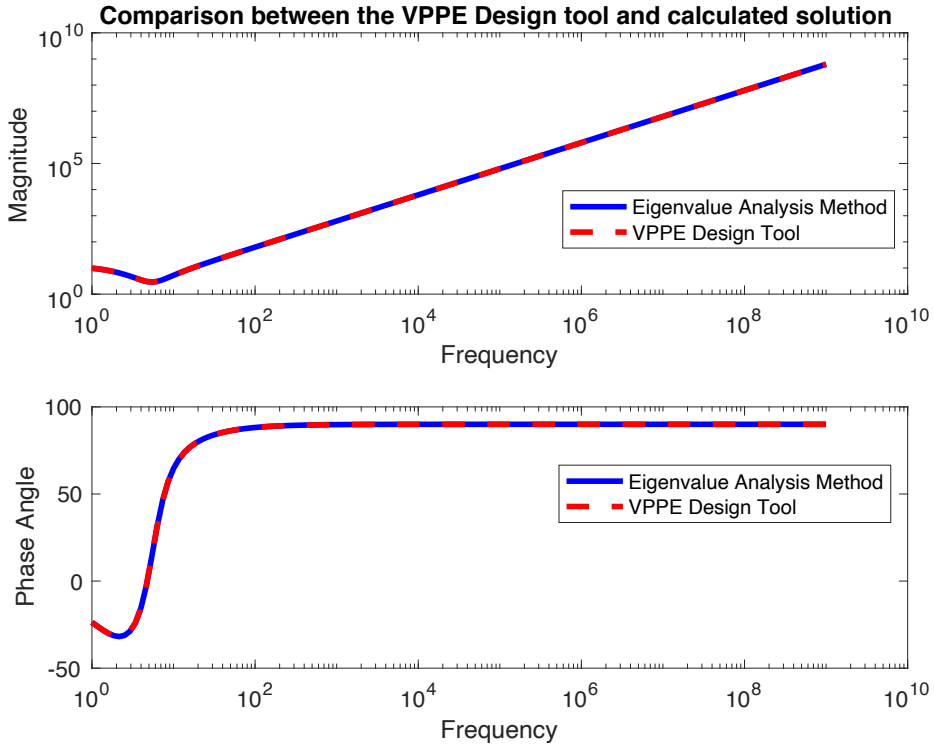

Figure 4.6 Comparison between the VPPE Design tool and calculated solution

It is clear that the results derived by eigenvalue analysis match the results given by VPPE designed tool. There is no obvious difference between eigenvalue analysis method and VPPE design tool. The error of eigenvalue analysis method is less than 0.1%. The comparison results show that the eigenvalue analysis method can give the accurate results in PEEC circuit model. The more complicated PEEC models include more meshing cells, there will be more state variable and more differential equation need to be generated.

The reduced model can be found through dominant eigenvalue analysis, the solution of the reduced model can be obtained by eigenvalue analysis, and this solution can be transfer back, using the transfer matrix *H*. The solution of the impedance curve of the original PEEC circuit model can be calculated by the transfer matrix. The comparison of the impedance curve between the original model and reduced model is shown in Figure 4.7:

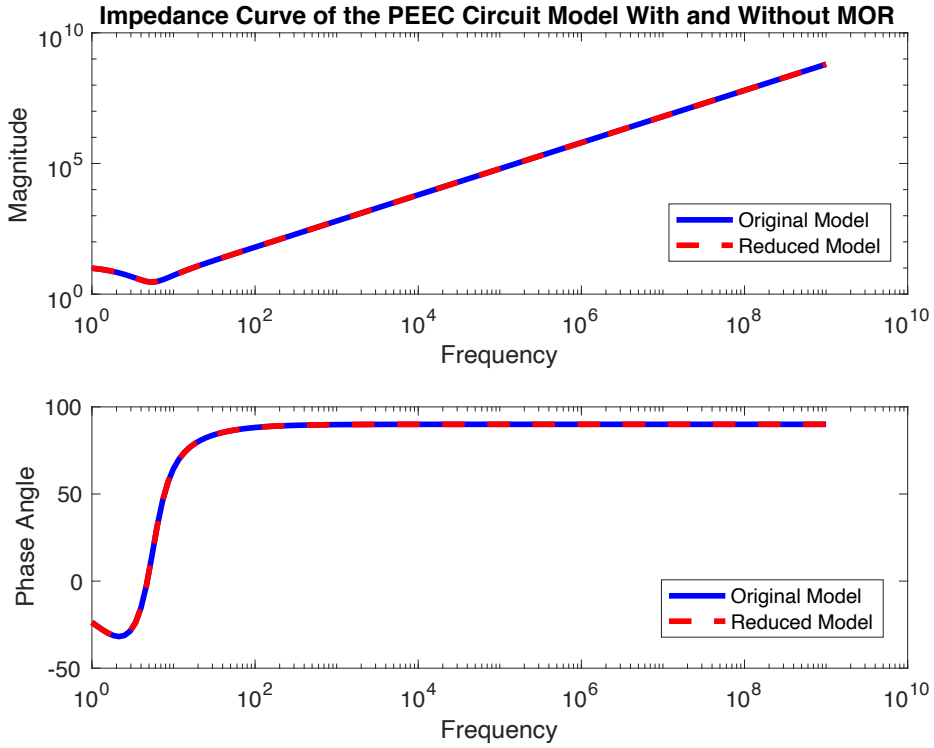

Figure 4.7 Impedance Curve of the PEEC Circuit Model With and Without MOR

The reduced model is generated using the dominant eigenvalues of the original model, and the results are the same. The error of the reduced model compared with original model is less than 0.1%. The reduced model can give the accurate solution when dominant eigenvalues are used to build the reduced model.

4.5.3 Relationship Between the Electrical Characteristic and the System Eigenvalue

The characteristic information is related to the eigenvalues and the dominant eigenvalue is related to the frequency range which has the most significant changes in the impedance characteristics.

Based on control theory, the general transfer function can be expressed in Equation 4.21:

$$G(s) = \frac{b_m s^m + b_{m-1} s^{m-1} + \cdots + b_1 s + b_0}{a_n s^n + a_{n-1} s^{n-1} + \cdots + a_1 s + a_0} \tag{4.21}$$

the transfer function of the system has a partial fraction expansion, so the system plant can be expressed in Equation 4.22:

$$G(s) = G_1(s) + G_2(s) + \cdots + G_k(s) \tag{4.22}$$

For each partial transfer function $G_i = \frac{N(s)}{D(s)}$, The denominator *D(s)* of transfer function *G(i)* can be expanded into two kind of the forms, the denominator of a first order system can be shown in Equation 4.23:

$$s + \sigma \tag{4.23}$$

The denominator of a second order system can be shown in Equation 4.24:

$$s^2 + 2\zeta\omega_n s + {\omega_n}^2 \tag{4.24}$$

So the system response is a linear combination of each individual term, and the term with the largest weight is the dominant eigenvalue.

The time constant is defined as:

$$\tau = \frac{1}{\zeta\omega_n} = \frac{1}{\sigma} \tag{4.25}$$

The poles can be expressed as the form of equation 4.26:

$$-\zeta\omega_n \pm j\omega_n\sqrt{1-\zeta^2} \quad (0 \le \zeta \le 1) \tag{4.26}$$

Considering different damping ratio situation ζ, the eigenvalues can be shown in Equation 4.27:

$$If\ \zeta < 1:\ \lambda = -\zeta\omega_n \pm j\omega_n\sqrt{1-\zeta^2} \tag{4.27}$$

$$If\ \zeta = 1\ :\ \lambda = -\omega_n$$

$$If\ \zeta \geq 1:\ \ \lambda = -\zeta\omega_n \pm j\omega_n\sqrt{1-\zeta^2}$$

The real part of the pole is -$\zeta\omega_n$. Small time constant means that the transient will decay very fast until reaching its steady-state. The real part of the eigenvalue is related to the frequency. For this simple PEEC circuit, the dominant characteristic is the resonant point which is determined by the capacitance and inductance values of the circuit. The resonant frequency is happened in lower frequency, and is close to the real part of the dominant eigenvalue.

The next step is to try to using dominant eigenvalue analysis to evaluate the MOR method on a more complicated and realistic PEEC circuit Model. A simple substrate example will be illustrated in the next section.

4.6 Evaluation of Eigenvalue Analysis of Standard MOR method (PRIMA) on a Substrate PEEC Model

4.6.1 Introduction to the substrate PEEC model

The theory of dominant eigenvalue analysis has been illustrated and validated on a circuit model that is representative of a small PEEC model. The next step is to analysis the results with a standard MOR technique and multi-expansion point MOR technique. The standard PRIMA algorithm usually chooses expansion point at DC, and identifies the dominant eigenvalues around the expansion point and so the eigenvalue analysis method may be used to investigate the poor performance of the reduced order model at higher frequencies.

The test case is a substrate model, the geometry of the model is shown in Figure 4.8:

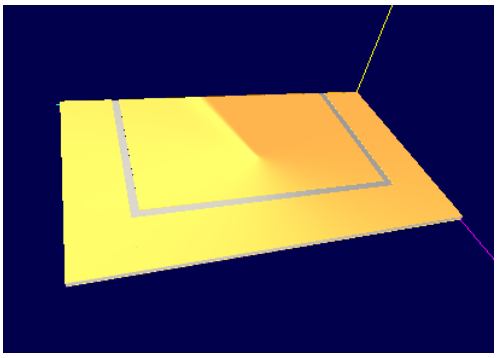

Figure 4.8 Substrate Model

There are three boundary conditions added to the model. A 1 Amp current source is added between the two end of the top copper layer. A fine mesh is used to generate good result. The meshing process generates 752 nodes, 308 cells and 1772 conductors, which results in 2527 equations.

4.6.2 Simulation Results of the Substrate Model With and Without MOR

4.6.2.1 Simulation Results of Impedance Curve

The simulation result of the impedance curve of the substrate with and without MOR is shown in Figure 4.9, where the DC expansion point is chosen for MOR.

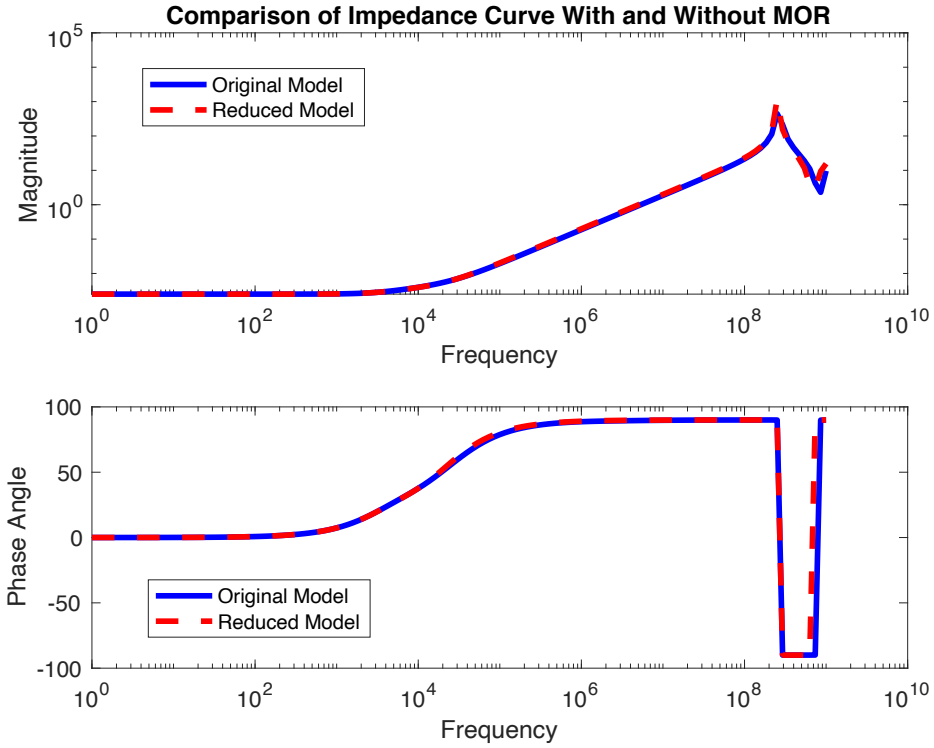

Figure 4.9 Impedance Curve of the substrate model

The simulation results for reduced model is almost the same as original model. From the impedance curve, the parasitic resistance is the dominant part, and the parasitic inductance tend to be the dominant part with the frequency increasing. The resonant frequency is between 205MHz and 215MHz.

From the impedance curve, the parasitic resistance, parasitic inductance and parasitic capacitance can be calculated. The *R, L, C* value of the model can be calculated from the magnitude and phase angle of the impedance curve, and is shown below:

$$R = 2.5e^{-3}\Omega, L = 3e^{-8}H, C = 2e^{-11}F$$

From the estimated value calculated by the impedance curve, the dominant frequencies in the system is around:

$$f_1 = \frac{1}{2\pi\sqrt{LC}} \approx 2.05468\times10^{8}Hz$$

$$f_2 = \frac{R}{L} = 83.3\times10^3 Hz$$

The resonance frequency is related to the system pole. Based on the control theory, the frequency response function is the transfer function evaluated along positive imaginary axis. The relationship between a system's eigen frequencies and system poles is shown in below:

$$f_{eig} = \frac{s}{2\pi} \tag{4.28}$$

Where *s* is the pole of a system. The dominant eigenvalue can be estimated by the resonant frequency from the impedance curve of the model.

The capacitive effect is disabled to evaluate the performance without capacitive coupling. Simulation results show that the impedance curve changes. The comparison of the impedance curve with and without capacitive effects is shown in Figure 4.10:

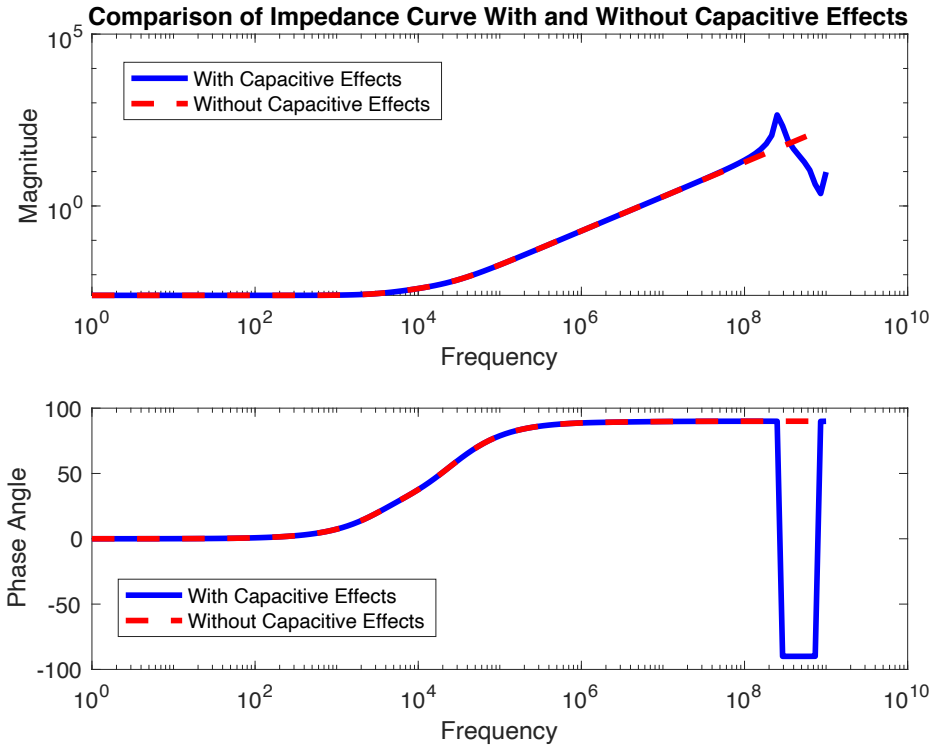

Figure 4.10 Comparison of Impedance Curve With and Without Capacitive Effects

From the impedance curve without capacitance effects, the capacitive effects start to play the dominant part in higher frequencies.

4.6.2.2 Simulation Results of Current Density

The surface current density is available to be plot through PEEC method. The interesting point is the influence of the MOR expansion point on the accuracy of the surface current density plots when applying MOR.

The standard MOR technique described in chapter 3 chooses only one point to expansion. The simulation time is very long if the MOR method is not being used. The simulation results for the surface current density distribution with and without MOR has been given in Table 3-1 from chapter 3.

From Table 3-1, It's clear that the simulation result applying single point MOR cannot give the accurate plot in higher frequency, which means it is missing the important information in the higher frequency range.

The substrate model can be simulated in Ansys software. The same model is simulated in Ansys Maxwell and the simulation results is shown in Table 4-2:

Table 4-2 Simulation Results of Current Density in Ansys Software

	Ansys	Standard MOR	
100Hz	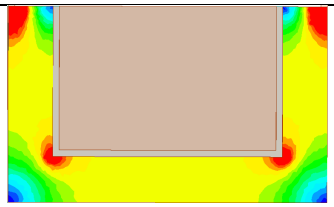		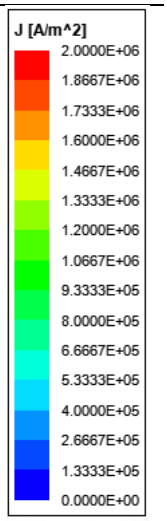
100KHz	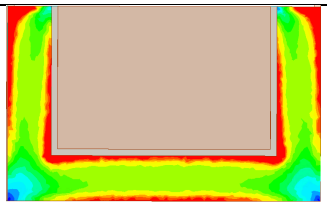	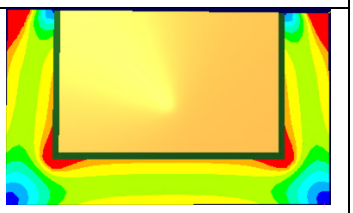	
100MHz	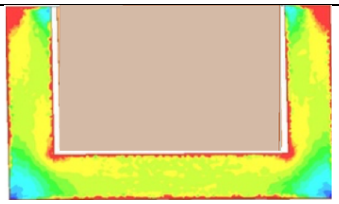	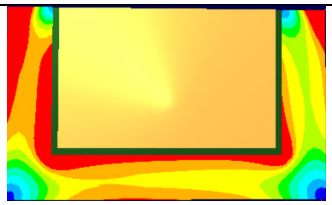	

From Table 4-2, the current density is only accurate at 100Hz when using standard MOR method. The current density at 100MHz is not symmetrical due to the limitation of standard MOR method and meshing issues. The next step is using dominant eigenvalue analysis method to analyse why standard MOR technique cannot give an accurate result in a wide range of frequency.

4.6.3 The Eigenvalue Analysis of the Reduced Order Model

The system matrix for this model can be extracted by VPPE software, and then the eigenvalue analysis can be used to find the dominant eigenvalue and the contribution coefficient for the original model. The system matrix of the reduced model can also be extracted and compared with the dominant eigenvalue of the original system. The process of how to find the dominant eigenvalue has been illustrated in the last section 4.3.2. The comparison of the eigenvalue distribution between the original model and reduced model with single expansion point is shown in Figure 4.11.

The y axis means the contribution percentage of the corresponding eigenvalue. The x axis means the value of eigenvalues, the first row corresponding to the real eigenvalues and the other two rows corresponding to the real part and imaginary part of the complex eigenvalues. To approximate the system response, the most important eigenvalues should be approximate in the reduced model. The eigenvalues with small imaginary part corresponding to the system response at lower frequencies; the eigenvalues with large imaginary part corresponding to the system response at higher frequencies.

The eigenvalues of the reduced model should close to the dominant eigenvalues of the original system to get accurate solutions. From the contribution of the real eigenvalues in Figure 4.11, only one of the dominant eigenvalues in the range from 10^4 to 10^5 can be extracted from the reduced model. It is obvious there is another dominant eigenvalue at 3×10^7, but not extracted by PRIMA algorithm. The dominant eigenvalue in low frequency is extracted, but the dominant eigenvalue in high frequency cannot be extracted from the reduced model.

From the dominant eigenvalue analysis, the PRIMA algorithm didn't identify the dominant eigenvalues in higher frequencies, and this is the reason of the existed error in current density approximation at higher frequencies.

In summary, the single point MOR cannot include all dominant eigenvalues from the contribution distribution. Single point MOR cannot give accurate results on current density plot through the whole frequency range.

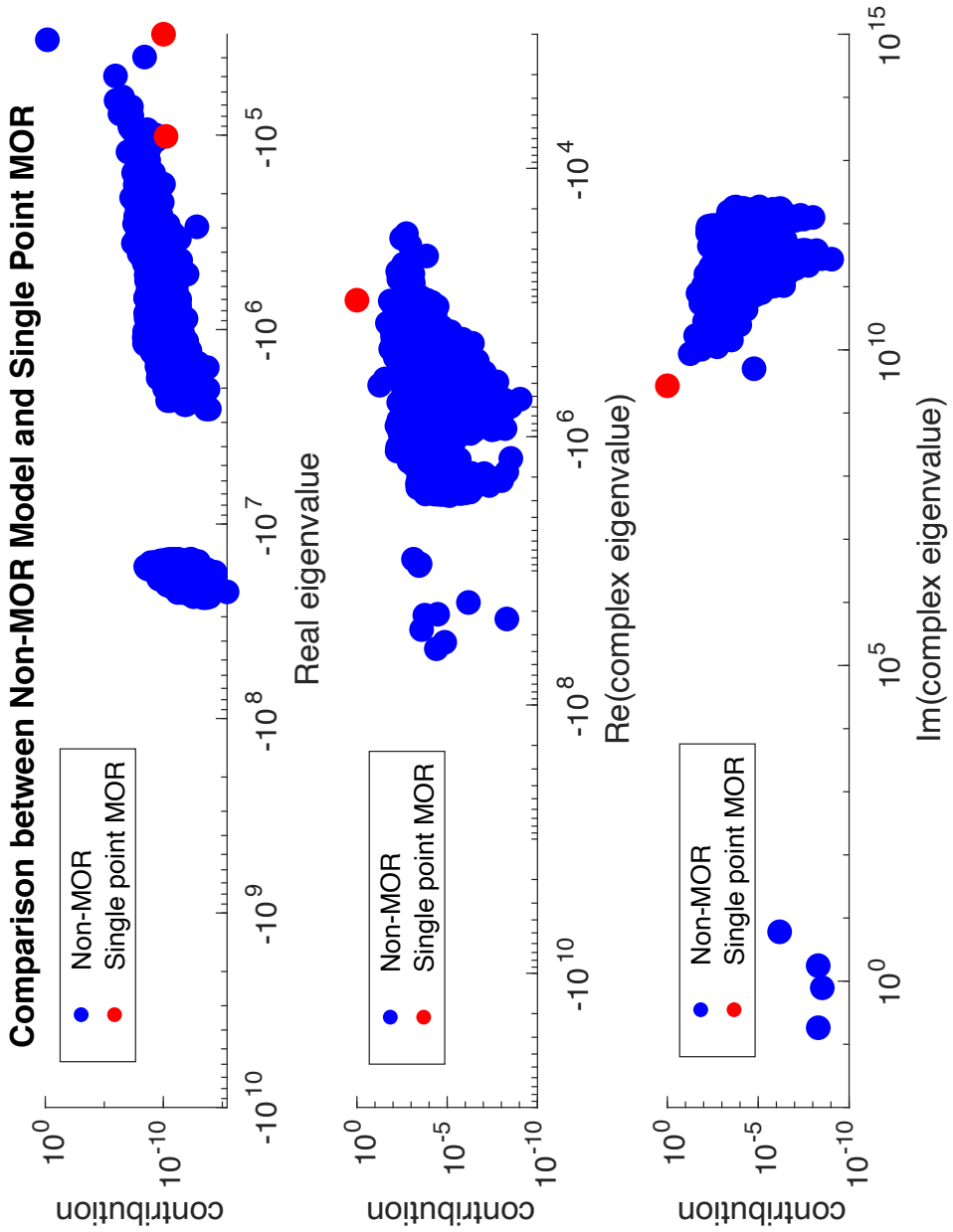

Figure 4.11 Comparison Between Non-MOR Model and Single MOR

The method used in Figure 4.12 is to analyse the dominant eigenvalue distribution of the original model and to find out whether the reduced model can extract the dominant eigenvalue correctly.

4.7 Summary

In this chapter, eigenvalue analysis method is proposed to analysis the simulation results. The aim of the eigenvalue analysis method is to find the reason why single point MOR cannot give accurate results.

The process of the analysis is illustrated in this chapter and a simple circuit model and substrate model is generated to show how the eigenvalue analysis method works.

From the analysis, it can be found that the accuracy of the simulation results is related to whether the dominant eigenvalues could be extracted from the original model. The difficulties are that how to choose the dominant eigenvectors for the dominant eigenvalues which are around the region of the frequencies of interest.

Chapter 5

5 Multipoint Model Order Reduction

5.1 Introduction

Electromagnetic characteristics of power electronic components are distributed across a wide range of frequencies. The limitation of the standard MOR method is that it cannot give accurate results across a wide frequency range because only one expansion point is used for reduced order model generation.

There exists multi-point MOR techniques, such as Rational MOR method[58], that can give accurate results across a wide range of frequencies through the uses of multiple expansion points.

A modified version of the PRIMA algorithm is proposed in section 5.3, the algorithm is a block type algorithm with multi expansion points. The algorithm is a solution to maintain accuracy over a wide-range of frequencies on 3D simulation, such as current density prediction.

In this chapter, the effectiveness of modified multi-point PRIMA applied to PEEC models will be investigated. It is important that not only does the multi-expansion

point approach lead to accurate inter-terminal characteristics but also an ability to predict internal variables (voltage and current density) for further analysis.

5.2 Background of Split MOR Approach

In the chapter 3, some basic Krylov subspace method are illustrated and the limitations of the standard MOR method are shown using simple examples. In summary, the Arnoldi method is based on moment matching at a single expansion point and cannot guarantee the global accuracy because it approximates the results near the expansion point.

This limitation can be optimized by multi-point expansion method, the principle is that the transfer function can be approximated by expanding at several points to produce a model formulated from the first moments matched at all expansion points[45]. Methods of this type have been developed and are called rational Krylov methods.

Rational Krylov methods can be used to solve large linear dynamic systems, such as large scale of electric radio RLC network[59]. They are based on standard methods to generate Krylov subspace, such as Lanczos method and Arnoldi method. The process for multi-point model order reduction is the extension to single-point model order reduction. The difference between them is the number of expansion points. A rational Lanczos algorithm which applied to large scale SISO (single input, single output) dynamic systems is introduced in [60] for model order reduction, two examples are given to show the advantages using multi-point Lanczos approaches compared with single-point Lanczos approaches. The issues of interpolation point selection for rational Lanczos algorithm is analysis in [61].

Arnoldi method is another approach widely used to generate Krylov subspace. For example, the Krylov based model order reduction can be extended to solve different type of problems, such as microwave circuits, EMC filters etc. It is more common to be used in wide frequency band. A block Rational Arnoldi algorithm with multiple expansion point is introduced in [58] which is applied for multiport RLC

networks. An Arnoldi based multipoint MOR algorithm is proposed in [62] to solve delayed PEEC Models and analyzed in a wide frequency range (0.0001Hz-20GHz), and two numerical examples are given to evaluate the accuracy between the reduced model and original model. Multipoint MOR method for inductive PEEC circuits is proposed in [63] and EMC filter is used as an example to evaluate the accuracy of adaptive multilevel fast multipole method(AMLFMM).

Multi-point MOR can also be used for scattering parameters extraction in electromagnetic systems, such as S parameter calculation in a wide frequency band for resonator antenna example described in [64].

In this work, the modified multi-point PRIMA algorithm is proposed. The difference between the proposed algorithm and conventional PRIMA is that multiple expansion points are chosen to achieve high accuracy within a wide frequency range. The proposed algorithm is applied to RLC PEEC model to achieve current density predictions in power electronics. Compared with other MOR techniques illustrated in chapter 3, the proposed algorithm keeps the advantages of passivity of PRIMA and provide comparable accuracy at higher frequencies.

In this chapter, the basic theory of multi-point MOR will be illustrated. Afterwards, the details of modified multi-expansion point MOR algorithm will be given in section 5.3. Finally, the validation and eigenvalue analysis on multi-point MOR algorithm will be given.

5.2.1 Multipoint Krylov Subspace Method

A general overview of the multi-point reduction procedure applied to PEEC models will now be given, subsequently this approach will be expanded to form a derivation of a modified, multi-point PRIMA algorithm.

Starting with the system matrix of the PEEC model can be written in state space form as shown in Equation 5.1:

$$M\dot{x} = Ax + Bu$$
$$y = Cx \tag{5.1}$$

In Krylov subspace methods, the state space model can be transferred to left-hand side representation because it is more convenient to generate Krylov subspace. The left hand representation form of state space model is shown in 5.2:

$$J\dot{x}(t) = x(t) + Ku(t)$$
$$y(t) = C \cdot x(t) \tag{5.2}$$

Where:

$$J = A^{-1}M$$
$$K = A^{-1}B$$

The transfer function of the general system is shown in Equation 5.3:

$$H(s) = C(sJ - I_n)^{-1}K \tag{5.3}$$

Padé approximation[65] can be used to approximate a function by a rational function of given order and is applied to estimate the system transfer function. The standard MOR technique usually choose one expansion point at 0 to make the Taylor series expansion of the transfer function. But more than one expansion points will be chosen in multi-point MOR approaches.

In standard MOR method, the Krylov subspace is defined as Equation 5.4:

$$Kr(J, K) = colsp[K, JK, J^2K, \cdots, J^{d-1}K] \tag{5.4}$$

Where *d* is the order number of Taylor expansion at expansion point. Multi-expansion point MOR will choose several expansion points, and the Krylov

subspace with multi-expansion points is constructed from vectors taken from each, as defined in Equation 5.5:

$$\begin{aligned} Kr(J,K) = colsp[K_0, \quad J_0K_0, \quad {J_0}^2K_0, \cdots, \quad {J_0}^{d_0-1}K_0, \\ \cdots K_{r-1}, \quad J_{r-1}K_{r-1}, \quad {J_{r-1}}^2K_{r-1}, \cdots, \quad {J_{r-1}}^{d_{r-1}-1}K_{r-1}] \end{aligned} \tag{5.5}$$

From the structure of the Krylov subspace, *r* is the number of the expansion points. The expansion points can be represented as σ_0, σ_1, ...σ_{r-1}. At each expansion point, a number of iterations are needed to generate the basis column vectors for that point, the number of iterations needed for each expansion point is represented by d_i. The general multi-point expansion reduction process is shown below:

Multi-Point MOR Process

Input: Original system matrix; $\{\sigma_r\}_{k=0}^{k=r}$ (expansion points); q (number of inputs); d_i
(number of reduced order for each expansion point)

1. Generate matrix V_1 through single-point model order reduction
2. $V=V_1$
3. For $k=0$, $k<=r$, $k++$
   Do: Generate Vk through single-point model order reduction
   V=[V Vk];
4. V=orth(V)

Output: Projection matrix V.

This is the general procedure of multi-point MOR method, there are different method to generate the subspace matrix V_k. The details on how to generate the basis vectors will be illustrated in next section.

5.3 Modified Multi-Point PRIMA Algorithm

PRIMA algorithm has been described in Chapter 3. The PRIMA algorithm is used for large scale coupled RLC circuit modelling and can guarantees passivity of the reduced model. The standard PRIMA algorithm uses a single expansion point, usually at 0Hz or DC. In this section, an algorithm for multi-point MOR based on conventional PRIMA algorithm is proposed. The modified multi-point PRIMA algorithm is the extended method from PRIMA algorithm. The inputs to the algorithm, matrices *A*, *B*, and *M* come from the PEEC state space model shown in Equation 5.1, and the output is the matrix V which can be used for reduced order model generation in the same way as the original algorithm.

The modified multi-point PRIMA algorithm is shown below:

Input: Matrix $A_{n\times n}$, $B_{n\times q}$, $M_{n\times n}$; Expansion points: σ_0, σ_1, …σ_{r-1} and integer orders, n is the size of the original model and q is the number of inputs, d_0, d_1, …d_{r-1} is the number of blocks for each expansion point.

Output: The orthonormal matrix V.

Set $m = 0$

//For each expansion point chosen

For ($k=0$; $k<r$; $k++$){

//Compute first block at each expansion point

For ($i=0$; $i< q$; $i++$){

// Get new vector from column i of input matrix B

Solve $(A+\sigma_k M)\boldsymbol{V_m} = \boldsymbol{B_i}$ for $\boldsymbol{V_m}$

// Orthogonalise against all previous vectors

For ($j=0$; $j<m$; $j++$){

$P_{jm} = \boldsymbol{V_j}^T \boldsymbol{V_m}$

$\boldsymbol{V_m} = \boldsymbol{V_m} - \boldsymbol{V_j} P_{jm}$

}

$\boldsymbol{V_m} = \boldsymbol{V_m}/|\boldsymbol{V_m}|$

// Add new vector as column of output matrix

$V = [V\ \boldsymbol{V_m}]$

m=m+1

}

// Generate remaining blocks for this expansion point

For ($p=1$, $p<d_k$;$p++$){

For ($i=m$; $i<m+q$; $i++$){

// Get new vector from corresponding vector in previous block

Solve $(A+\sigma_k M)\boldsymbol{V_i} = M\boldsymbol{V_{i-q}}$ for $\boldsymbol{V_i}$

// Orthogonalise against all previous vectors

For ($j=0$; $j<i$; $j++$){

$P_{ji} = \boldsymbol{V_j}^T \boldsymbol{V_i}$

$\boldsymbol{V_i} = \boldsymbol{V_i} - \boldsymbol{V_j} P_{ji}$

}

// Check for convergence

If($|\boldsymbol{V_i}|$ < tol) break;

$\boldsymbol{V_i} = \boldsymbol{V_i}/|\boldsymbol{V_i}|$

// Add new vector as column of output matrix

$V = [V\ \boldsymbol{V_i}]$

```
        }
// Increase total vector count by number of new vectors
      m=i+1
      }
   }
   Output: V = [V_0, V_1, ... V_{m-1}]
```

The modified PRIMA algorithm is similar to standard PRIMA algorithm, the difference between them is the modified multi-point PRIMA algorithm chooses several expansion points to generate the subspace. The first step is to generate the first block vector from each column in Matrix *B*, then generate new block of vectors from previous vectors at each expansion point and orthogonalise these vectors.

When the algorithm converges the new basis vector may have no significant component that is orthogonal to all previous vectors and therefore the normalization can fail, in this case the iterations for the current expansion point are terminated and the algorithm continues at the next expansion point.

In summary, the output matrix generated through modified multi-point PRIMA algorithm is $V_{n\times m}$. In other words, the total number of column vectors is *m*. Each expansion point is repeated a number of iteration steps to generate basis vectors. Gramm-Schmidt process [66] is applied to each column vector generated and make sure the vector is orthogonal to each previous one.

5.4 Evaluation of Multi-Expansion Point PRIMA

In this section, test examples will be used to evaluate the accuracy of multi-point MOR algorithm. The simulation results of terminal impedance and current density will be given in following sections.

5.4.1 Evaluation on Terminal Impedance Prediction

With the development of WBG devices, the EMI issues caused by high switching frequency is the challenge. The parasitic inductance and parasitic capacitance can affect the performance of power devices. There is a tradeoff between the switching

speed and the efficiency of power devices. One solution is to optimize the design of PCB layout at the design stage. Parasitic parameter extraction is important at the design stage for power electronics. One example will be used as an example to validate the performance of terminal impedance.

5.4.1.1 Test Example

The test example is shown in Figure 5.1:

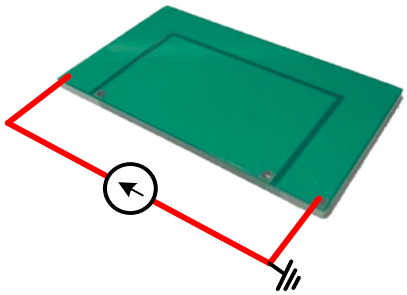

Figure 5.1 Test Example for Terminal Impedance Validation

This example is typical of a current carrying ceramic substrate that might be found in a power electronic semiconductor module. There are three boundary conditions added to the model. A 1A current source is added between the two ends of the top copper layer.

5.4.1.2 Simulation and Experimental Results

The U shape copper conductor on the PCB is modelled in VP software and the terminal impedance between the two ends of the copper track is extracted. The experimental tests for this PCB on ENA analyzer and impedance analyzer can be used as reference. The PCB board in measurement equipment is shown in Figure 5.2 :

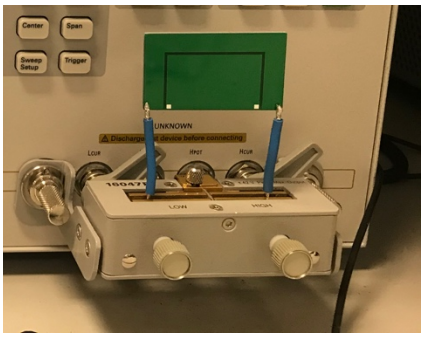

Figure 5.2 Experimental Test on Impedance Analyser

The model is simulated in VP software with different MOR settings and all other simulation settings are the same. The meshing process generates 752 capacitive nodes, and 1772 current carrying conductors, which results in 2527 equivalent circuit equations for the system.

The comparison of the terminal impedance between the experimental tests and simulation results is shown in Figure 5.3:

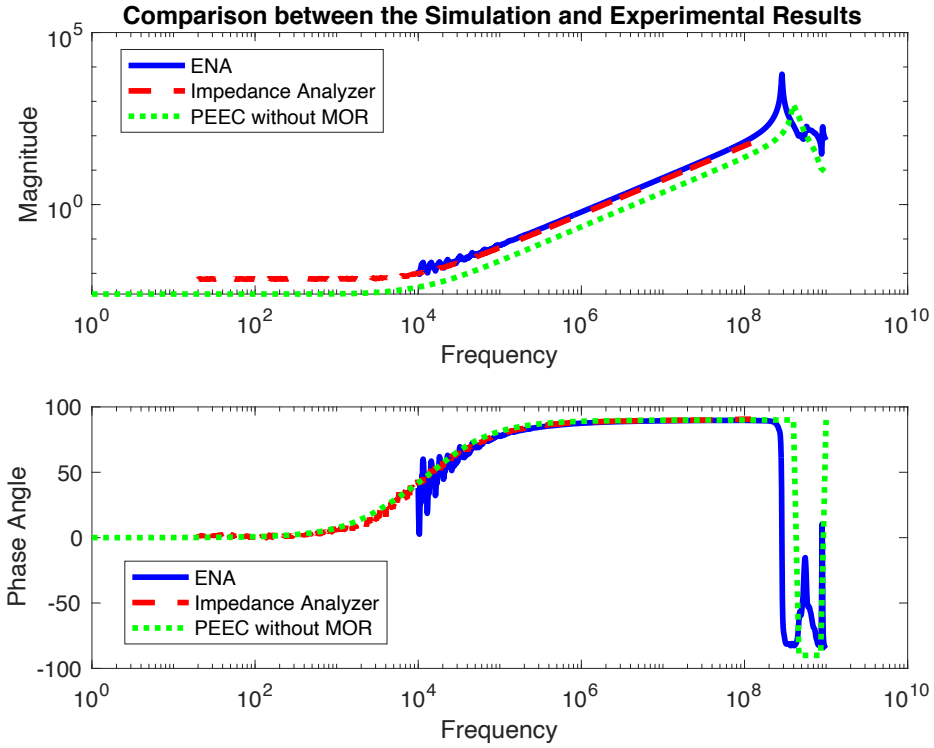

Figure 5.3 Comparison Between Simulation and Experimental Results without MOR

The extracted terminal impedance from VP software almost match the experimental results from Figure 5.3. The small magnitude of the impedance is because the connector and cable affected the terminal impedance on measurement equipment. There is a steady state test rig error between the simulation results and experimental results. It is affected by test environment, such as the connector and cable. The offset can be compensated in every specific test case. For this specific test case, the offset is around 0.02 Ω at 100KHz.

The comparison of terminal impedance among different MOR settings are shown in Figure 5.4:

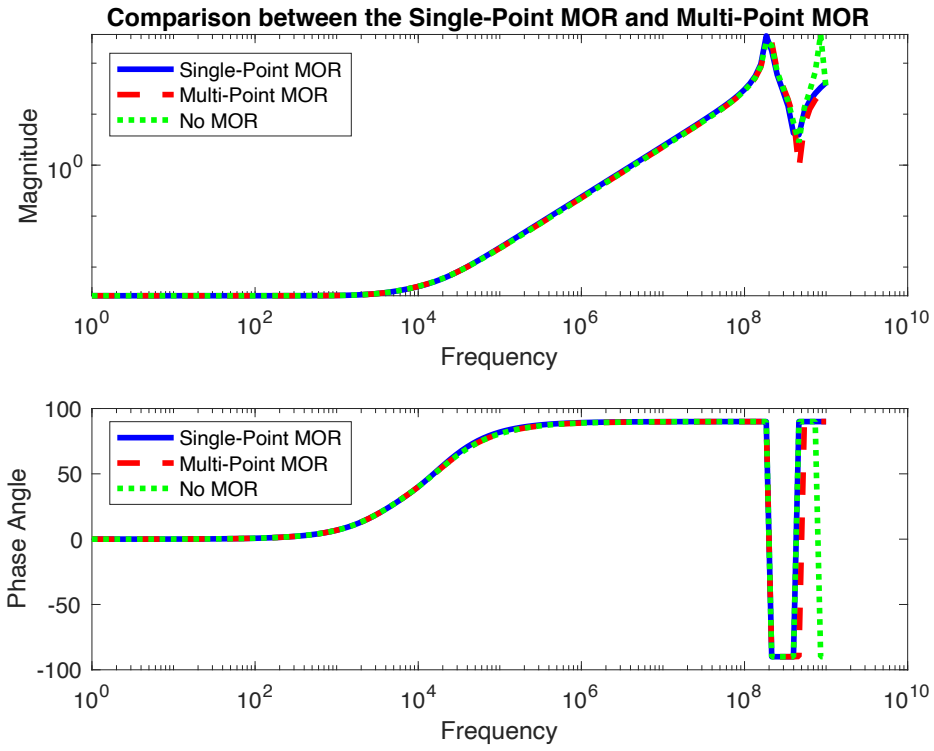

Figure 5.4 Comparison between the Single-Point (DC) MOR and Multi-Point MOR with Expansion Points at (100Hz,100KHz,100MHz)

For simulation with multi-point MOR, there are three expansion points and they are 100Hz, 100KHz, and 100MHz. More analysis of expansion point placement will be given in chapter 6. The total simulation time without MOR is 1954.6s. Total simulation time for single-point MOR and multi-point MOR are 122s and 127s

separately. The initial results show that multi-point Model Order Reduction has only a small increase in simulation time compared with single point MOR.

At high frequencies, the simulation results on different settings may have a bit deviation, this is because PEEC method is not full wave electromagnetic modelling method. It won't affect the EM modelling in power electronics because the frequency of interest for WBG devices is in the range of MHz.

From the Figure 5.4, The terminal impedance predictions for multi-point MOR and almost identical to those for single point MOR and so the use of multiple expansion points does not appear to offer significant benefits. The evaluation of multi-point MOR method on current density distribution, where the limitations of single point MOR are more pronounced, will be discussed in next session.

5.4.2 Evaluation on Current Density Distribution

The current density is important for thermal management on power electronics because it may cause in high temperature due to heat generation. The current level can affect the circuit performance and determined the dimension and layout on the design stage of power electronics. Especially at high frequencies, the current density will increase on the surface region due to skin effect. So the analysis of current density is needed for power electronics [67].

5.4.2.1 Test Example

The same test example is chosen to evaluate the accuracy of multi-point MOR algorithm on current density distribution. The test case is the same substrate PCB board shown in Figure 5.1.

This 3D model of the substrate in VP Software is shown in Figure 5.5:

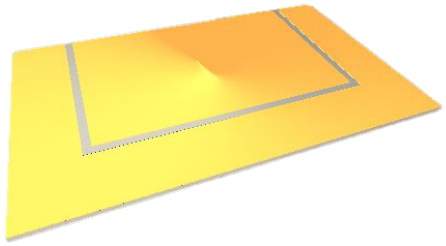

Figure 5.5 Substrate Model in VPPE

5.4.2.2 Simulation Results

To capture more details of current density plot, a fine mesh is needed to get accurate results of current density distribution. The mesh structure is denser than the mesh structure used for terminal characteristics. The simulation time will increase because of the fine mesh structure. The meshing process generated 1948 capacitive nodes, and 4646 current carrying conductors, which results in 6602 equivalent circuit equations for the system. The total simulation time without MOR is 33379.6s. The composition of the simulation time for this test case is shown in Table 5-1:

Table 5-1 Simulation Time

	PEEC Model Generation	MOR (optional)	Time/Freq. Stepping	Total Simulation Time
Original Model	90s	No	244s×136steps	33379.6s
Single Point MOR	90s	260s	0.015ms×136steps	350s
Multi-Point MOR	90s	410s	0.013ms×136steps	503s

There is overhead involved in computing the reduced order model during simulation process. The advantage is that the subsequent time/frequency stepped simulation is much faster per step.

To evaluate the current density distribution, Ansys Software can be used as reference of the simulation results. 100Hz and 100KHz are chosen to show the changes of current density distribution when increasing the frequency. The simulation results in Ansys software and VP software are shown in Figure 5.6 :

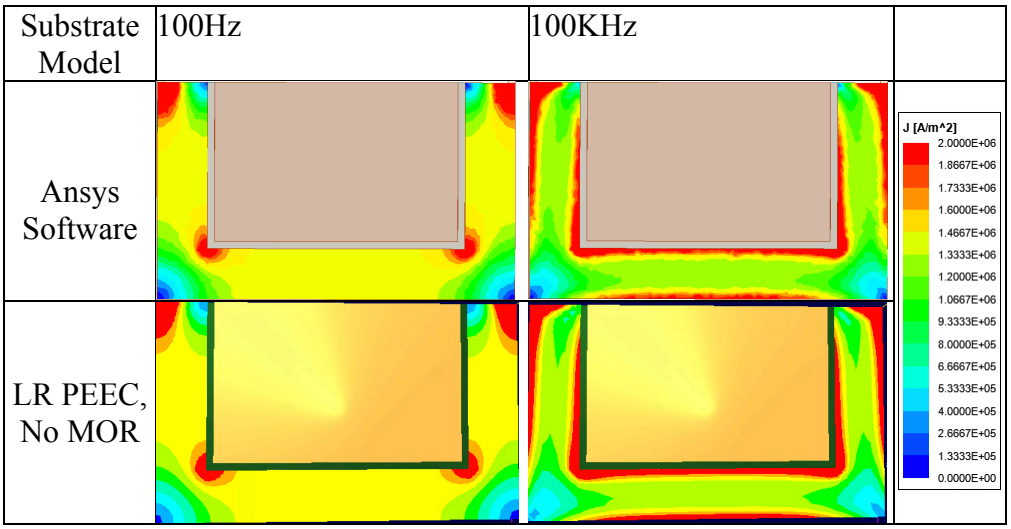

Figure 5.6 Comparison on Current Density Distribution

The PEEC simulation results (obtained using the VPPE power electronics virtual prototyping tool) matched the simulation results in Ansys software at 100Hz and 100KHz. From the figure, the current density is largest near the edge surface of the copper track, and decreases from surface towards the centre. This is expected due to "skin effects" which lead to the majority of current flowing within a small distance of the conductors outer surface – the skin depth. The important observation from these result is that the non-MOR enabled PEEC model and meshing settings used are sufficient to accurately capture this effect in the 100Hz-100KHz frequency range.

The accuracy of the MOR enabled models was then tested and a comparison of the current density plot with different MOR settings is shown in Figure 5.7:

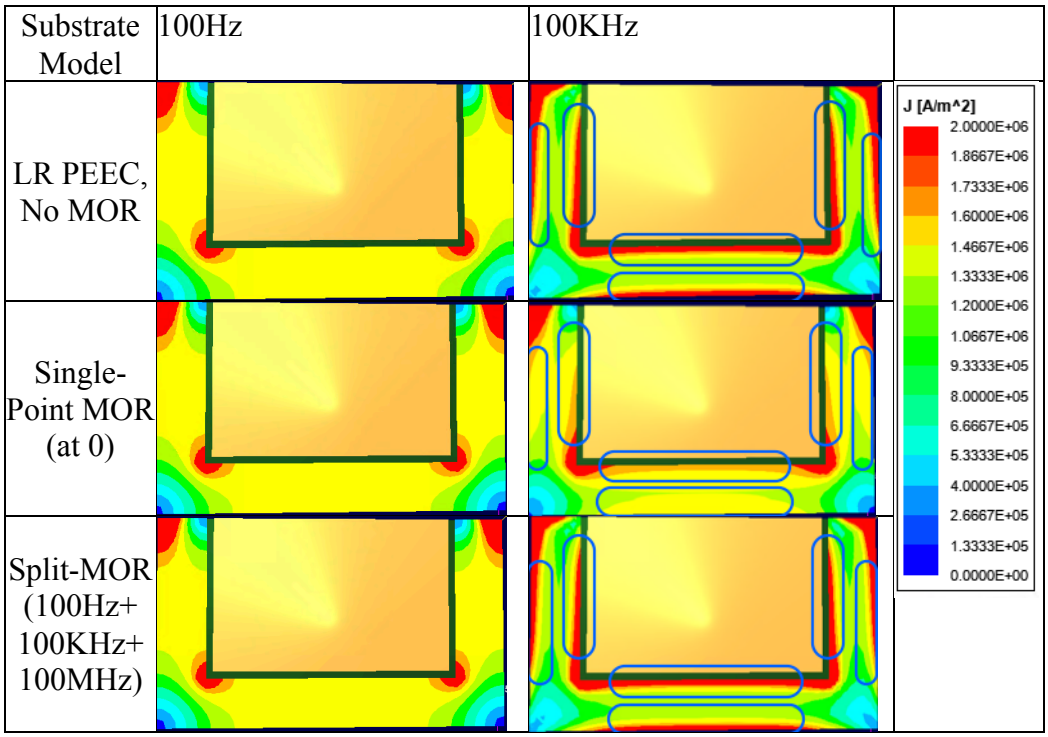

Figure 5.7 Comparison Between different MOR settings

The differences among the single-point MOR, multi-point MOR and non-MOR model on current density prediction at 100KHz has been highlighted on images with rectangular in blue colour.

The total simulation time with single-point MOR and multi-point MOR are 350s and 503s separately, and the size of the reduced model is 10 equations and 37 equations separately. To generate accurate 3D current density plot, more equations are generated after meshing process. 3D current density plot will take longer simulation time than terminal impedance prediction. The iterations for expansion point 100Hz are terminated at vector 5 because |V5| = 1.63665e-017, which is too small. There are two blocks generated through first expansion point. Then the algorithm will start the iterations for next expansion point at 100KHz, and terminated at vector 31, which generate 8 blocks.

The simulation results with single-point MOR is shown at the second row. The current density plot at 100Hz is correct, but the current density at 100KHz is different compared with original simulation results without MOR. This limitation

of single-point MOR can be improved by multi-point MOR method. The third row of Figure 5.7 shows the correct results at both 100Hz at 100KHz.

In summary, the simulation results applying more shift points can give the accurate results in a wide frequency range compared with single-point MOR method.

5.5 Eigenvalue Analysis on Reduced Model with Multi-Expansion Point MOR

In MOR process, the transfer matrix can be generated through MOR algorithm, then reduced model can be transferred from the original model. To get more accurate solution from the reduced model, the eigenvalue of the reduced model need to be very close to the dominant eigenvalues of the original model with number of iterations.

The dominant eigenvalue analysis has been described in chapter 4, the contribution coefficient can be used to analysis the contribution of the system response from each eigenvalue.

The eigenvalue distribution of original model and single-point reduced model is shown in Figure 5.8 and the eigenvalue distribution of original model and multipoint reduced model is shown in Figure 5.9:

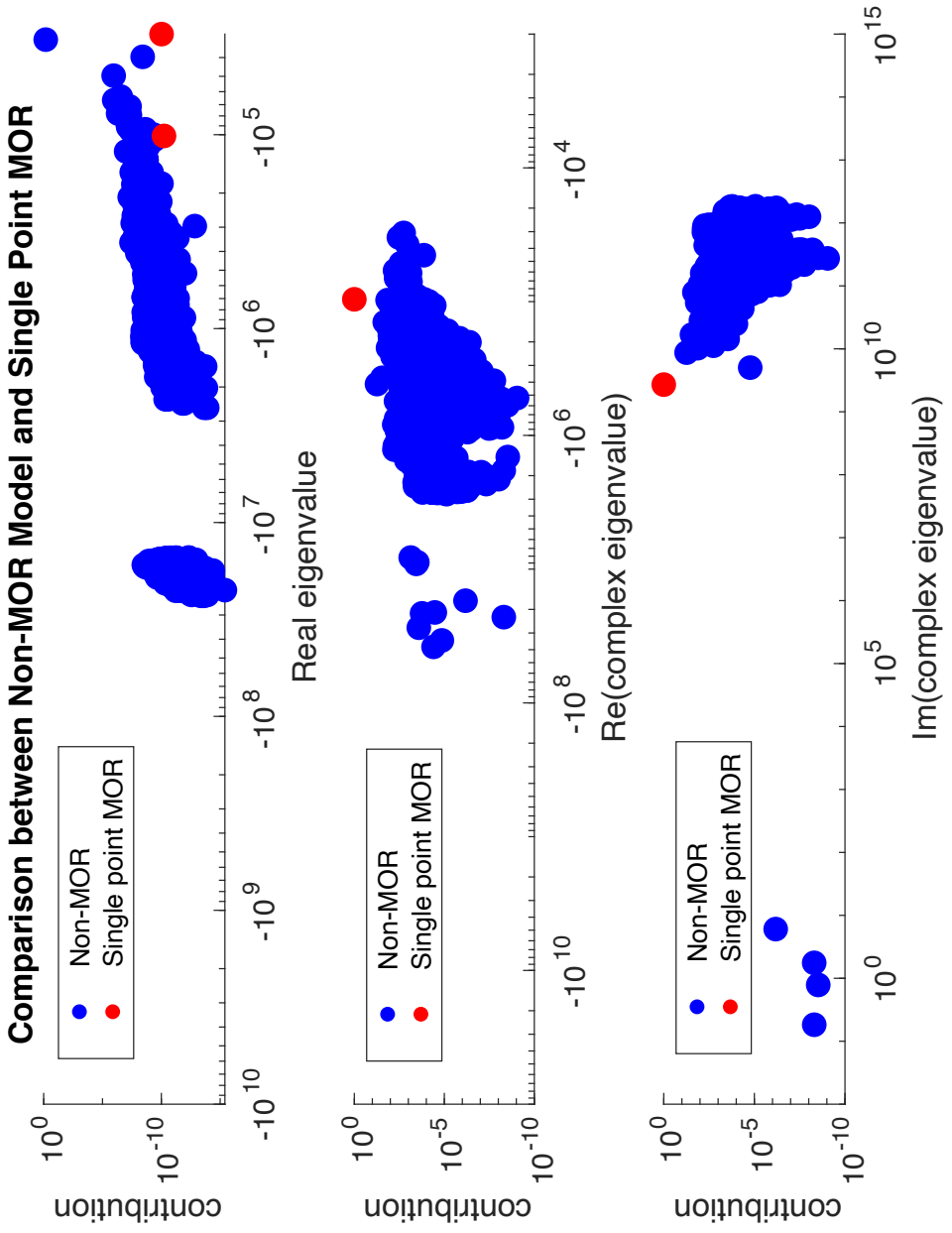

Figure 5.8 Comparison between Non-MOR model and Single-Point MOR

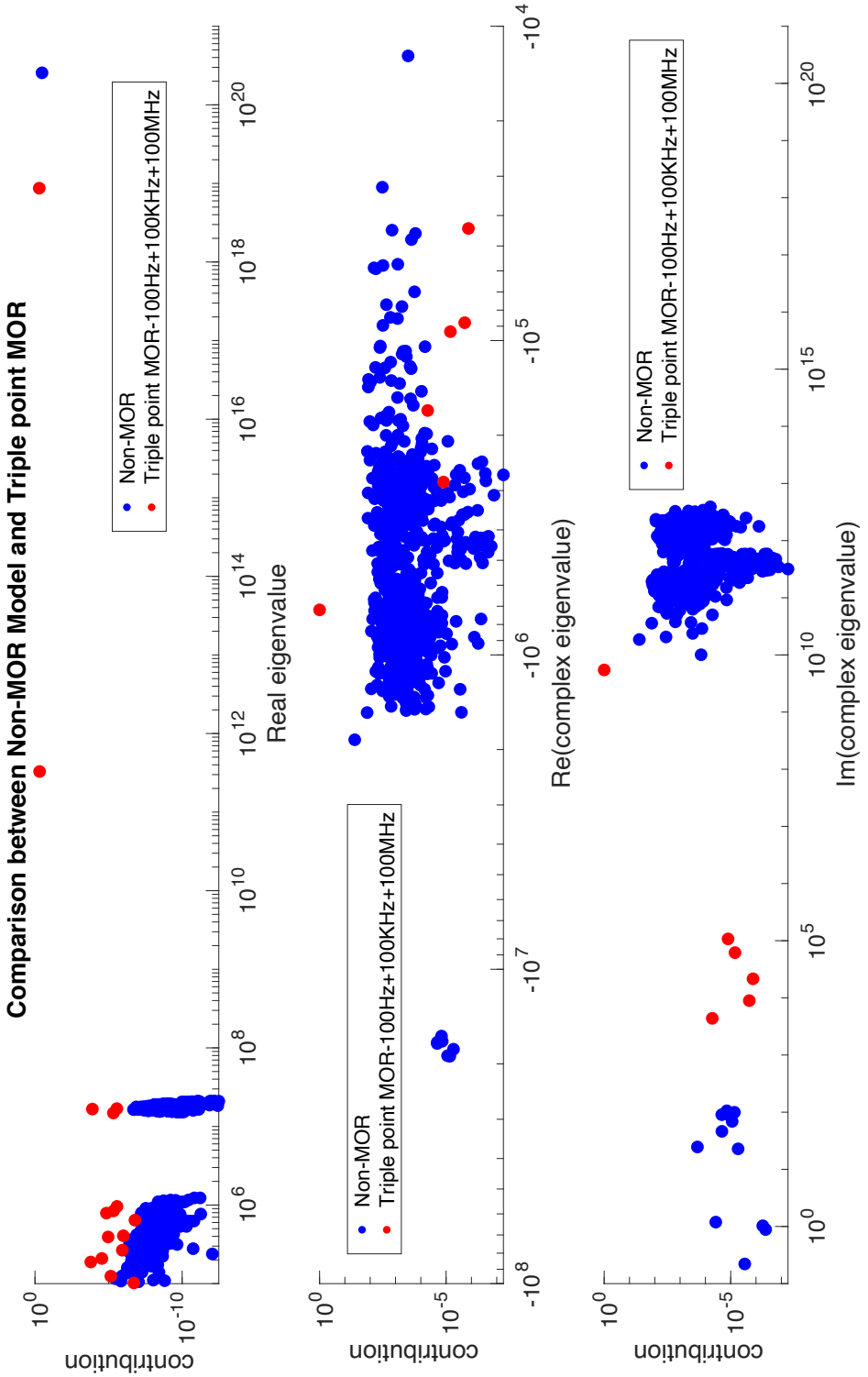

Figure 5.9 Eigenvalue Distribution of Original and Reduced Model

From Figure 5.9, it can be seen that there are three expansion points used in the multi-point MOR method. The eigenvalue distribution and corresponding contribution coefficient among the wide frequency range are shown in Figure 5.9. Compared with Figure 5.8, the eigenvalue distribution of multi-point MOR method matched eigenvalue distribution of the original model better than single-point MOR method, which extracted the dominant eigenvalues in the range from -10^4 to -10^6 and the range from -10^7 to -10^8. From the contribution of the real eigenvalues in Figure 5.8, only one of the dominant eigenvalues in the range from -10^4 to -10^5 can be extracted from the reduced model. Therefore, the eigenvalue of the reduced model can match the dominant eigenvalue of the original system if multiple expansion points are selected.

5.6 Summary

This chapter introduces the multi-point MOR method. Firstly, background of the multi-point MOR and its application are introduced. In section 5.3, the technical details of modified multi-point PRIMA algorithm are described.

To evaluate the accuracy of multi-point MOR method, an example test case is used to evaluate the performance of multi-point MOR method. The evaluation is from two direction: terminal impedance and current density distribution. Experimental results and simulation results from Ansys software are given as reference. From these results, the results of current density distribution improved and becomes better after applying multi-point MOR method. The eigenvalue analysis of the reduced model is given in this chapter, which shows more dominant eigenvalues are captured by multi-point MOR method.

In summary, given these simulation results and eigenvalue analysis in this chapter, the improvement of the accuracy of current density prediction by generate the Krylov subspace with a few expansion points are discussed. The work has been validated on a simple example to show the accuracy on multi-expansion point MOR technique used in developed VP design tool. Multi-expansion point MOR

can give better results compared with single point MOR when modelling EM performance in a wide frequency range.

Chapter 6

6 Expansion Point Selection for Model Order Reduction

6.1 Introduction

In previous chapters, standard model order reduction and multi point model order reduction has been evaluated on impedance prediction and current density prediction. The limitations of single point model order reduction can be improved by multi point model order reduction.

The computation cost of Krylov subspace generation through multi point model order reduction is more increased compared with standard model order reduction. The number of expansion points and the placement of selected expansion point of model order reduction is therefore very important.

In this chapter, firstly, the effect of expansion point placement will be analysed on an example for single point model order reduction, and the effects on different expansion points combination for multi-point model order reduction will be analysed.

6.2 Expansion Point Selection with Single-Point MOR

6.2.1 Current Density Prediction

The same example will be used to evaluate the influence on expansion point selection on current density prediction with single point model order reduction technique. The test case is shown in Figure 6.1:

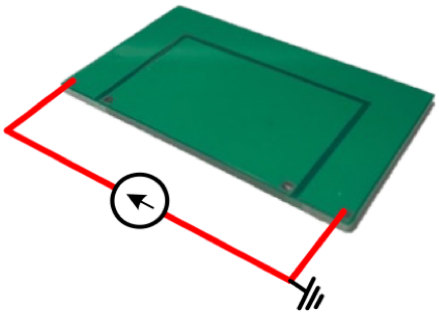

Figure 6.1 Test Case

The simulation results with single point model order reduction on current density is shown in Table 6-1:

Table 6-1Current Density Plot with Single Expansion Points at Different Frequencies

	100Hz	100KHz	100MHz
No MOR			
Single-Point (at 0)		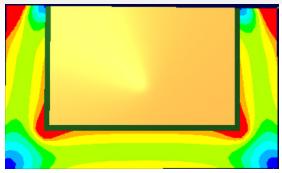	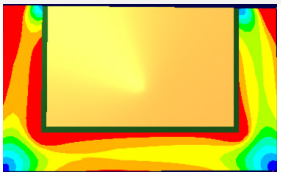
Single-Point (100KHz)	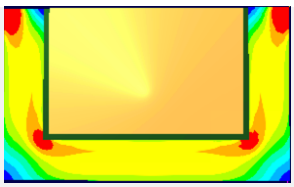	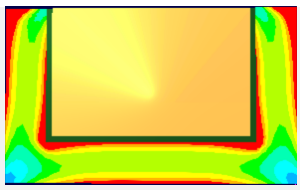	
Single-Point (100MHz)	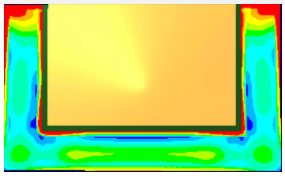	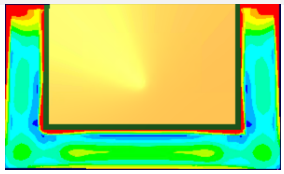	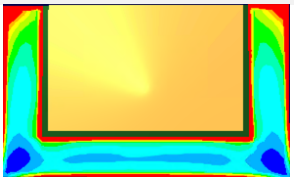
	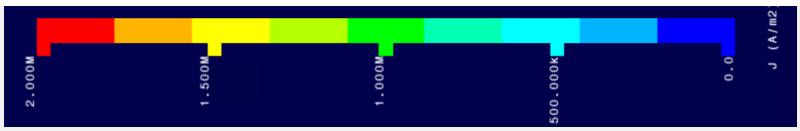		

The simulation results with single-point model order reduction at different point placement is given in Table 6-1. All the simulation results are obtained with same mesh settings and the scale is from 0 (A/m^2) to $2e^6$ (A/m^2).

From the simulation results above, the simulation results on current density prediction are more accurate towards the expansion point. For example, When the expansion point is chosen at low frequency, the current density is more accurate towards the expansion point. When the expansion point is chosen at higher frequency, the current density is more accurate towards high frequency.

In summary, conventional single-point MOR technique can be used when only specific frequency is required for simulation. The expansion point selection is chosen based on frequency of interest. The closer the expansion point is to the required frequency, the more accurate the results are.

6.2.2 Eigenvalue Analysis

Based on the comparison of simulation results with different expansion point, eigenvalue analysis can be applied to different reduced model. The comparison of eigenvalue analysis on different reduced model is shown in Figure 6.2:

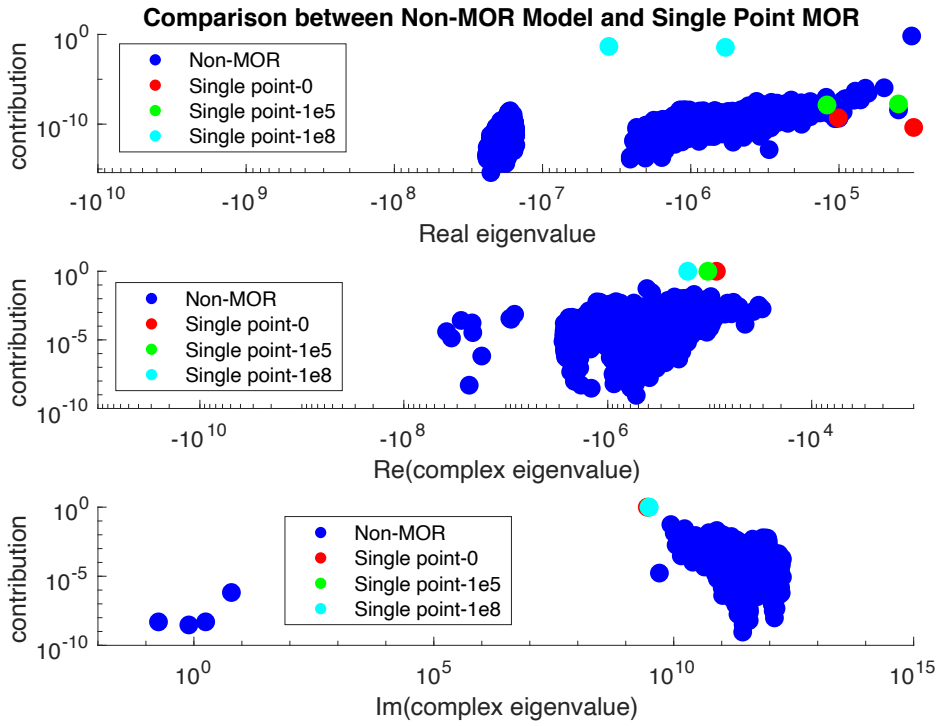

Figure 6.2 Eigenvalue Analysis on Single Point MOR

From the analysis, comparison of numerical values of eigenvalues in reduced model with different expansion point is shown in Table 6-2:

Table 6-2 Comparison of Eigenvalues in Reduced Model

Expansion Point	Eigenvalues in Reduced Model
0	-3.03×10^{4}, -1×10^{5}
1×10^{5}	-4×10^{4}, -1.2×10^{5}
1×10^{8}	-5.8×10^{5}, -3.57×10^{6}

From the eigenvalue analysis, it is clear that the reduced model with higher expansion point will extract the dominant eigenvalues at higher frequencies. And the smaller expansion point will extract the dominant eigenvalues at lower frequencies. In summary, the eigenvalue analysis shown the conventional MOR method can extract the dominant eigenvalue in the range close to the expansion point but cannot guarantee the accuracy when wide frequency range is applied.

6.3 Expansion Point Selection with Multi-Point Model Order Reduction

6.3.1 Current Density Prediction

Chapter 5 has shown the advantage of multi-expansion point model order reduction on 3D EM simulation within a wide frequency range. This section will give the simulation results in different expansion points combination and evaluate the effects on accuracy.

The comparison of the simulation results on current density plot through different MOR setting are shown in Table 6-3:

Table 6-3 Comparison on Current Density with Multi Point MOR

	100Hz	100KHz	100MHz
No MOR	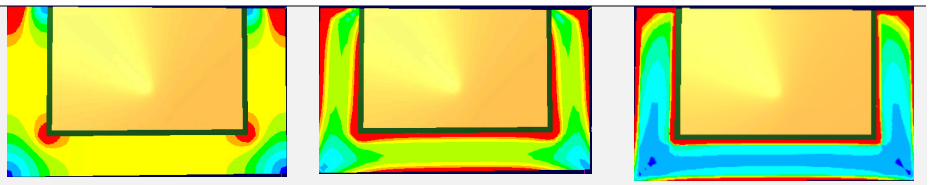		
Multi-Point(0 +1e3	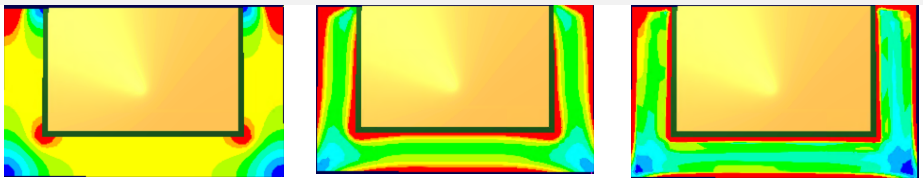		
Multi-Point(0 + 1e8)	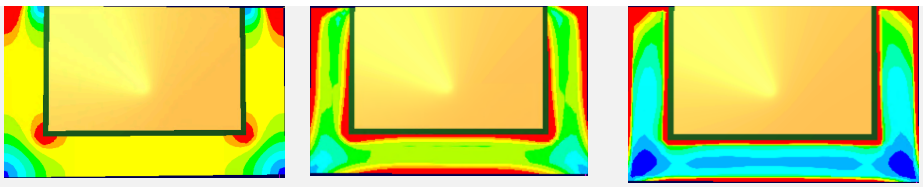		
Multi-Point(1e5+ 1e8)	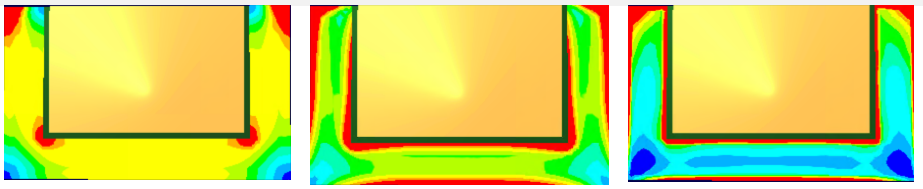		
Multi-Point (0+1e5 + 1e8)	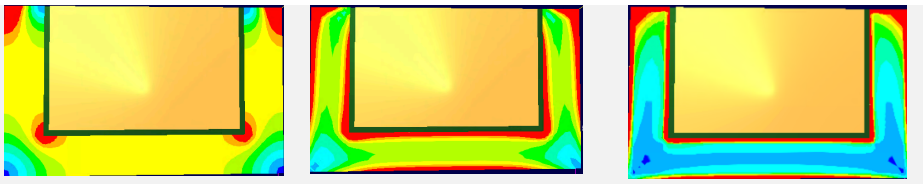		
	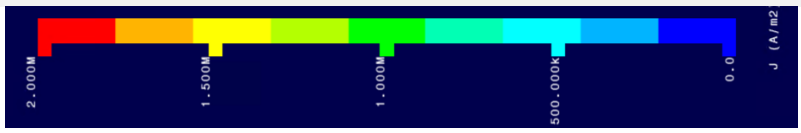		

Multi expansion point MOR techniques are applied to generate current density plot with different combination. All the simulation results are obtained with same mesh settings and the scale is from 0 (A/m^2) to $2e^6$ (A/m^2). From the simulation results, the results with two expansion point is more accurate than the single point MOR, and the simulation results with three expansion points are the best.

The methodology of expansion points selection depends on the requirement of accuracy and the frequency range of simulation. The more expansion points were chosen, the more accurate results will be given. The appropriate points chosen also

depends on the frequency range of interest. The wider frequency range used, the more expansion points needs to be chosen.

The selection of expansion point is very important as well, the best combination is to include the minimum and maximum frequency, with an additional expansion point at the middle range.

6.3.2 Eigenvalue Analysis on Simulation Results with Different Expansion Points Combination for Multi-point MOR methods

The eigenvalue analysis of the reduced model with multi point MOR is shown in Figure 6.3:

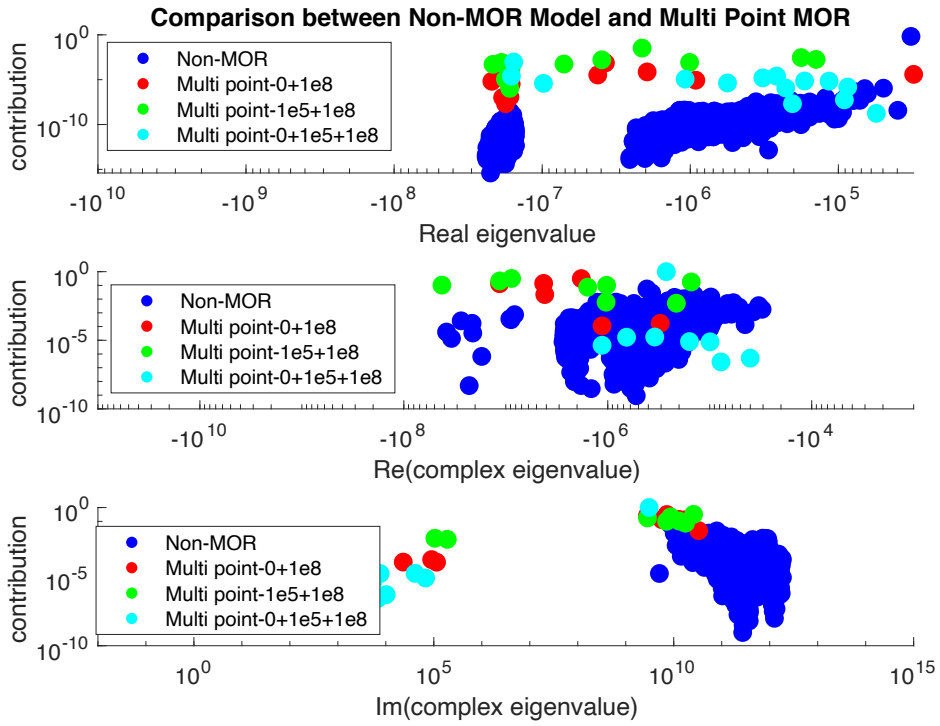

Figure 6.3 Eigenvalue Analysis with Multi Expansion Point MOR

From the eigenvalue analysis, it is clear that the reduced model with multi expansion points will extract the dominant eigenvalues in a wide frequency range.

In summary, the eigenvalue analysis shown the more expansion points chosen, the more dominant eigenvalues will be extracted through MOR method.

6.4 High Resolution Frequency Sweep

Three frequencies are chosen for current density plot in previous section, but sometimes there might be issues between the different frequencies. In this section, high resolution frequency sweep is shown to validate the accuracy of modified model order reduction with three expansion points at 100Hz, 100Khz, and 100 MHz. The simulation results are shown in Figure 6.4:

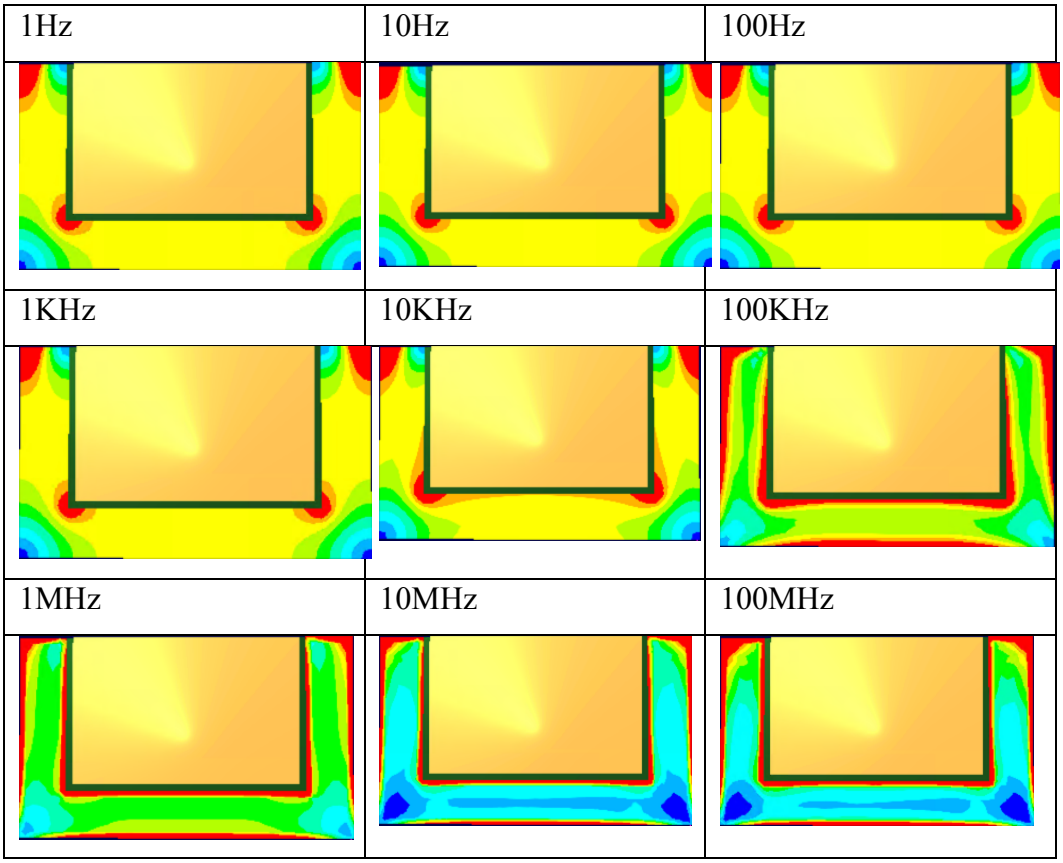

Figure 6.4 Current Density Plot with Three Expansion Point

From the results, 9 plots over the frequency range would fully validate the modified model order reduction method.

6.5 Summary

From simulation results and eigenvalue analysis above, the single expansion point model order reduction is suitable to be used with narrow frequency range. Multi expansion point model order reduction method is suitable to be used with wide frequency range.

The chosen demonstrator in this chapter can be representative for substrate tail for power electronics application, such as GaN device half bridge circuit board etc. The limitation is that it is difficult to model complicated power electronics converters, such as inverter etc.

The criterion for expansion point selection with single expansion point MOR method is to choose the closest point with required frequency. For example, one expansion point is sufficient up to frequency 1KHz, and two expansion points for a frequency up to 100KHz, three expansion points are needed above this frequency range. The expansion points should be evenly spaced in the frequency range. The criterion for expansion point selection with multi expansion point MOR method is depends on the frequency range of interest, usually including minimum frequency, maximum frequency, and another point in the frequency range.

Chapter 7

7 Conclusion

7.1 Conclusions and Summary of Work

In summary, the aim of this work is to optimize the simulation speed and accuracy in iterative virtual prototyping design process through the application of Model Order Reduction techniques, to evaluate a coupled 3D physical model and wide band gap semiconductor models, specifically looking at the variables such as the parasitic characteristic and current density prediction.

There are challenges on the development of wide band gap semiconductors due to the features such as high voltage, high temperature, and high switching frequency. The physical design of the application circuit such as the passive filter components may cause issues related to thermal management and electromagnetic interference (EMI).

Nowadays some different types of commercial software exist which are used for simulating power electronics systems, including circuit simulation, 3D electromagnetic simulation, or system simulation, such as Ansys software and PLECS, SPICE etc. These software are difficult to meet the requirements with increasing operating frequencies because they are usually designed for one domain and is difficult for coupling with accurate semiconductor models.

In this thesis, PEEC method, a finite element analysis method is applied in electromagnetic modelling process using the Ansys simulation software. The limitation with the original model generated by PEEC method is the simulation time when many time steps or frequency steps are needed in one simulation.

An effective model order reduction technique is then proposed and applied to a multi-domain virtual prototyping (VP) design tool which is under development to achieve the objective of rapid virtual prototyping design. The principle of MOR is to make a projection from a high dimensional model to a low dimensional model. A conventional model order reduction method, PRIMA is used to enhance the simulation speed, but the standard method with only one expansion point may lose some important information of the model. Evaluation and analysis of limitations with standard model order reduction are given in this thesis through some test examples. These limitations are particularly evident when the reduced order model is used for prediction of 3D fields such as current density, a key requirement for use in a virtual prototyping tool. An eigenvalue analysis methods is proposed to enable the limitation of MOR methods to be analyzed and understood.

A modified model order reduction method is then proposed to solve the issues with 3D current density prediction with single point model order reduction method. The multi-expansion point MOR method is able to achieve accurate 3D simulation within a wide range frequencies. The same test cases are used for validation, and eigenvalue analysis is applied to check whether the dominant eigenvalues are extracted through MOR process.

Finally, analysis on expansion point selection is performed and recommendations for optimum expansion point choice are given.

7.2 Future work

In this thesis, model order reduction techniques have been proposed and shown that it can be used to optimize the 3D field prediction, specifically for current density. One of the main reasons for doing this is to analyse losses for thermal simulation,

such as in inductor windings or bus bars. MOR methods for thermal simulation[45, 68] also exist and now work is needed to understand how to couple the methods together. It is not easy because distributed coupling between the models requires many independent power inputs to the thermal model and as has been shown, block based MOR methods then require large block sizes.

Future work includes applying PEEC method with magnetic materials and doing electromagnetic modelling in nonlinear system.

Work is also needed to increase the speed for reduced order model generation. The model generation time increases with the square of original matrix dimension. More efficient solvers for the MOR process are needed.

Appendix-Published Papers

A conference paper has been published during PhD period which is listed below:

1. Multi Expansion Point Reduced Order Modelling for Electromagnetic Design of Power Electronics
   Presented at DMC 2021, Bath, 2021

References

[1] E. M. Petriu, M. Cordea, and D. C. Petriu, "Virtual prototyping tools for electronic design automation," *IEEE Instrumentation & Measurement Magazine,* vol. 2, no. 2, pp. 28-31, 1999.

[2] A. K. Morya *et al.*, "Wide bandgap devices in AC electric drives: Opportunities and challenges," *IEEE Transactions on Transportation Electrification,* vol. 5, no. 1, pp. 3-20, 2019.

[3] D. Han, S. Li, W. Lee, and B. Sarlioglu, "Adoption of wide bandgap technology in hybrid/electric vehicles-opportunities and challenges," in *2017 IEEE Transportation Electrification Conference and Expo (ITEC)*, 2017: IEEE, pp. 561-566.

[4] J. He, T. Zhao, X. Jing, and N. A. Demerdash, "Application of wide bandgap devices in renewable energy systems-benefits and challenges," in *2014 International Conference on Renewable Energy Research and Application (ICRERA)*, 2014: IEEE, pp. 749-754.

[5] K. Takahashi, A. Yoshikawa, and A. Sandhu, "Wide bandgap semiconductors," *Springer-Verlag Berlin Heidelberg.,* p. 239, 2007.

[6] P. G. Neudeck, R. S. Okojie, and L.-Y. Chen, "High-temperature electronics-a role for wide bandgap semiconductors?," *Proceedings of the IEEE,* vol. 90, no. 6, pp. 1065-1076, 2002.

[7] M. S. Hybertsen and S. G. Louie, "Electron correlation in semiconductors and insulators: Band gaps and quasiparticle energies," *Physical Review B,* vol. 34, no. 8, p. 5390, 1986.

[8] J. Casady and R. W. Johnson, "Status of silicon carbide (SiC) as a wide-bandgap semiconductor for high-temperature applications: A review," *Solid-State Electronics,* vol. 39, no. 10, pp. 1409-1422, 1996.

[9] T. Kachi, "Recent progress of GaN power devices for automotive applications," *Japanese Journal of Applied Physics,* vol. 53, no. 10, p. 100210, 2014.

[10] F. Qi, Z. Wang, and Y. Wu, "650V GaN Based 3.3 kW Bi-Directional DC-DC Converter for High Efficiency Battery Charger with Wide Battery Voltage Range," in *2019 IEEE Applied Power Electronics Conference and Exposition (APEC)*, 2019: IEEE, pp. 359-364.

[11] B. Ozpineci and L. M. Tolbert, *Comparison of wide-bandgap semiconductors for power electronics applications*. United States. Department of Energy, 2004.

[12] O. Bouketir, "Advances and challenges in WBG devices and their applications in power conversion and conditioning," *Diamond,* vol. 100, p. 5.5, 2016.

[13] B. Zhang and S. Wang, "A survey of EMI research in power electronics systems with wide-bandgap semiconductor devices," *IEEE Journal of Emerging and Selected Topics in Power Electronics,* vol. 8, no. 1, pp. 626-643, 2019.

[14] K. Li, P. Evans, and M. Johnson, "Developing power semiconductor device model for virtual prototyping of power electronics systems," in *2016 IEEE Vehicle Power and Propulsion Conference (VPPC)*, 2016: IEEE, pp. 1-6.

[15] C. Winterhalter, R. Kerkman, D. Schlegel, and D. Leggate, "The effect of circuit parasitic impedance on the performance of IGBTs in voltage source inverters," in *APEC 2001. Sixteenth Annual IEEE Applied Power Electronics Conference and Exposition (Cat. No. 01CH37181)*, 2001, vol. 2: IEEE, pp. 995-1001.

[16] A. S. Martyanov and N. I. Neustroyev, "ANSYS Maxwell Software for electromagnetic field calculations," *Eastern European Scientific Journal,* no. 5, 2014.

[17] P. V. Hung, N. Q. Dinh, Y. Yamada, N. Michishita, and M. T. Islam, "Parametric Analysis of Negative and Positive Refractive Index Lens Antenna by ANSYS HFSS," *International Journal of Antennas and Propagation,* vol. 2020, 2020.

[18] H. Ansys, "High frequency electromagnetic field simulation," *Retrieved from,* 2019.

[19] L. R. C. S. U. PLECS, "LLC Resonant Converter Simulation Using PLECS."

[20] M. H. Rashid, *Spice for power electronics and electric power*. CRC press, 2005.

[21] P. L. Evans, A. Castellazzi, and C. M. Johnson, "A design tool for rapid, multi-domain virtual prototyping of power electronic systems," in *2015 IEEE Energy Conversion Congress and Exposition (ECCE)*, 2015: IEEE, pp. 3069-3076.

[22] P. Evans, A. Castellazzi, S. Bozhko, and C. Johnson, "Automatic design optimisation for power electronics modules based on rapid dynamic thermal analysis," in *2013 15th European Conference on Power Electronics and Applications (EPE)*, 2013: IEEE, pp. 1-10.

[23] S. M. Lee, "Finite-difference vectorial-beam-propagation method using Yee's discretization scheme for modal fields," *JOSA A,* vol. 13, no. 7, pp. 1369-1377, 1996.

[24] D. M. Sullivan, *Electromagnetic simulation using the FDTD method*. John Wiley & Sons, 2013.

[25] G. A. Vandenbosch, "Computational Electromagnetics in Plasmonics," *Plasmonic-Principles and Applications,* pp. 23-48, 2012.

[26] J. B. Schneider, "Understanding the finite-difference time-domain method," *School of electrical engineering and computer science Washington State University,* p. 28, 2010.

[27] J. Ekman, "Electromagnetic modeling using the partial element equivalent circuit method," Luleå tekniska universitet, 2003.

[28] R. F. Harrington, *Field computation by moment methods*. Wiley-IEEE Press, 1993.

[29] J. E. Garrett, "Advancements of the partial element equivalent circuit formulation," 1998.

[30] T. Bauernfeind, P. Baumgartner, O. Bíró, C. A. Magele, K. Preis, and R. Torchio, "PEEC-based multi-objective synthesis of non-uniformly spaced linear antenna arrays," *IEEE Transactions on Magnetics,* vol. 53, no. 6, pp. 1-4, 2017.

[31] K. Priyadharshini and G. Brenie Sekar, "Design of Dipole Antenna Using Mom," in *Proceedings of International Conference on Global Innovations in Computing Technology (ICGICT'14)*, 2014, vol. 2, pp. 1469-1476.

[32] M. B. Allen III, I. Herrera, G. F. Pinder, and W. K. Liu, "Numerical modelling in science and engineering," 1988.

[33] P. Evans and C. M. Johnson, "Fast extraction of dynamic thermal impedance for multi-chip power modules," in *2010 6th International Conference on Integrated Power Electronics Systems*, 2010: IEEE, pp. 1-6.

[34] P. Evans, A. Castellazzi, F. Carastro, and C. Johnson, "A computationally efficient electro-thermal modelling technique for coupled Multi-Disciplinary Analysis of Multi-Chip Power Modules," in *2010 22nd International Symposium on Power Semiconductor Devices & IC's (ISPSD)*, 2010: IEEE, pp. 297-300.

[35] Y. S. Cao, Y. Wang, L. J. Jiang, A. E. Ruehli, J. L. Drewniak, and J. Fan, "Characterizing EMI radiation physics corresponding to distributive

geometry features using the PEEC method," in *2016 IEEE International Symposium on Electromagnetic Compatibility (EMC)*, 2016: IEEE, pp. 764-769.

[36] J.-P. Keradec, E. Clavel, J.-P. Gonnet, and V. Mazauric, "Introducing linear magnetic materials in PEEC simulations. Principles, academic and industrial applications," in *Fourtieth IAS Annual Meeting. Conference Record of the 2005 Industry Applications Conference, 2005.*, 2005, vol. 3: IEEE, pp. 2236-2240.

[37] A. E. Ruehli, G. Antonini, and L. Jiang, *Circuit oriented electromagnetic modeling using the PEEC techniques*. Wiley Online Library, 2017.

[38] C.-W. Ho, A. Ruehli, and P. Brennan, "The modified nodal approach to network analysis," *IEEE Transactions on circuits and systems,* vol. 22, no. 6, pp. 504-509, 1975.

[39] U. Wali, R. Pal, and B. Chatterjee, "On the modified nodal approach to network analysis," *Proceedings of the IEEE,* vol. 73, no. 3, pp. 485-487, 1985.

[40] A. Goldman, *Magnetic components for power electronics*. Springer Science & Business Media, 2002.

[41] M. K. Kazimierczuk, *High-frequency magnetic components*. John Wiley & Sons, 2009.

[42] L. V. Bewley, "Flux Linkages and Electromagnetic Induction," *American Journal of Physics,* vol. 33, no. 4, pp. 355-356, 1965.

[43] J. B. Faria, *Electromagnetic foundations of electrical engineering*. John Wiley & Sons, 2008.

[44] A. Odabasioglu, M. Celik, and L. T. Pileggi, "PRIMA: Passive reduced-order interconnect macromodeling algorithm," in *The Best of ICCAD*: Springer, 2003, pp. 433-450.

[45] T. Bechtold, E. B. Rudnyi, and J. G. Korvink, *Fast simulation of electro-thermal MEMS: efficient dynamic compact models*. Springer Science & Business Media, 2006.

[46] L. C. Westphal, *Handbook of Control Systems Engineering*. Springer Science & Business Media, 2012.

[47] G. Obinata and B. D. Anderson, *Model reduction for control system design*. Springer Science & Business Media, 2012.

[48] B. Datta, *Numerical methods for linear control systems*. Academic Press, 2004.

[49] A. C. Antoulas, *Approximation of large-scale dynamical systems*. SIAM, 2005.

[50] B. Moore, "Principal component analysis in linear systems: Controllability, observability, and model reduction," *IEEE transactions on automatic control,* vol. 26, no. 1, pp. 17-32, 1981.

[51] R. W. Freund, "Reduced-order modeling techniques based on Krylov subspaces and their use in circuit simulation," *Applied and computational control, signals, and circuits,* pp. 435-498, 1999.

[52] B. N. Datta, *Applied and Computational Control, Signals, and Circuits: Volume 1*. Springer Science & Business Media, 2012.

[53] A. El Guennouni, K. Jbilou, and A. Riquet, "Block Krylov subspace methods for solving large Sylvester equations," *Numerical Algorithms,* vol. 29, no. 1-3, pp. 75-96, 2002.

[54] B. Liu *et al.*, "Block SAPOR: Block second-order arnoldi method for passive order reduction of multi-input multi-output RCS interconnect circuits," in *Proceedings of the 2005 Asia and South Pacific Design Automation Conference*, 2005, pp. 244-249.

[55] B. Salimbahrami, B. Lohmann, T. Bechtold, and J. Korvink, "Two-sided Arnoldi algorithm and its application in order reduction of MEMS," in *Proc. 4th MATHMOD*, 2003: Citeseer, pp. 1021-1028.

[56] P. Dawkins, "Systems of Differential Equations," 2007.

[57] P. L. Evans, A. Castellazzi, and C. M. Johnson, "Automated fast extraction of compact thermal models for power electronic modules," *IEEE transactions on power electronics,* vol. 28, no. 10, pp. 4791-4802, 2012.

[58] I. M. Elfadel and D. D. Ling, "A block rational Arnoldi algorithm for multipoint passive model-order reduction of multiport RLC networks," in *iccad*, 1997, vol. 97, pp. 66-71.

[59] A. Ruhe and D. Skoogh, "Rational Krylov algorithms for eigenvalue computation and model reduction," in *International Workshop on Applied Parallel Computing*, 1998: Springer, pp. 491-502.

[60] K. Gallivan, G. Grimme, and P. Van Dooren, "A rational Lanczos algorithm for model reduction," *Numerical Algorithms,* vol. 12, no. 1, pp. 33-63, 1996.

[61] E. Grimme, K. Gallivan, and P. Van Dooren, "A rational Lanczos algorithm for model reduction II: Interpolation point selection," *Numerical Algorithms,* vol. 12, pp. 33-63, 1998.

[62] F. Ferranti, M. S. Nakhla, G. Antonini, T. Dhaene, L. Knockaert, and A. E. Ruehli, "Multipoint full-wave model order reduction for delayed PEEC models with large delays," *IEEE Transactions on Electromagnetic Compatibility,* vol. 53, no. 4, pp. 959-967, 2011.

[63] T.-S. Nguyen, T. Le Duc, T.-S. Tran, J.-M. Guichon, O. Chadebec, and G. Meunier, "Adaptive multipoint model order reduction scheme for large-

scale inductive PEEC circuits," *IEEE Transactions on Electromagnetic Compatibility,* vol. 59, no. 4, pp. 1143-1151, 2017.

[64] M. Rewieński, A. Lamecki, and M. Mrozowski, "Greedy multipoint model-order reduction technique for fast computation of scattering parameters of electromagnetic systems," *IEEE Transactions on Microwave Theory and Techniques,* vol. 64, no. 6, pp. 1681-1693, 2016.

[65] G. A. Baker Jr and J. L. Gammel, "The padé approximant," *Journal of Mathematical Analysis and Applications,* vol. 2, no. 1, pp. 21-30, 1961.

[66] W. Cheney and D. Kincaid, "Linear algebra: Theory and applications," *The Australian Mathematical Society,* vol. 110, pp. 544-550, 2009.

[67] R. M. Martin, *Electronic structure: basic theory and practical methods*. Cambridge university press, 2020.

[68] L. Codecasa *et al.*, "Novel MOR approach for extracting dynamic compact thermal models with massive numbers of heat sources," in *2016 32nd Thermal Measurement, Modeling & Management Symposium (SEMI-THERM)*, 2016: IEEE, pp. 218-223.